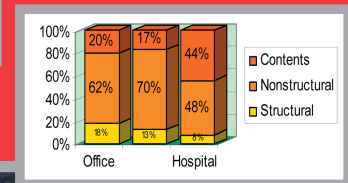
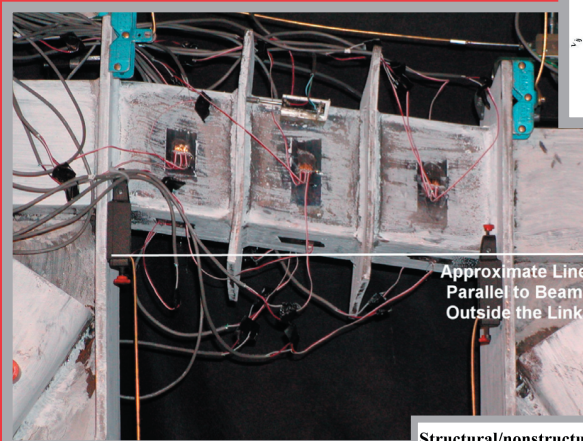
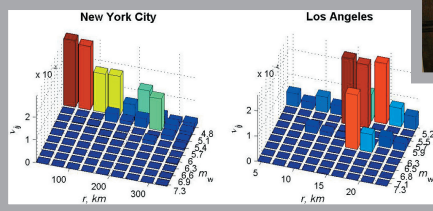
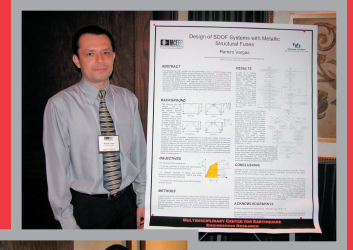
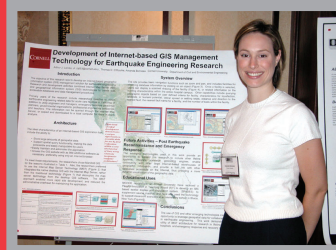
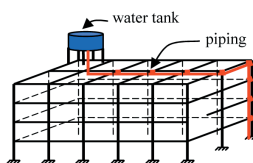


Student Research Accomplishments 2003 – 2004



Structural/nonstructural system definition





The Multidisciplinary Center for Earthquake Engineering Research

The Multidisciplinary Center for Earthquake Engineering Research (MCEER) is a national center of excellence in advanced technology applications that is dedicated to the reduction of earthquake losses nationwide. Headquartered at the University at Buffalo, State University of New York, the Center was originally established by the National Science Foundation (NSF) in 1986, as the National Center for Earthquake Engineering Research (NCEER).

Comprising a consortium of researchers from numerous disciplines and institutions throughout the United States, the Center's mission is to reduce earthquake losses through research and the application of advanced technologies that improve engineering, pre-earthquake planning and post-earthquake recovery strategies. Toward this end, the Center coordinates a nationwide program of multidisciplinary team research, education and outreach activities.

Funded principally by NSF, the State of New York and the Federal Highway Administration (FHWA), the Center derives additional support from the Federal Emergency Management Agency (FEMA), other state governments, academic institutions, foreign governments and private industry.

Student Research Accomplishments

2003-2004

Multidisciplinary Center for Earthquake Engineering Research
University at Buffalo, State University of New York

Edited by Amanda Bonneau
December 2004

MCEER-04-SP06

Red Jacket Quadrangle, Buffalo, New York 14261

Phone: (716) 645-3391; Fax: (716) 645-3399

E-mail: mceer@mceermail.buffalo.edu

World Wide Web: <http://mceer.buffalo.edu>

Foreword

The Student Leadership Council (SLC) is a formal incarnation of the students who are involved in performing MCEER research under a faculty advisor. Since its inception, MCEER has included and encouraged student efforts throughout its research program and in all of the disciplinary specialties concerned with earthquake engineering.

Throughout the years, students have been an integral component in advancing research in earthquake hazard mitigation. Many former students are now employed in academia, professional practice or government agencies applying knowledge gained during their exposure to MCEER research. While associated with MCEER, students participate in Center annual meetings, attend conferences, workshops and seminars, and have the opportunity to make presentations at these events. The SLC was formed in the year 2000 to formalize these programs and to afford students from many different institutions the opportunity to meet with each other and develop/improve interaction.

The idea for the *Student Research Accomplishments* was conceived by the SLC and features the work of MCEER's current students. Topics range from traditional civil and lifeline engineering to applications of advanced technologies to social impacts and economic modeling.

This volume was coordinated and edited by Amanda Bonneau, MS/Ph.D. student in the School of Civil and Environmental Engineering at Cornell University. Previous editors were Ramiro Vargas, Benedikt Halldorsson, and Diego Lopez Garcia, all from the Department of Civil, Structural and Environmental Engineering, University at Buffalo, and Gauri Guha, Department of Energy, Environmental and Mineral Economics, the Pennsylvania State University.

All papers included in this volume were entered into MCEER's *Best Student Article Competition*. Members of MCEER's Industry Advisory Board (IAB) judged the 11 submissions, and selected a winner and two honorable mentions. The winner of this year's competition is outgoing SLC President Jeffrey Berman, University of Buffalo, and honorable mentions were awarded to Anita Jacobson, Cornell University and Michael Astrella, University of Buffalo, for their outstanding efforts. All three students were invited to present their research at the 2005 MCEER Annual Meeting. Our thanks go to John Abruzzo, Thornton-Tomasetti Group, Sreenivas Alampalli, New York State Department of Transportation, Scott Campbell, Kinetics Noise Control, Inc., Paul Hough, Armstrong World Industries, Inc., Amarnath Kasalanati, Dynamic Isolation Systems, Inc., Leon Kempner, Bonneville Power Administration, Peter Lee, Skidmore, Owings & Merrill, Paul Senseny, FM Global Research, Andy Taylor, KPFF Consulting Engineers, Doug Taylor, Taylor Devices, Inc. and Michael Willford, ARUP for their reviews and recommendations.

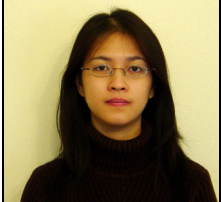
Finally, MCEER wishes to extend its thanks to the Student Leadership Council for its endeavors, and in particular to Jeffrey Berman, current president, and A. Natali Sigaher, past president, for their able guidance of the SLC.

Best Student Article Competition: 2004

Winner

	Jeffrey Berman
	<i>Ph.D. Student, Department of Civil, Structural & Environmental Engineering, University at Buffalo</i> <i>Research Supervisor: Michel Bruneau, Professor and Director of MCEER</i> Testing of a Laterally Stable Eccentrically Braced Frame for Steel Bridge Piers page 1

Honorable Mentions

	Anita Jacobson
	<i>Ph.D. Student, School of Civil and Environmental Engineering, Cornell University</i> <i>Research Supervisor: Mircea Grigoriu, Professor</i> A Methodology to Assess Seismic Performance of Water Supply Systems page 7

	Michael Astrella
	<i>Graduate Student, Department of Civil, Structural & Environmental Engineering, University at Buffalo</i> <i>Research Supervisor: Andrew S. Whittaker, Associate Professor</i> Changing the Paradigm for Performance-Based Design page 15

Contents

Winner: Best Student Article Competition

- 1 Testing of a Laterally Stable Eccentrically Braced Frame for Steel Bridge Piers
Jeffrey W. Berman, University at Buffalo..... 1

Honorable Mentions

- 2 A Methodology to Assess Seismic Performance of Water Supply Systems
Anita Jacobson, Cornell University..... 7
- 3 Changing the Paradigm for Performance-Based Design
Michael Astrella, University at Buffalo..... 15

Papers

- 4 Global Fragility Evaluation of Health Care Facilities with Structural and Nonstructural Components
Gian Paolo Cimellaro, University at Buffalo..... 23
- 5 An Experimental Verification of the Eigensystem Realization Algorithm for Vibration Parameter Identification
Marlon D. Hill, Florida A&M University..... 29
- 6 Evolutionary Methodologies for Decision Support
Yufeng Hu, University at Buffalo..... 39
- 7 Fragility Based Rehabilitation Decision Analysis
Cagdas Kafali, Cornell University..... 47
- 8 A Wavelet Based Approach for Estimating the Steady State Response of Nonlinear Systems
Jale Tezcan, Rice University..... 55
- 9 Floor Response of Single Degree of Freedom Systems with Metallic Structural Fuses
Ramiro E. Vargas, University at Buffalo..... 61
- 10 Response of Seismically Isolated Bridges Considering Variation in the Mechanical Properties of Individual Isolators
Gordon Warn, University at Buffalo..... 69
- 11 A Novel Nonlinear Control System with Emphasis on Nonstructural Performance
Xin Xu, University at Buffalo..... 75

Testing of a Laterally Stable Eccentrically Braced Frame for Steel Bridge Piers

Jeffrey W. Berman

Ph.D. Student, Dept. of Civil Structural and Environmental Engineering, University at Buffalo

Research Supervisor: Michel Bruneau, Professor and Director of MCEER

Summary

This paper describes the design and testing of a proof-of-concept eccentrically braced frame specimen that utilizes a hybrid rectangular shear link that is not laterally braced. Equations used for design are given and references for their derivations are provided. The quasi-static cyclic proof-of-concept testing is described and results are reported. Stable and full hysteretic loops were obtained and no signs of flange, web, or lateral torsional buckling were observed. The link was subjected to 0.15 radians of rotation in the final cycle, which is almost twice the maximum rotation allowed in building codes for links with I-shaped cross-sections. Although the final failure mode was fracture of the bottom link flange, the large rotations achieved were well above what would be required in a seismic event, indicating that hybrid rectangular links without lateral bracing of the link can indeed be a viable alternative for applications in steel bridge piers in seismic regions.

Introduction

Eccentrically braced frames have been shown to exhibit excellent seismic performance. However, eccentrically braced frames have had limited use in the steel piers of bridges due to the difficulty of providing the lateral bracing required to prevent possibility of lateral torsional buckling of the link. An eccentrically braced frame system in which lateral bracing of the link is not necessary would make it desirable in the context of seismic design and retrofit of bridges, especially since eccentrically braced frames have been shown to exhibit excellent seismic performance (Roeder and Popov (1977), Hjelmstad and Popov (1983), Kasai and Popov (1986), Engelhardt and Popov (1989), among others).

From this motivation, the concept of an EBF utilizing a rectangular hybrid cross-section for the link is explored (hybrid in this case meaning the yield stresses of the webs and flanges may be different). Rectangular cross-sections inherently have more torsional stability than I-shaped cross-sections and may not require lateral bracing.

This paper describes the design and testing of a proof-of-concept EBF having a link with a hybrid rectangular cross-section. First, equations used for design, including plastic shear force, and plastic moment are given and references for their derivations are provided. Then, the specimen design and test setup are described. Finally, the experimental results are discussed and conclusions are drawn.

Design Equations

A link with a hybrid rectangular cross-section is shown in Figure 1. Assuming the moment on the section is less than the reduced plastic moment (described below), the plastic shear force, V_p , for the cross-section is (Berman and Bruneau, 2004):

$$V_p = \frac{2}{\sqrt{3}} F_{yw} t_w (d - 2t_f) \quad (1)$$

where F_{yw} is the yield stress of the webs, t_w is the web thickness, d is the depth of the section, and t_f is the flange thickness. The plastic moment, M_p , for the cross-section shown in figure is:

$$M_p = F_{yf} t_f (b - 2t_w)(d - t_f) + F_{yw} \frac{t_w d^2}{2} \quad (2)$$

where F_{yf} is the yield stress of the flanges, b is the section width, and other terms are as previously defined. This plastic moment may also be reduced the presence of the plastic shear force, as a simple way of accounting for shear-moment interaction in the presence of the full plastic shear. The reduced plastic moment, M_{pr} , can be written as:

$$M_{pr} = F_{yf} t_f (b - 2t_w)(d - t_f) + 2F_{yw} t_f t_w (d - t_f) \quad (3)$$

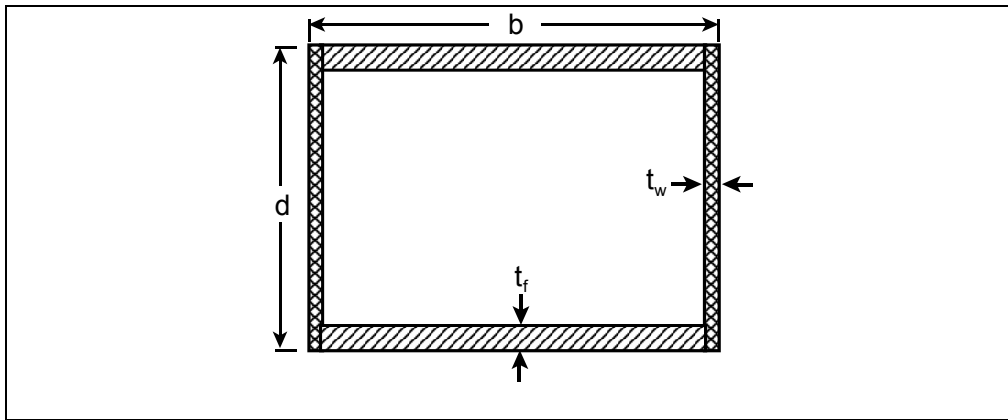


Figure 1. Hybrid Rectangular Link Cross-Section

As with links having I-shaped cross-sections, hybrid links with rectangular cross-sections fall into one of three categories, shear links, intermediate links, and flexural links. Classification of links can be done using the normalized link length, ρ , defined as $e/(M_p/V_p)$, where e is the link length. Links having $\rho \leq 1.6$ are shear links and the inelastic behavior is dominated by shear yielding of the webs. Links having $1.6 < \rho \leq 2.6$ are intermediate links, for which inelastic behavior is a mix of shear and flexural behavior, and links having $2.6 < \rho$ are flexural links where inelastic behavior is dominated by flexural yielding. These ranges are the same as those for I-shaped links, since there is no expected difference in the factors used to determine them, namely, overstrength and strain hardening (Berman and Bruneau, 2004). For I-shaped links, the AISC Seismic Provisions (AISC, 2002) limit the inelastic link rotation for shear links and flexural links to 0.08 rads and 0.02 rads, respectively, with linear interpolation based on normalized link length to be used for intermediate links. At this point there is no data indicating these limits should be different for hybrid rectangular links.

The necessity for using hybrid rectangular cross-sections arises from the short link lengths required for HSS shapes that are listed in the AISC LRFD Manual of Steel Construction (AISC, 1998) to be shear links (i.e. have $\rho \leq 1.6$). The maximum length for a shear link, that also meets the compactness limits would be 460 mm and would be obtained with a HSS 250x250x16. Considering a 7.3 m wide by 3.7 m tall frame the drift at a plastic rotation of 0.08 rads is only 0.5% from (Bruneau et al., 1998):

$$\theta = \gamma \frac{e}{L} \quad (4)$$

where θ is the frame drift, γ is the link rotation, L is the frame width, and e is the link length. There may be instances where ductility demand exceeds this drift value. Additionally, a short link has a greater stiffness, which can translate into increased seismic demands on the surrounding framing and foundation. Furthermore, as a minor point, short links can cause congested details and fabrication difficulties. Therefore, hybrid rectangular cross-sections which offer the ability to change the M_p over V_p ratio by changing the web and flange thicknesses independently, are desirable since they will allow longer link lengths while still having a shear link and the desired shear strength.

Specimen Design and Test Setup

The proof-of-concept EBF with a hybrid rectangular shear link was designed to be as large as possible considering the constraints of the available equipment in the Structural Engineering and Earthquake Simulation Laboratory (SEESL) at the University at Buffalo (UB). Quasi-static cyclic loading was chosen and the maximum force output of the actuator available (1115 kN) was divided by 2.5 to account for the possibility of obtaining material with a higher than specified yield stress as well as strain hardening, making the design base shear 445 kN. The general test setup is shown in Figure 2. Assuming the moments at the middle of the link and clevises are zero, the design link shear can be found to be 327 kN for the dimensions shown. To design the link, the equations described above (i.e., link shear force, Eq. (1), and the AISC web and flange compactness limits) were used in conjunction with enforcing a minimum link length such that a drift of at least 1% corresponds to a maximum link rotation of 0.08 rads and assuring $\rho < 1.6$ (i.e., maintaining a shear link). The following link dimensions were selected: $d = b = 150$ mm, $t_f = 16$ mm, $t_w = 8$ mm, and $e = 460$ mm. A yield stress of 345 MPa was assumed for the steel during the design process and ASTM A572 Gr. 50 steel was specified for fabrication of the link beam which gave an anticipated link shear of 381 kN.

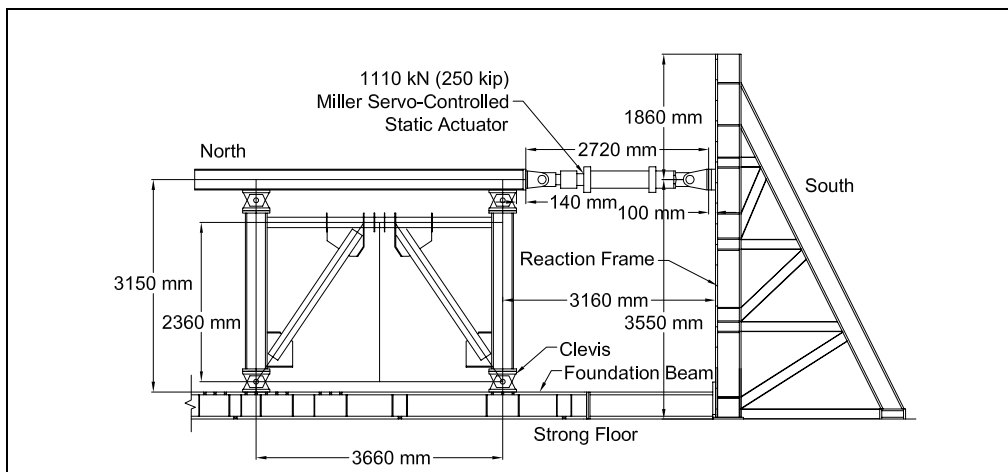


Figure 2. Test Setup

The framing outside the link was designed using capacity principles. Factors to account for the difference between specified and expected (i.e., mean) yield stress of the link material as well as strain hardening were incorporated, resulting in the member sizes shown in Figure 3.

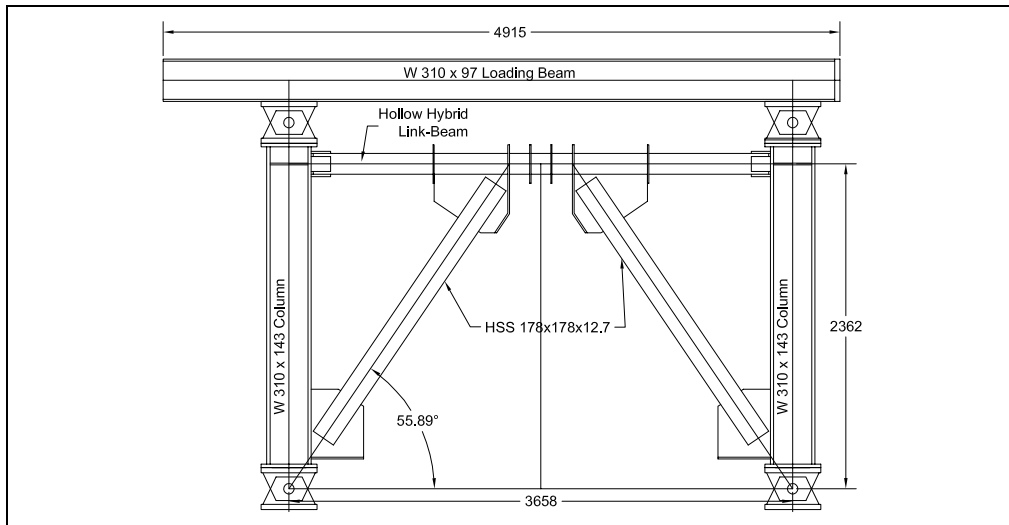


Figure 3. Test Specimen with Dimensions

Experimental Results

The experimentally obtained base shear versus frame drift hysteresis is shown in Figure 4a and the link shear force versus link rotation hysteresis is shown in Figure 4b. From the elastic cycles of Figure 4a, the initial stiffness of the specimen was found to be 80 kN/mm. The yield base shear and frame drift were 668 kN and 0.37% while the maximum base shear and drift were 1009 kN and 2.3%, respectively. Link shear force and rotation at yield were 490 kN and 0.014, while the maximum link shear and rotation achieved were 742 kN and 0.151 rads, respectively. Projecting the elastic and inelastic slopes of Figure 4b leads to an approximation of the plastic link shear force of 520 kN. The link shear force at 0.08 rads of rotation (the current limit for shear links) was 689 kN. Assuming equal link end moments, the end moments at specimen yield, development of V_p , and 0.08 rads of rotation were 112 kN-m, 119 kN-m, and 158 kN-m, respectively, and the maximum link end moment was 170 kN-m.

The link achieved a rotation level 0.151 rads, which is almost twice the current limit for shear links in EBF for buildings (0.08 rads) and the target rotation for the specimen. Furthermore, the EBF reached a frame displacement ductility 6.0 and link rotation ductility of over 10 (the difference in these is due to the flexibility of the surrounding framing). Figure 5a shows the deformed link at 0.123 rads (1.92% drift) during Cycle 19.

Link failure occurred when the bottom flange at the north end of the link fractured as shown in Figure 5b. The fracture occurred in the heat affected zone (HAZ) of the flange adjacent to the fillet weld used to connect the stiffener for the gusset of the brace-to-link connection to the link. Inspection of the failure surface was performed using a magnifying glass and light-microscope with 30x magnification (personal communication, Mark Lukowski, metallurgist, and Dr. Robert C. Wetherhold, mechanical engineer, Department of Mechanical and Aerospace Engineering, University at Buffalo, September 2003). The fracture was assessed as having initiated by cracking in

the HAZ of the previously mentioned fillet weld and the propagation of those cracks under load reversals. There was no evidence of crack initiation in the full penetration groove weld used to assemble the webs and flanges of the link

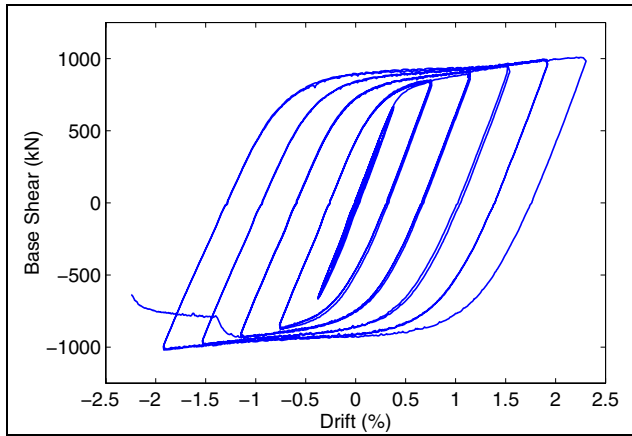


Figure 4a. Base Shear vs. Frame Drift

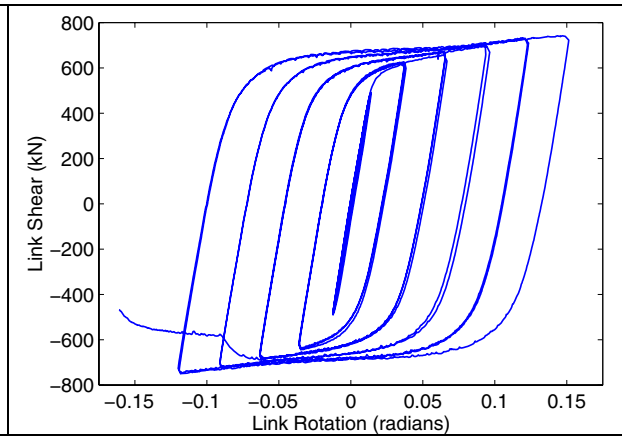


Figure 4b. Link Shear vs. Link Rotation

The framing outside the link remained elastic for the duration of testing. Out-of-plane moments in the beam segments outside the link and eccentric braces remained less than 2.5% of those members' yield moments. This small moment can be resisted by the connections to the columns and need not be considered in design. Small out-of-plane moments and the fact that no evidence of lateral torsional buckling was observed, indicates that the goal of developing a link that does not require lateral bracing was achieved.



Figure 5a. Link Deformed at 0.123 rads of Rotation During Cycle 19

Figure 5b. Fractured Bottom Flange at North End of Link

Conclusions

A laterally stable link for eccentrically braced frames for use in bridge piers where lateral bracing to prevent lateral torsional buckling is difficult to provide, has been developed. Selected design equations to achieve laterally stable hybrid rectangular links have been given and references for their

derivations have been provided. The proof-of-concept testing of a single eccentrically braced frame with a hybrid rectangular shear link was successful in that it reached a link rotation of 0.151 rads (almost twice the maximum allowed in building codes for I-shaped links) without strength degradation and showed no signs of lateral torsional buckling. Link failure occurred after reaching a frame displacement ductility of 6 (which corresponded to a link rotation ductility of more than 10) when the bottom flange fractured at the north end of the link. The fracture was found to have started in the heat affected zone of the flange near the fillet weld used to connect the gusset stiffener for the eccentric brace connection to the link and was not affected by the full penetration groove weld used to connect the webs and flanges of the link.

Acknowledgements

This research was conducted by the State University of New York at Buffalo and was supported by the Federal Highway Administration under contract number DTFH61-98-C-00094 to the Multidisciplinary Center for Earthquake Engineering Research. However, any opinions, findings, conclusions, and recommendations presented in this paper are those of the authors and do not necessarily reflect the views of the sponsors.

References

AISC (1998): *Manual of Steel Construction: Load and Resistance Factor Design*. 3rd Ed. American Institute of Steel Construction, Chicago, IL.

AISC (2002): *Seismic Provisions for Structural Steel Buildings*. American Institute of Steel Construction, Chicago, IL.

Berman, J. W., and Bruneau, M., (2004): Approaches for the Seismic Retrofit of Braced Steel Bridge Piers and Proof-of-Concept Testing of a Laterally Stable Eccentrically Braced Frame. *Technical Report MCEER-03-0001*, Multidisciplinary Center for Earthquake Engineering Research, (submitted for review 9/04).

Bruneau, M., Uang, C.M., and Whittaker, A. (1998): *Ductile Design of Steel Structures*. McGraw-Hill, New York, NY.

Engelhardt, M.D., and Popov, E.P. (1989): Behavior of Long Links in Eccentrically Braced Frames. *Report No. UCB/EERC-89-01*, Earthquake Engineering Research Center, College of Engineering, University of California Berkeley, Berkeley, CA.

Hjelmstad, K.D., and Popov, E.P. (1983): Cyclic Behavior and Design of Link Beams. *Journal of Structural Engineering*, ASCE, 109(10), 2387-2403.

Kasai, K., and Popov, E.P. (1986): General Behavior of WF Steel Shear Link Beams. *Journal of Structural Engineering*, ASCE, 112(2), 362-382.

Roeder, C.W., and Popov, E.P. (1977): Inelastic Behavior of Eccentrically Braced Steel Frames Under Cyclic Loadings. *Report No. UCB/EERC-77/18*, Earthquake Engineering Research Center, College of Engineering, University of California Berkeley, Berkeley, CA.

A Methodology to Assess Seismic Performance of Water Supply Systems

Anita Jacobson

Ph.D student, School of Civil and Environmental Engineering, Cornell University

Research Supervisor: Mircea Grigoriu, Professor

Summary

A methodology to assess the seismic performance of water supply systems has been developed, which estimate the probability that a given system response violating some specified conditions or limit states. The methodology requires input on: seismic hazard at the site of the system, fragility information of each component of the system, and the limit states imposed on the system. The proposed methodology consists of three steps: (1) generate samples of damaged system, (2) perform hydraulic analysis on the generated damaged systems, and (3) develop system fragility to assess the seismic performance of the water supply system based on specified criteria.

Introduction

It is essential that water supply systems will be able to deliver the required amount of water needed to help recovery process during the aftermath of seismic occurrences, especially if fire breaks during those events. Many researchers have come up with ways to assess seismic performance of water supply systems or seismic network reliability in general, such as those proposed by [Hwang, Lin, and Shinozuka (1998)] and [Selçuk and Yüçemen (1999), (2000)]. In this paper, the author proposes a new methodology which incorporates a new seismic activity model to represent the seismic hazard at the location of the system.

Seismic Hazard

A probabilistic model, shown in Figure 1, is developed to generate random samples of seismic occurrences at a collection of sites during a time period τ , which usually equals the lifetime of the analyzed system. The inputs for the model consist of: system lifetime τ , seismic activity matrix V_{ij} , and soil properties at the collection of sites.

Each sample of seismic activity generated by the model gives the number and temporal distribution of the seismic events, along with the seismic moment magnitude m_m , and site-to-source distance r of each event. For each event, given the soil properties at the collection of sites, samples of spatially distributed seismic ground acceleration can be generated using a ground motion stochastic model such as the specific barrier model by [Papageorgiou and Aki (1983a), (1983b), (1988)] and incorporating a coherence function to obtain a spatially correlated ground motion such as [Harichandran and Vanmarcke (1986)] coherence function.

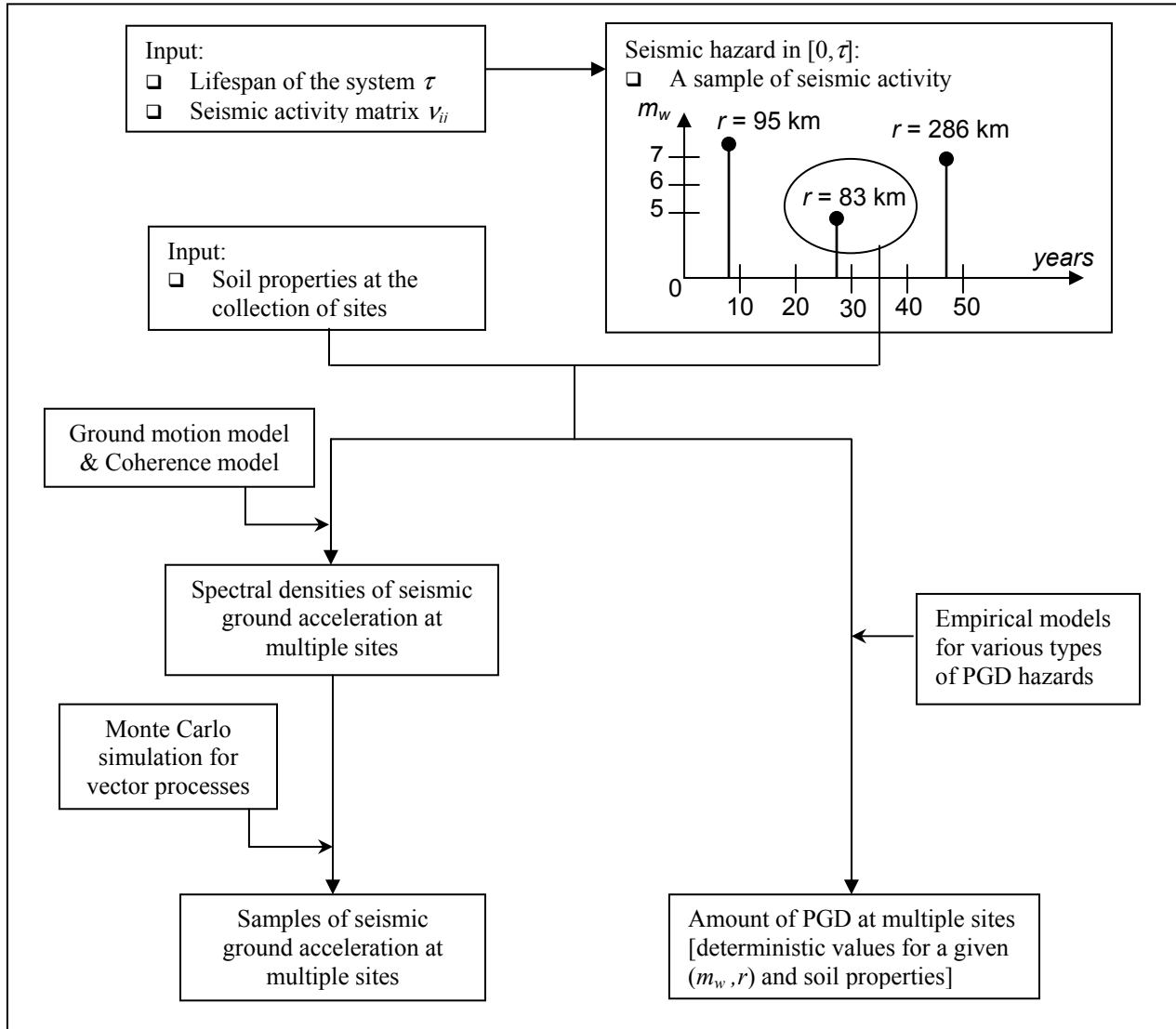


Figure 1. A seismic activity model for multiple sites

Consider a site, in which the area surrounding the site can be discretized into rings R_j and the range of possible earthquake magnitudes into bins M_j . Then, seismic activity matrix provides the mean annual rate of seismic occurrences at the site v_{ij} in the bin (R_j, M_j) . Figure 2 shows the seismic activity matrix for New York City and Los Angeles.

Permanent ground displacement (PGD) hazards consists of landslides, liquefactions, and surface ruptures (or fault displacements). Various researchers have come up with empirical relationships to estimate the amount of ground displacement caused by these hazards. For example: [Jibson and Keefer (1993)] model provides a method to compute the expected amount of ground displacement caused by landslides, or [Barlett and Youd (1995)] model gives an estimate of ground displacement caused by lateral spreads induced by liquefactions.

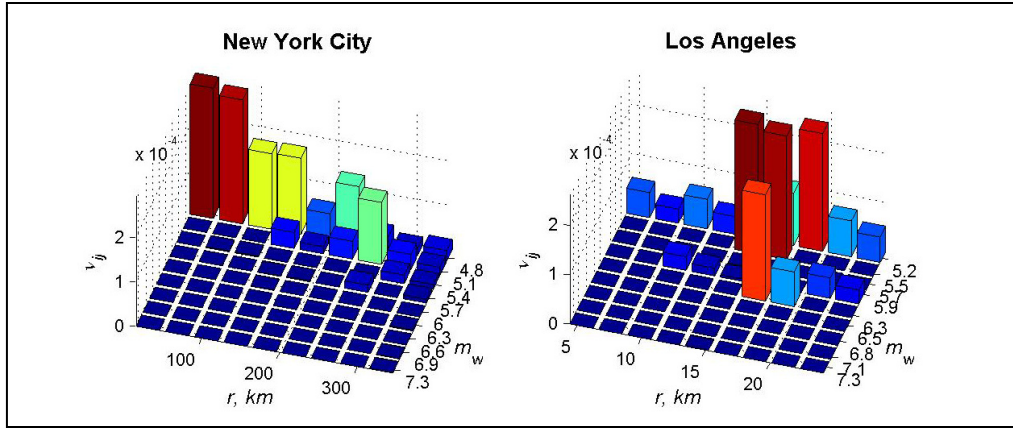


Figure 2. Seismic activity matrix for New York City and Los Angeles.

Component Fragility

Fragility is described as the conditional probability of failure or damage for a system/system component with some earthquake parameters. The probability of a system exceeding different levels of limit states can be given as a function of either a ground motion intensity (i.e. fragility curves) or a function of moment magnitude and site-to-source distance (i.e. fragility surfaces).

Fragility corresponds to the i -th limit state is the conditional probability that the damage index DI exceeds a critical value DI_i given the seismic occurrence with ground motion intensity y , that is $F_i(y) = P(DI > DI_i | y)$, or seismic occurrence with moment magnitude and site-to-source distance (m_w, r) , that is $F_i(m_w, r) = P(DI > DI_i | m_w, r)$. Damage index DI is the seismic demand of the component/system, while DI_i is the seismic capacity of the component/system.

Fragility can be obtained empirically based on historical data or can be generated by Monte Carlo simulation when sufficient data is not available. Figure 3 shows examples of fragility curves obtained for water tanks as a function of fill level and anchorage [ALA (2001)].

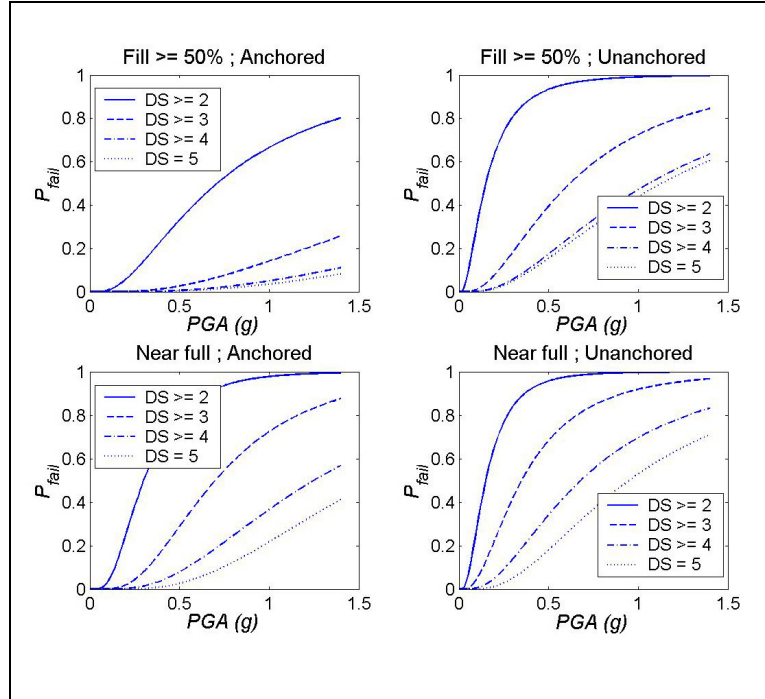


Figure 3. Fragility curves for water tanks [ALA (2001)]

When no existing fragility information can be found for a certain component, we can try to produce one analytically by using the general methodology given in Figure 4 [Jacobson (2004)].

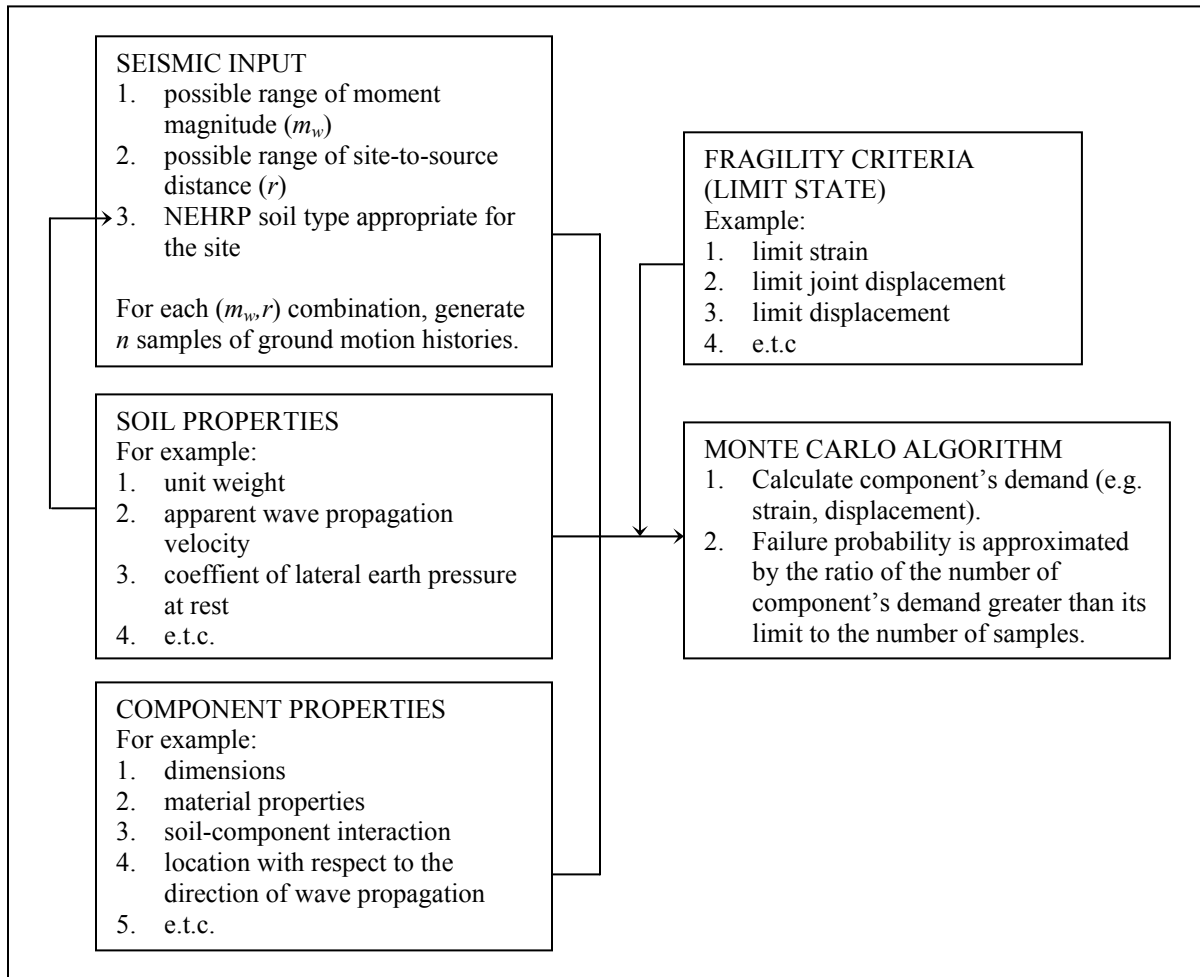


Figure 4. General methodology to obtain component's fragility

Example: Fragility surfaces are obtained for a continuous pipe with 12-inch diameter and 0.5-inch wall thickness with 48-inch of depth to its centerline. The pipe is made of steel with elastic modulus of 29000 ksi. It is assumed that the angle between pipeline and seismic wave is 45° , and the specified limit strain is 0.005%. Figure 5 shows fragility surfaces of the pipe for various NEHRP soil types. The fragility surfaces are calculated for m_w from 4.0 to 8.0, r from 50 km to 250 km with 250 samples for each (m_w, r) pair.

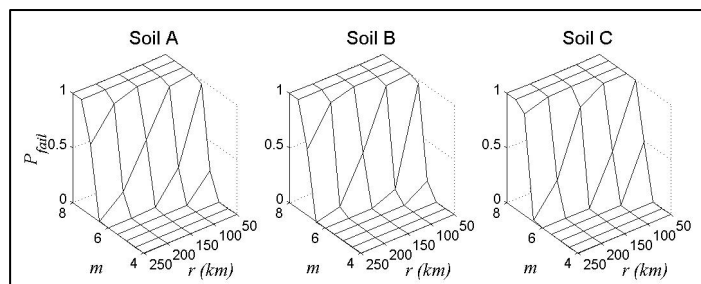


Figure 5. Fragility surfaces of an example continuous pipe.

Water Supply System Fragility

A methodology to assess the seismic performance of water supply systems is proposed, which provides an estimation of failure probability of a water supply system. A water supply system fails when it is no longer capable to deliver the minimum required performance that it is assigned to do, such as if it fails to provide the minimum pressure at certain demand nodes.

The methodology requires data on: (1) the moment magnitude of the earthquake, (2) site-to-source distances from the source to each component in the system, (3) the soil properties at each location of the component, (4) the fragility information for each component in the system, and (5) the performance criteria or limit states for the water supply system.

The methodology consists of three steps as illustrated in Figure 6:

Step 1: Generate samples of damaged systems.

The analysis is initiated by shaking the system with a seismic ground motion having a moment magnitude m^* to obtain the ground motion intensity (e.g. peak ground acceleration) values at each location at its components. For each component, generate a random variables having a uniform distribution $U(0,1)$ to determine the damage state of the component based on its fragility information.

Step 2: Perform hydraulic analysis on the damaged systems.

Evaluation of damaged systems can be done using hydraulic analysis to check the amount of flow at critical pipes and/or amount of pressures at critical nodes. When the system is no longer capable to deliver its minimum requirement, then it fails.

Step 3: Develop system fragilities.

Failure probability of the system under seismic occurrence with moment magnitude m^* can be approximated by the ratio of the number of damaged system samples that fail to satisfy the predetermined limit state over the number of samples generated. Repeat the procedure with a range of moment magnitude m_w values to obtain a fragility curves.

Conclusion

A methodology to assess the seismic performance of water supply systems has been developed, which utilize a probabilistic model in order to capture the spatial variation in seismic ground acceleration existing in a system covering a large area and to also account for PGD hazards. The proposed methodology consists of three steps: generate samples of damaged systems, perform hydraulic analysis on the damaged systems, and develop system fragilities.

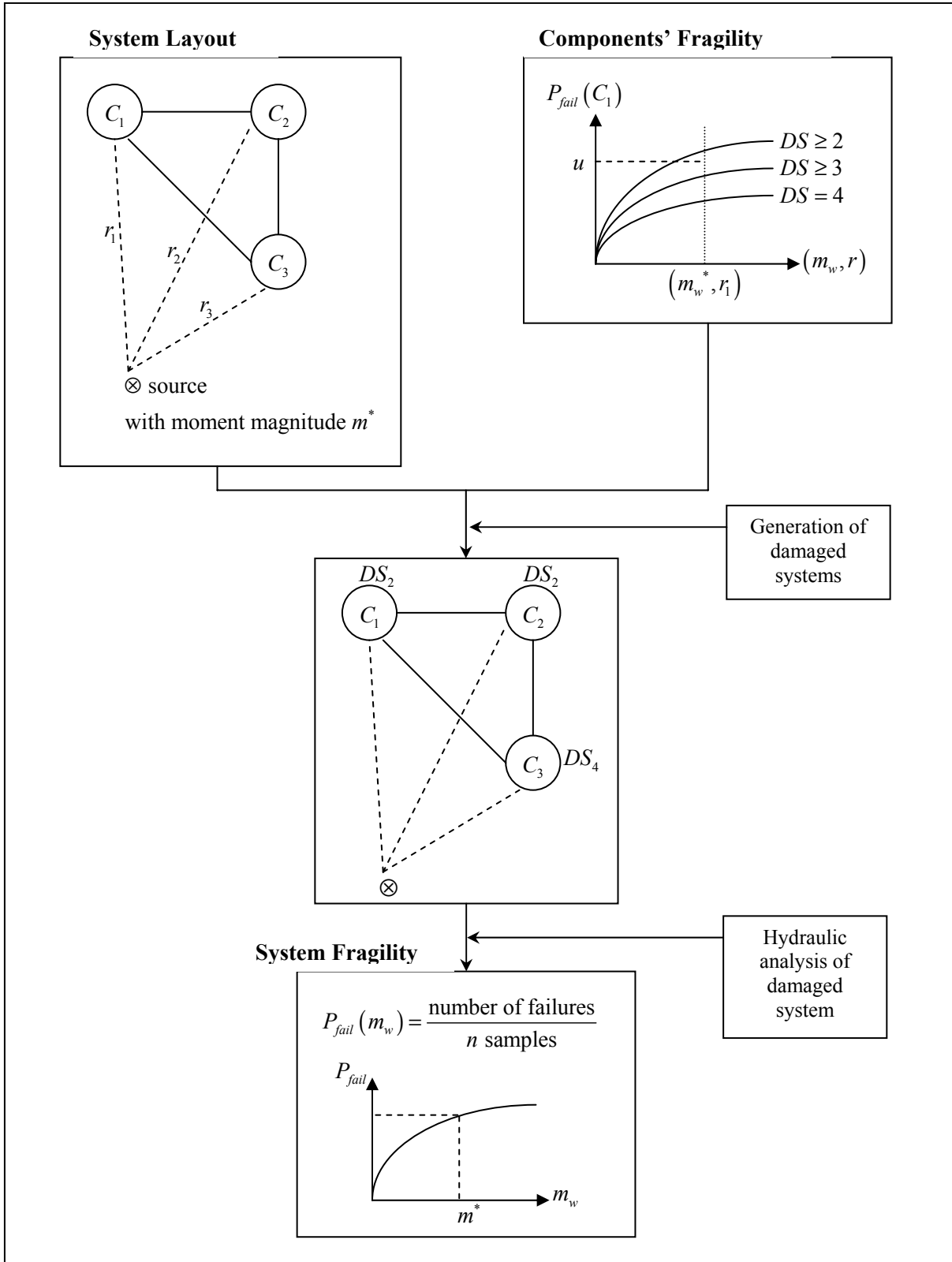


Figure 6. Methodology of fragility analysis of water supply systems

Acknowledgements

This research was carried out under the supervision of Dr. Mircea Grigoriu and primarily supported by the Earthquake Engineering Research Centers Program of the National Science Foundation, under award number EEC-9701471. This financial support is gratefully acknowledged.

References

- ALA (2001): Seismic Fragility Formulations for Water Systems: Part I – Guideline. <http://www.americanlifelinesalliance.org>.
- Barlett S. and Youd T.(1995): Empirical Prediction of Liquefaction-Induced Lateral Spreads. *J.Geotech.Engrg., ASCE 121(4)*, 316-329.
- Hwang H., Lin H., and Shinozuka M. (1998): Seismic Performance Assessment of Water Delivery System. *Journal of Infrastructure Systems 4(3)*, 118-125.
- Jacobson A. (2004): Fragility Analysis of Water Supply Systems. Master's thesis, Cornell University, Ithaca, NY, USA.
- Jibson R.W. and Keefer D.K. (1993): Analysis of the Seismic Origin of Landslides: Examples from the New Madrid Seismic Zone. *Geological Society of America Bulletin 105*, 521-536.
- Kafali C. and Grigoriu M. (2003): Non-Gaussian Model for Spatially Coherent Seismic Ground Motions. *Proceedings of the 9th International Conference on Applications of Statistics and Probability in Civil Engineering*, San Francisco, CA, 321-327.
- Papageorgiou A.S. and Aki K. (1983a): A Specific Barrier Model for the Quantitative Description of Inhomogeneous Faulting and the Prediction of Strong Ground Motion. Part I: Description of the Model. *Bulletin of the Seismological Society of America 73(3)*, 693-722.
- Papageorgiou A.S. and Aki K (1983b): A Specific Barrier Model for the Quantitative Description of Inhomogeneous Faulting and the Prediction of Strong Ground Motion. Part II: Application of the Model. *Bulletin of the Seismological Society of America 73(4)*, 953-978.
- Papageorgiou A.S. (1988): On Two Characteristic Frequencies of Acceleration Spectra: Patch Corner Frequency and f_{max} . *Bulletin of the Seismological Society of America 78(2)*, 509-528.
- Selçuk A. and Yüçemen M. (1999): Reliability of Lifeline Networks Under Seismic Hazards. *Reliability Engineering and System Safety 65*, 213-227.
- Selçuk A. and Yüçemen M. (2000): Reliability of Lifeline Networks With Multiple Sources Under Seismic Hazards. *Natural Hazards 21*, 1-18.

Changing the Paradigm for Performance-Based Design¹

Michael Astrella

Graduate Student, Department of Civil, Structural & Environmental Engineering, University at Buffalo

Research Supervisor: Andrew Whittaker, Professor

Summary

The principal investments in building construction are made in non-structural components and contents (NCCs). An efficient performance-based design paradigm should focus on these key investments and a new design paradigm is needed in order to do so. Structural framing systems should be selected on the basis of the required performance of NCCs. Protective systems appear to offer significant advantages over traditional framing systems in terms of both smaller median demands and smaller dispersion in demand for acceleration- and displacement-sensitive NCCs. The impact of structural framing system type on the NCCs demands is illustrated through response-history analysis of a 1960s-era hospital building located in Southern California.

Introduction

To date, tools for performance-based earthquake engineering have focused on performance *assessment* of structural framing. Only modest attention has been paid to *assessment* of nonstructural components and contents (NCCs) and to the development of tools for *design* of structural framing and NCCs.

HAZUS (NIBS 1997) provides important information on the financial importance of NCCs in a wide variety of building structures. Figure 1 displays the average percent investment in structural framing, nonstructural components and building contents for three types of building structures:

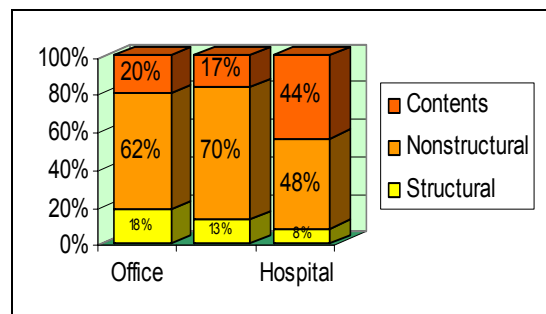


Figure 1. Investments in building construction (after E. Miranda)

office, hotel and hospital. In all cases, the investment in the structural framing is less than 20% of the total investment, and the percent investment in hospital construction is a mere 8% of the total. If a goal of performance-based earthquake engineering is to protect financial investments by minimizing total cost (including construction cost, annual maintenance cost and annualized earthquake-damage-related cost), close attention must be paid to those parts of a building in which the greatest investment is made.

Updating the design paradigm

Traditionally, structural engineers have paid scant attention to NCCs because their design and detailing had not formed part of the structural-engineering scope of work. In those cases where structural engineers have designed and detailed NCCs, the components have been analyzed and designed (albeit indirectly) for the output of the structural framing. We contend that such an approach is inappropriate and that the performance-based design process should focus first and foremost on the most significant investments in the building, namely, the nonstructural components and contents. A preliminary design of the framing system (framing layout, system type, material, etc), should be selected considering both structural and nonstructural components and then analyzed for *performance capability*. If the computed performance is unacceptable, the design of the structural and nonstructural components is revised and then re-analyzed for performance capability. Assuming that fragility functions are developed in sufficient number and detail to characterize the vulnerability of NCCs for common building occupancies, guidance will be required to assist the structural engineer to select the structural system type (incl. material, seismic framing system, strength, ductility) that will deliver the intended building performance.

Studies are under way at the University at Buffalo to aid in the identification of optimal structural framing systems, noting that the optimal solution will vary as a function of the performance objectives. Weak and flexible, strong and stiff, and *protected* framing systems are being studied. A hospital structure was chosen for the baseline building because of the high value (measured as a percentage of the total investment) of the nonstructural components and building contents in such buildings (see Figure 1). Sample *preliminary* results from these studies are presented in the following sections with emphasis on demands on acceleration- and drift-sensitive NCCs.

Assessment of an acute care facility

To illustrate the impact of structural-system choice on the response of acceleration- and drift-sensitive NCCs, a four-story mathematical model was developed based on the MCEER demonstration hospital. The lateral-load resisting system is composed of perimeter steel moment-resisting frames. The column bases and beam-column connections were modeled as rigid in all MRFs and as pin connections in all non-MRFs.

Protection of structural framing systems against gross damage during severe earthquake shaking motivated the initial development (in the 1970s and 80s) and implementation (1980s) of seismic protective systems: seismic isolation bearings and supplemental passive damping devices. Hospital buildings were early candidates for the use of protective systems because of the need to maintain hospital function after a major earthquake: essentially eliminating damage to the structural framing. Nowadays, seismically isolated buildings are designed to restrict substantial (or all) inelastic action to the isolators in maximum capable earthquake shaking. Buildings incorporating supplemental dampers are designed typically to restrict substantial inelastic action (damage) to the damping devices in design and maximum earthquake shaking and thus to eliminate damage to components of the gravity-load-resisting system.

Fifteen mathematical models representing different traditional and *protected* lateral-force-resisting systems were developed in the OpenSees software environment (<http://opensees.berkeley.edu/>) for analysis and evaluation. The 15 models are summarized in Table 1; the baseline model was M3. The *traditional* framing systems are M3 and M6: moment-resisting frames. Buckling restrained braces (BRBs), displacement-dependent dampers, were implemented in M7. Fluid viscous dampers (FVDs),

velocity-dependent dampers, were implemented in M8 and M9. Models M10 through M13 include linear viscoelastic seismic isolation bearings: one mathematical model used for low- and high-damping rubber bearings. Models M14 and M15 include bilinear seismic isolation bearings: the mathematical model used typically for lead-rubber and Friction Pendulum™ bearings. Much additional information will be available in Astrella (2004).

Table 1. Description of mathematical models

Model	Description	T_1^1 (secs)
M1	Baseline model of 1970s in-situ building; designed for the strength and drift limits of the 1970 Uniform Building Code; best-estimate model for <i>non-moment</i> -resisting connections.	0.70
M2	Similar to M1 except rigid connections used for <i>non-moment</i> -resisting connections.	0.68
M3	Similar to M1 except pinned connections used for <i>non-moment</i> -resisting connections.	0.71
M4	1960s variant of M1: design drift limits of M1 not imposed.	1.74
M5	Similar to M4 except rigid connections used for <i>non-moment</i> -resisting connections.	1.58
M6	Similar to M4 except pinned connections used for <i>non-moment</i> -resisting connections.	1.81
M7	M6 augmented with buckling restrained braces (BRBs) to provide approximately a 300% increase in lateral stiffness. BRBs installed in paired diagonal braces in the exterior bays on grid lines B and H.	0.97
M8	M6 equipped with fluid viscous dampers (FVDs) to provide approximately 25% of critical damping in the first mode. FVDs installed in paired diagonal braces in the exterior bays on grid lines B and H.	1.81
M9	M6 equipped with fluid viscous dampers (FVDs) to provide approximately 40% of critical damping in the first mode. FVDs installed in paired diagonal braces in the exterior bays on grid lines B and H.	1.81
M10	M3 equipped with viscoelastic seismic isolation bearings; isolated period is 2.5 seconds; approximately 10% of critical damping in the first mode.	2.60
M11	M3 equipped with viscoelastic seismic isolation bearings; isolated period is 2.5 seconds; approximately 20% of critical damping in the first mode.	2.60
M12	M3 equipped with viscoelastic seismic isolation bearings; isolated period is 3.5 seconds; approximately 10% of critical damping in the first mode.	3.57
M13	M3 equipped with viscoelastic seismic isolation bearings; isolated period is 3.5 seconds; approximately 20% of critical damping in the first mode.	3.57
M14	M3 equipped with coupled bilinear seismic isolation bearings: $Q_d = 0.06W$; second-slope isolation period is 2.5 seconds; isolator yield displacement is 25 mm.	2.60 ¹
M15	M3 equipped with coupled bilinear seismic isolation bearings: $Q_d = 0.06W$; second-slope isolation period is 3.5 seconds; isolator yield displacement is 25 mm.	3.57 ¹

1. First mode period in transverse (short) direction.

2. Period calculation based on second slope (post-yield) isolator stiffness.

Preliminary results are presented in this paper for 11 of the 15 models: M3, M6, M7, M8, M9, M10, M11, M12, M13, M14 and M15. Seismic demands on NCCs in the 11 buildings was assessed by nonlinear response-history analysis in the transverse (north-south) direction only. The earthquake histories used for the response-history analysis were those generated for a NEHRP Soil Type S_D (firm soil) site in Los Angeles as part of the SAC Steel Project (Somerville et al. 1997). Three bins of 20 histories were developed, each representing a different probability of exceedance (2% in 50 years, 10% in 50 years and 50% in 50 years).

Sample results from the response-history analysis are presented in Figures 2 through 5 for the 10/50 motions. Figure 2 presents a summary of the maximum drift responses for the 11 models noted above. Median, maximum, minimum, 16th percentile and 84th percentile results are presented assuming that the maximum responses are lognormally distributed. Drift data (relative displacement as a percentage of height) are presented for the 2nd story and the roof.² The horizontal axis in each subplot denotes the model number (e.g., M3 per Table 1). The yield drift in each story for M3 and M6, based on nonlinear static analysis, are shown in the subplots of Figure 2 to identify the degree of inelastic action (damage) in the non-isolated building frames. The trends of Figure 2 are well established, namely, that adding lateral stiffness, viscous damping and seismic isolation reduce interstory drift. As expected, the drifts in the isolated frames (M10 through M15) are substantially smaller than those in the *traditional* frames (M3 and M6) and the frames equipped with supplemental damping devices (M7, M8 and M9). The addition of the displacement and velocity-dependent dampers led to significant reductions in the median maximum displacement response of the weak and flexible frame (M6). Based on median response data, a) the traditional moment frames (M3 and M6) each sustained structural damage; b) damage in the building equipped with BRBs (M7) was limited primarily to the BRBs; and c) the viscous damped frames (M8 and M9) sustained negligible damage. For the non-isolated buildings (M3, M6, M7, M8 and M9), the coefficient of variation in the peak roof drift is greatest (0.33) for M6 (mean peak roof drift = 2.3 %) and smallest (0.28) for M9 (mean peak roof drift = 0.95 %). The addition of viscous dampers (M8 and M9) to the weak and flexible building (M6) reduced substantially the median maximum roof drift (by 44% for M8 and 56% for M9) and the coefficient of variation in the maximum roof drift (from 0.33 for M6 to 0.29 for M8 and 0.28 for M9).

Figure 3 summarizes the maximum *peak* floor acceleration responses at the 3rd and roof levels. Median, maximum, minimum, 16th percentile and 84th percentile results are presented assuming that the maximum responses are lognormally distributed. The trends seen in the four subplots of Figure 3 are also well established, namely, that adding lateral stiffness increases peak floor accelerations, and adding viscous damping or seismic isolation bearings reduce peak floor accelerations. For the non-isolated models, the coefficient of variation in the peak 2nd floor acceleration is greatest (0.37) for M7 (mean peak acceleration = 0.98 g) and smallest (0.30) for M8 and M9 (mean peak acceleration = 0.49 g). The addition of viscous dampers to the weak and flexible building (M6) reduced the median peak 2nd floor acceleration (by 29% for M8 and M9) and the coefficient of variation in the peak 2nd floor acceleration (from 0.32 for M6 to 0.30 for M9).

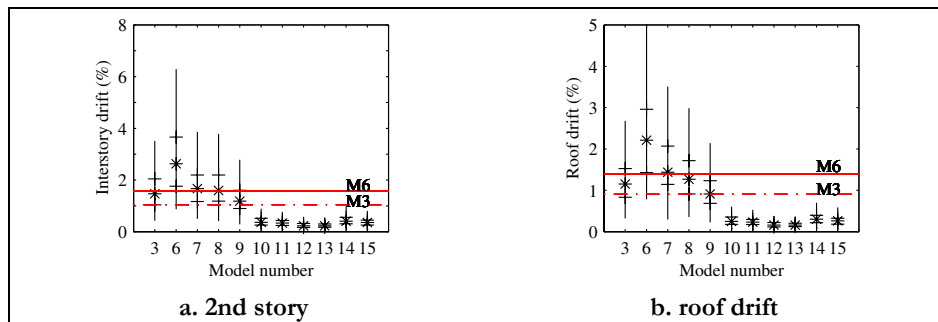


Figure 2. Maximum drift responses for 10/50 earthquake histories

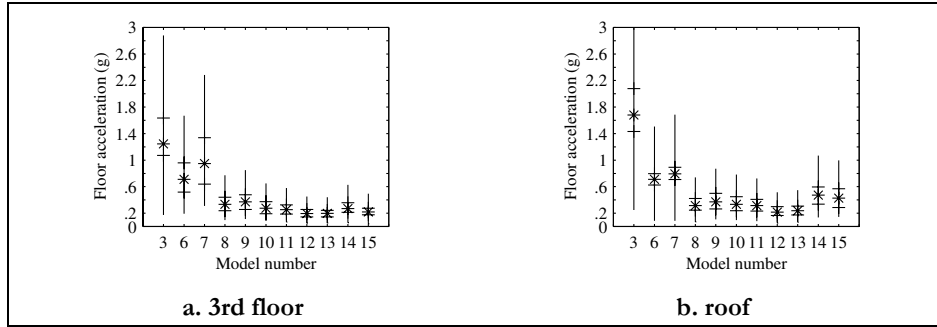


Figure 3. Maximum acceleration responses for 10/50 earthquake histories

In FEMA 273/356, the intersection of the median capacity (pushover) and median demand (hazard) curves is termed a *performance point*. Such a point, although instructive, provides no information on the impact of uncertainty and randomness on the capacity and demand calculations and by extension on the building performance. Reinhorn extended the concept of the performance point to a *performance space*, to account for both uncertainty and randomness in a rigorous manner. Figure 4 presents performance points using median maximum drift (ID*) and median peak floor acceleration (A*) as the performance metrics (ID* and A* are defined in the figure) and performance spaces as boxes defined by the 16th and 84th percentile maximum drift and zero-period floor acceleration responses. Alternate groupings of ID* and A* (e.g., A2/ID1) might be more appropriate for nonstructural components such as suspended ceiling systems. In terms of demands on NCCs, performance points adjacent to the origin and performance spaces that are small in size (indicating small variability in displacement and acceleration responses) are preferable to points remote from the origin and spaces that are large in size. On the basis of the chosen metrics, the performance of the buildings equipped with supplemental fluid viscous dampers or seismic isolation bearings is superior to that of the *traditional* moment-frame buildings or the building equipped with BRBs.

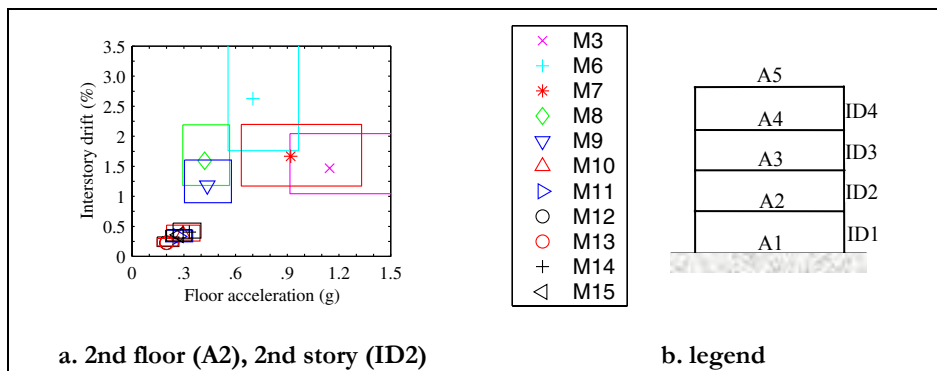


Figure 4. Performance points and spaces for 10/50 earthquake histories

On the basis of the data presented in Figure 4, the performance of the isolated buildings is superior to that of the other buildings in terms of smaller displacement and acceleration demands on NCCs. Of the remaining *traditional* and *protected* lateral-force-resisting systems, the buildings equipped with fluid viscous dampers (M8 and M9) outperform the remaining 3 buildings (M3, M6 and M7).

For many acceleration-sensitive NCCs, peak floor acceleration alone is an inefficient predictor of damage. Better estimates of the vulnerability of acceleration-sensitive NCCs can be developed through the use of floor (in-structure) acceleration spectra. Median 5% damped median floor acceleration spectra for the 2nd floor (A2) and 4th floor (A4) of the 11 models for the 10/50 earthquake histories are presented in Figures 5a and 5b. The stiff and strong moment frame building (M3) and the building equipped with BRBs (M7) produce the highest spectral acceleration demands across a frequency range from 1 Hz to 100 Hz. The smallest acceleration demands are associated with the viscous damped frames (M8 and M9) and the isolated frames (M10 through M15). Importantly, the spectral peaks of the moment-frame structures (M3 and M6) are suppressed through the addition of viscous damping: an observation reported first by Pavlou and Constantinou (2004).

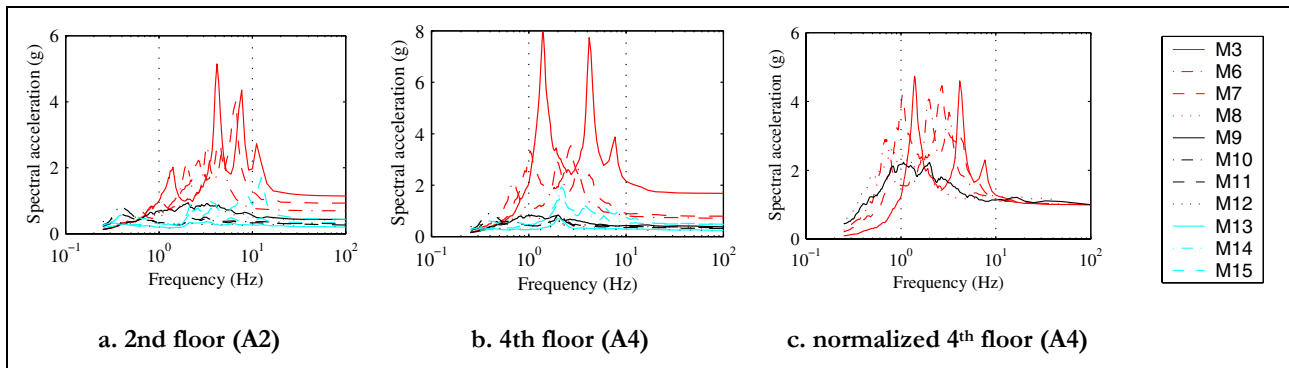


Figure 5. Floor acceleration spectra for 10/50 earthquake histories

Normalized 5-percent damped 4th floor acceleration spectra are presented in Figure 5c for the 5 non-isolated buildings (M3, M6, M7, M8 and M9). The figure shows the amplification of the peak floor acceleration as a function of structural framing system. For the same peak floor acceleration, the performance of the viscous damped buildings, M8 and M9, is clearly superior to the *traditional* moment-frame buildings and the building equipped with BRBs

Closing remarks

The next generation tools for PBEE will recognize the substantial financial investment in nonstructural components and contents (Figure 1). Significant research work is underway at the three NSF-funded earthquake research centers to develop performance assessment tools for NCCs (Whittaker and Soong, 2003).

To reduce losses in buildings in future earthquakes, the current performance-based design paradigm must be updated to shift the focus to NCCs. The geometry, type and materials that comprise a structural framing system should be selected by the structural engineer so as to protect the primary investment: the NCCs. Guidance on the appropriate choice of structural framing system to meet NCCs-driven performance objectives is needed. The *preliminary* studies reported in this paper illustrate the benefits of seismic protective systems in reducing the median seismic demand and/or the variability in seismic demand on acceleration- and displacement-sensitive NCCs. On the basis of the limited studies reported herein, framing systems incorporating seismic isolation bearings and/or supplemental fluid viscous dampers appear to offer superior performance to traditional framing systems.

Acknowledgements

Financial support for the studies described in this paper was provided by the Multidisciplinary Center for Earthquake Engineering Research (MCEER) through grants from the Earthquake Engineering Centers Program of the National Science Foundation (Award Number EEC-9701471) and the State of New York. These studies form part of the MCEER research program on the seismic retrofit of acute care facilities. I acknowledge and appreciate both the NSF/MCEER support and the advice and assistance of Ms. Pavlou and Professor Michael Constantinou at the University at Buffalo.

The opinions, findings, conclusions expressed in this paper are those of the authors and do not necessarily reflect the views of the sponsors or the Research Foundation of the State University of New York.

References

- Astrella, M and A. S. Whittaker. "Changing the paradigm for performance-based design." *Conference on Performance-Based Seismic Design*. Bled, Slovenia. July 2004.
- Astrella, M. (2004). "Changing the paradigm for performance-based earthquake design." *M.Sc. Thesis*, Department of Civil, Structural and Environmental Engineering, State University of New York, Buffalo, NY, August.
- FEMA. (1997). "NEHRP Guidelines for the seismic rehabilitation of buildings." *Report FEMA 273*, Washington, D.C.: Federal Emergency Management Agency.
- NIBS. (1997). "Earthquake loss estimation technology – HAZUS; user's manual." Washington, D.C.: National Institute of Building Sciences.
- Pavlou, E. and M. C. Constantinou. (2004). "Response of nonstructural components in structures with damping systems." Paper submitted for review, *Journal of Structural Engineering*, Reston, VA: American Society of Civil Engineers.
- Somerville, P., N. Smith, S. Punyamurthula and J. Sun. (1997). "Development of ground motion time histories for Phase 2 of the FEMA/SAC Steel Project." *Technical Report SAC/BD-97/04*, Sacramento, CA: SAC Joint Venture.
- Whittaker, A. S. and T. T. Soong. (2003). "An overview of nonstructural components research at three U.S. Earthquake Engineering Research Centers." *Proc., ATC Seminar on Seismic Design, Performance, and Retrofit of Nonstructural Components in Critical Facilities*, Report ATC-29-2, Redwood City, CA: Applied Technology Council.

Notes

¹ This paper has been adapted from Astrella and Whittaker (2004).

² The earthquake shaking is imposed at the 1st (ground) floor level (A1) in the non-isolated models M3, M6, M7, M8 and M9, and at the basement level (A0) for the isolated models M10, M11, M12, M13, M14 and M15.

Global Fragility Evaluation of Health Care Facilities with Structural and Nonstructural Components

Gian Paolo Cimellaro

Research Assistant, Department of Civil, Structural & Environmental Engineering, University at Buffalo

Research supervisors: Andrei Reinhorn, Professor and Director of SEESL

Michel Bruneau, Professor and Director of MCEER

Summary

A multi-dimensional definition of fragility is developed considering multiple variables such as floor acceleration and interstory drifts. The limit states which have uncertainties are defined as random variables in the calculation of fragility. A random description of the limit state has been adopted to calculate fragility and different cases have been considered. A case study of a Hospital located in California has been considered. The development of fragility for different cases show how important is a correct evaluation of the limit state for comparison of different techniques. The paper investigates how conservative or unconservative are the fragility curves when uncertainties in limit states are considered. Among the different parameters that influence fragility damping has a considerable effect in reducing displacements; Influence of such parameters is investigated.

Introduction

The knowledge of structural damage is crucial for the evaluation of the economic losses in a region that has been or might be affected by earthquakes. It should be prepared with an acceptable degree of certainty to mitigate the potential losses that depend on the seismic performances of all types of building structures typically constructed in that region. To describe the structural damage distribution over a given region two techniques can be used: the fragility curves and the damage probability matrix (DPM). They both describe the conditional probabilities of sustaining different degrees of damage at given levels of ground motion. Engineers usually make their recommendations using fragility curves or DPM that are being build using deterministic performance limit state fixed by public policies, provisions etc.. The reason of using crisp quantities derives from the large uncertainties in the earthquake loads that are larger than the uncertainties in the limit states. The goal of this paper is to show that the limit states should be properly modeled as random variables. If uncertainties in limit states are not considered the results may be non-conservative and wrong decision could be made.

Definition of Multidimensional fragility

Fragility curves are functions that represent the conditional probability that the response of a structure for various seismic excitations exceeds performance limit states. Theoretically the definition of fragility using multidimensional parameters, like for instance displacements and accelerations of a story building, can be written in mathematical form as (Reinhorn et al., 2001):

$$Fragility = P\{\Delta \geq D_{lim} \cup Z \geq A_{lim} / I\} \quad (1)$$

Where Δ is the random variable representing the displacement response, Z is the random variable representing the acceleration response, D_{lim} is the determined displacement threshold and A_{lim} is the determined acceleration threshold. The response is represented by a “bell surface” in the pseudo acceleration (PSA) - interstory drifts (SD floor) plane and the limit space in this case can be expressed (Bruneau and Reinhorn, 2004) in term of accelerations, displacements, or velocity [Fig.1]. One time the probability of exceeding the limit states is calculated (volume underneath the surface) it can be represented using fragility curves. The peak ground acceleration (PGA) is usually used to represent the intensity of the seismic ground motion in the x axis of the fragility curves even though other quantities like return period, peak ground velocity, spectral intensity can be used. In this paper both PGA and return period are used to represent the seismic intensity ground motion.

Procedure to calculate fragility

The limit state represents the level of response at which the loss of function or undesirable damage occurs in the structure, but it requires damage descriptors describing the physical conditions of the building during and after the earthquake. Definition of limit states plays an important role in the construction of fragility curves because its value directly affects on the fragility curve parameters. Damage states of structural and non structural components depend on their mechanical properties such as strength and deformability which are characterized to be uncertain; therefore a crisp description of limit states can not be performed.

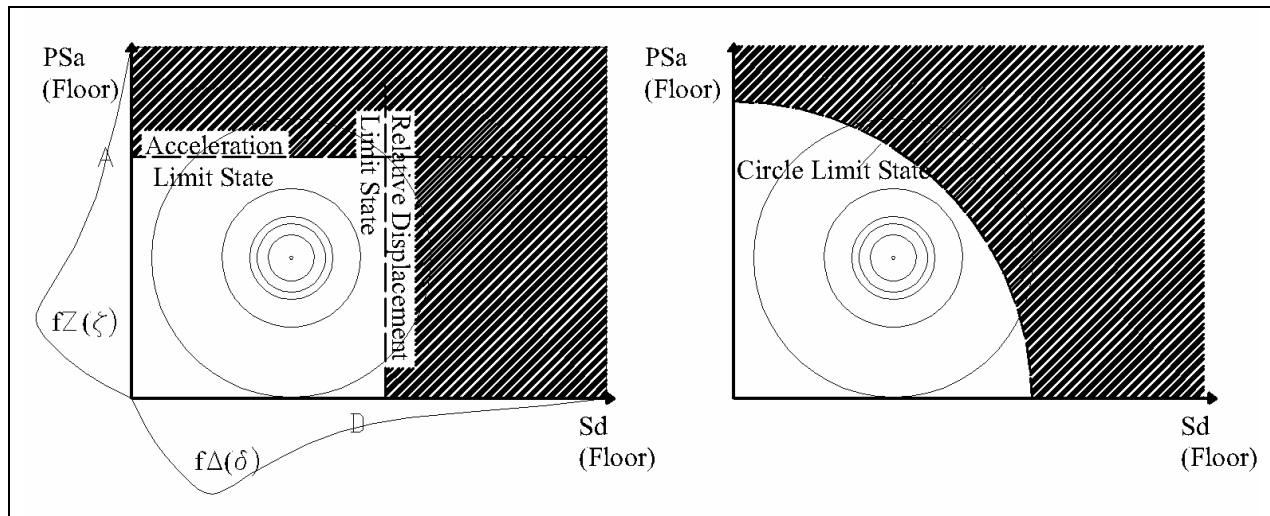


Figure 1. Probability of two random variables of exceeding two deterministic limit states
(a) uncorrelated or (b) related

The limit states should be properly modeled as random variables. In this study the limit states are considered as random variables and defined in term of interstory drift and accelerations. Five different cases have been considered to calculate the probability of exceeding a certain limit state assuming that the considered limit states are randomly distributed as the response of the structure and considering two different types of responses: displacements and accelerations. Both the response of the structure in term of displacements and accelerations are considered lognormal

distributed. This assumption is reasonable, because we are considering the maximum of the response that is always positive. For each case the linear case has been separated from the non linear case and various assumptions have been made regarding the random variables considered. In figure 1 limit states are represented by straight lines, and by a circle curve, but it is also possible to define different curves limit state like ellipses and so on.

Case study: West coast Hospital W70

A non linear MDOF model and SDOF model equivalent to the Hospital W70 located in the West coast of California has been used. The model is used by multiple research teams at MCEER for evaluation of various aspects of hospital seismic issues. The non linear MDOF model has been developed in the computer platform IDARC2D 6.0 (Reinhorn et al., 2004) and non linear springs have been used in all hinge connections of the non moment resisting frames. The SDOF system is modeled as elastic perfectly plastic with a yield shear strength equal to $V_y = 0.62 \cdot W$ that have been calculated by non linear static pushover analysis of the hospital. Different deterministic limit states related to the interstory drift have been considered according to FEMA 356 (0.7% - 2.5% - 5% of interstory drift) and SEAOC (0.2% - 0.5% - 1.5% - 2.5% of interstory drift).

Characterization of ground motion for SDOF and MDOF system

In this study three different families of accelerograms have been used.

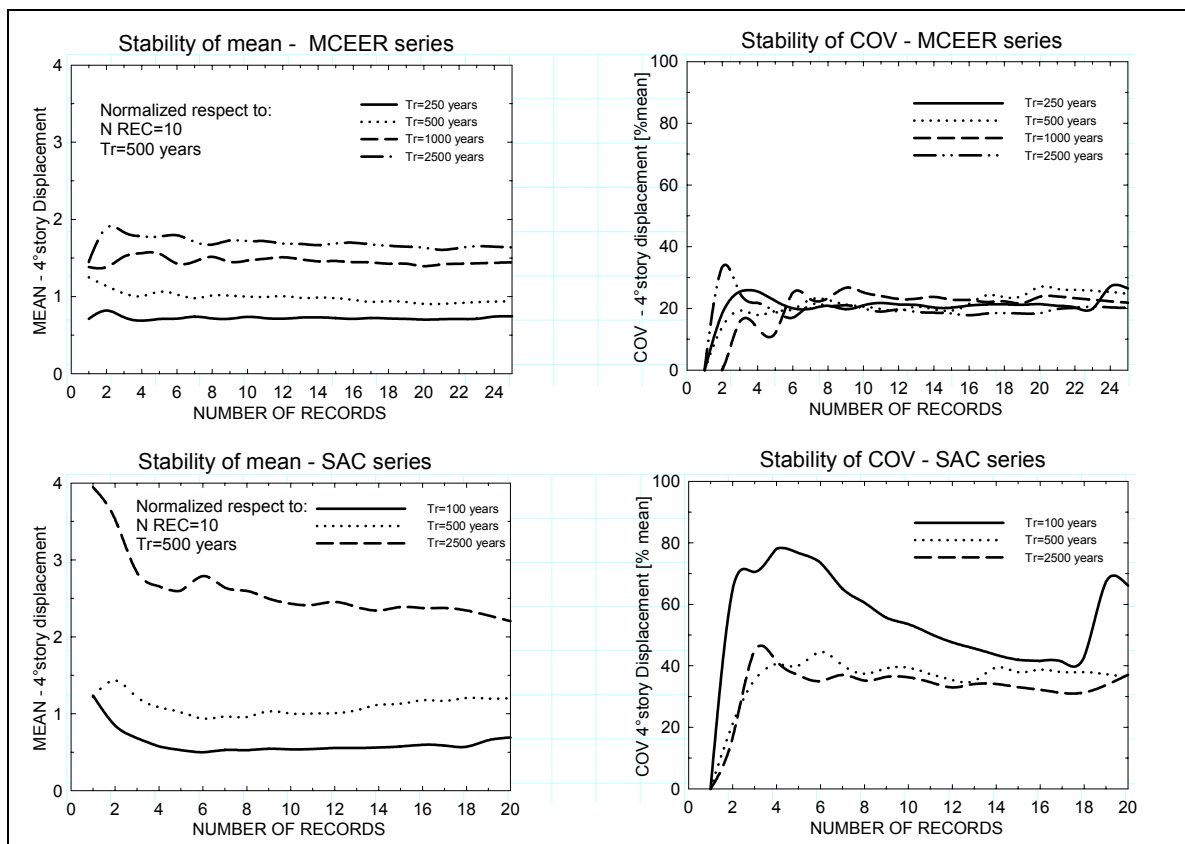


Figure 2. Stability of Mean and of CoV for MCEER and SAC series.

For the SDOF model the accelerograms used have been derived by the frequency content of the modified Kanai-Tajimi spectral density function (Clough and Penzien, 1993). The selected parameters for the model are the following: $\omega_g = 15.0 \text{ rad/s}$; $\zeta_g = 0.6$; $\omega_k = 1.5 \text{ rad/s}$ and $\zeta_k = 0.6$. These parameters have been used to reflect firm-soil conditions. of some literature (Heredia-Zavoni and Vanmarcke, 1994). For the MDOF system two series of accelerograms related to different return period have been used: the MCEER series and the SAC series [Fig. 2].

Influence of structural parameters on fragility

Fragility curves can be used for decisions to strength buildings that are at high risk of being damaged and for this purpose it is necessary to know the effects of different structural parameters such as strength, stiffness, and damping on fragility. The following figure describes the influence of stiffness on fragility and it shows how the increments of stiffness reduce fragility. This is due to reduction in displacements obtained when we increase the stiffness of the structure.

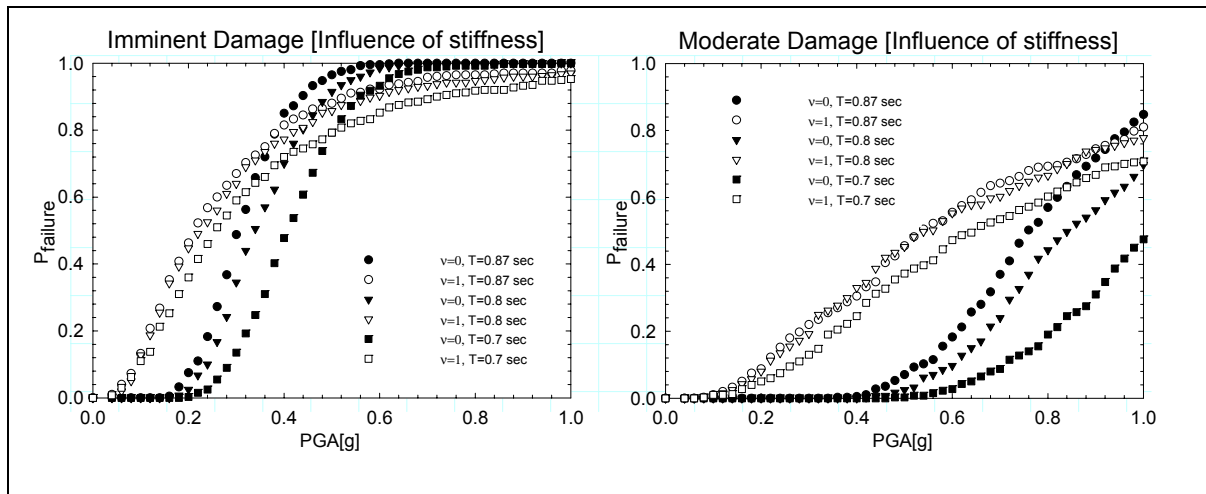


Figure 3. Comparison between different values of dispersion of limit state and different values of stiffness.

If we plot in the same figure the effect of stiffening the structure together with the effect of uncertainties of limit state, we can clearly see that the randomness of limit states generate bigger increases in the probability of exceeding the limit state if compared with the reduction of the probability of exceed the l.s. due to the stiffening of the structure. This show important is a correct evaluation of the l.s. for a comparison among different retrofit techniques. One of the advanced technologies studied by the MCEER for retrofitting structures consists in adding damping for displacement reduction; therefore it is desirable to know the effect of added damping to fragility (Barron, 2000; Reinhorn et al., 2001). In the following figure the fragility curves are plotted for the Imminent Damage State and for the Moderate Damage State for three different values of damping ratios [5%, 15% and 25%]. It can be seen that a considerable reduction of fragility is obtained when damping is added. However this reduction is not proportional. From the second figure we can see that the reduction is more significant for low values of damping ratio [$\zeta = 15\%$] than for high values of damping ratio [$\zeta = 25\%$]. Also in this case from the first figure one can see do not consider dispersion of limit state it can be unconservative for values of PGA below a range that varies between 0.4g and 0.6g, depending on the kind of damping considered, and conservative for

upper values of PGA, while for the second limit state do not consider the randomness of the limit state is always not conservative for every value of damping considered and PGA. Other parameters like strength have been considered, but increments of strength do not produce significant improvements on fragility and this is due to the fact that changes in strength do not affect displacement in the inelastic range.

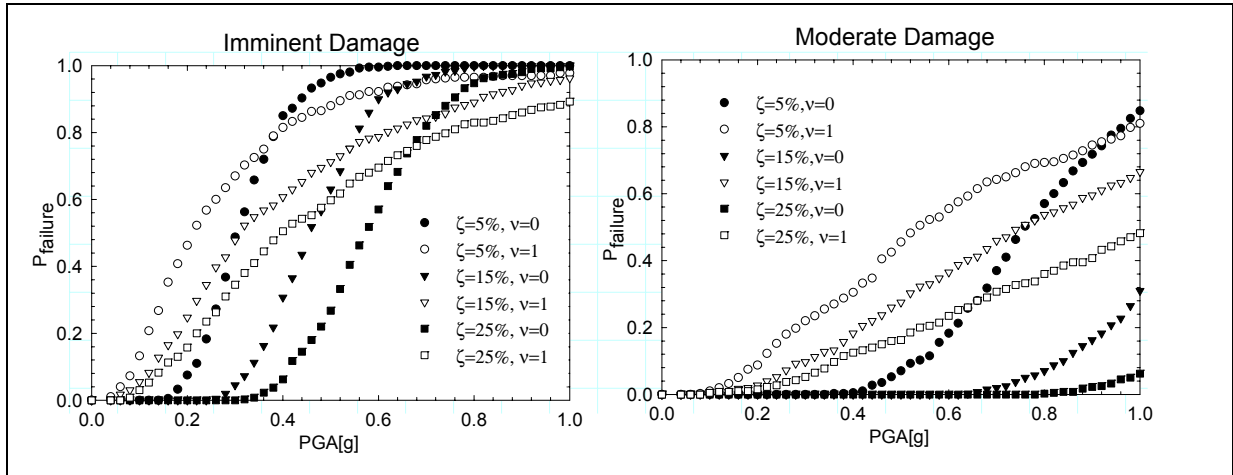


Figure 4. Comparison between different values of dispersion of limit state and different values of Damping.

Influence of acceleration threshold on fragility

In figure 5 is reported the fragility curve related to the 4^o story for the limit state of immediate occupancy according to FEMA 356, calculated using the MCEER series as input.

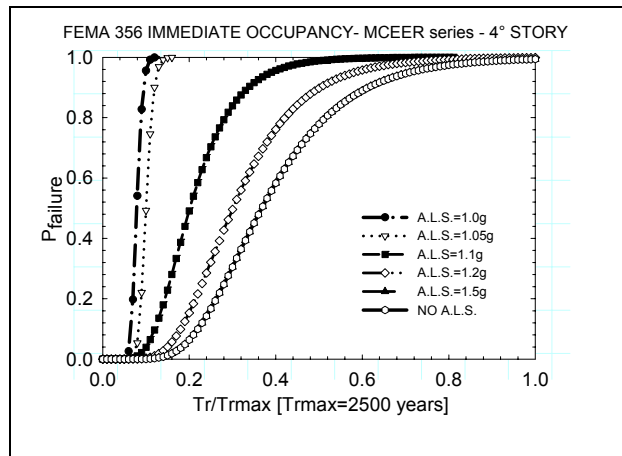


Figure 5. Influence of acceleration threshold on fragility calculated using two random variables.

In the x axis instead of PGA is used the return period, normalized respect to the maximum return period. Different values of acceleration limit state have been considered from 1 to 1.5g. It can be clearly see that the probability of exceed the limit increases quickly with small increasing value of acceleration. So fragility curves show to be really sensitive to acceleration limit state.

Concluding Remarks

A random description of the limit state has been adopted in this paper to calculate fragility and different cases have been considered. The development of fragility for different cases show how important is a correct evaluation of the limit state for comparison of different techniques. Besides to not consider randomness of the limit state can develop not conservative results. Among the different parameters that influence fragility damping has a considerable effect in reducing displacements; therefore it clearly produces changes in fragility.

Acknowledgements

The research described in this paper is supported by a grant from the Multidisciplinary Center for Earthquake Engineering Research (Buffalo, NY) supported by National Science Foundation and by the State of New York. This study is part of the Master Thesis developed under supervision of Prof. A. M. Reinhorn. His guidance and encouragement are gratefully acknowledged.

References

- Barron R. Corvera, "Spectral Evaluation of Seismic Fragility in Structures", PhD Thesis (A.M. Reinhorn, supervisor), Department of Civil, Structural & Environmental Engineering, University at Buffalo, 2000.
- Bruneau, M., Chang, S., Eguchi, R. Lee, G., O'Rourke, T., Reinhorn, A., Shinozuka, M., Tierney, K., Wallace, W., von Winterfelt, D., "A framework to Quantitatively Assess and Enhance the Seismic Resilience of Communities", EERI Spectra Journal, Vol. 19, No.4, pp. 733-752, 2003.
- Bruneau, M., Reinhorn, A. "Seismic resilience of communities - conceptualization and operationalization", Proceedings of International workshop on Performance based seismic-design, Bled - Slovenia, June 28-July 1, 2004 (in print).
- Cimellaro G.P., "Multidimensional Fragility of Structures – Formulation and Evaluation", M.S. Thesis (A.M. Reinhorn, supervisor), Department of Civil, Structural & Environmental Engineering, Buffalo, NY December 2004.
- Clough, R.W., Penzien, J., "Dynamic of structures", 2nd edition. NY, McGrawHill, 1993.
- Heredia-Zavoni E, Vanmarcke EH. Seismic random-vibration analysis of multisupport-structural systems. J Eng Mech ASCE; Vol. 120, No.5:pp.1107–28, 1994.
- Reinhorn, A.M., Barron-Corverra, R and Ayala, A.G., "Spectral Evaluation of Seismic Fragility of Structures", Proceedings ICOSSAR 2001, Newport Beach CA, June 2001.
- Reinhorn A.M., et al. "IDARC2D Version 6.0 - A computer Program for the Inelastic Damage Analysis of Reinforced Concrete Buildings", latest release retrieved from <http://civil.eng.buffalo.edu/idarc2d50>, July 2004.
- Shinozuka, M., Feng, M. Q, Lee, J., and Naganuma, T., "Statistical Analysis of Fragility Curves," J Eng Mech ASCE; Vol.126, No.12, pp 1224-1231, 2000.

An Experimental Verification of the Eigensystem Realization Algorithm for Vibration Parameter Identification

Marlon D. Hill

Ph.D. Student, Civil & Environmental Engineering Department, Florida A&M University

Research Supervisor: Makola M. Abdullah, Professor

Summary

In recent years structural health monitoring (SHM) has become an important problem. One of the challenges in this new field is an accurate representation of structural properties by which the health of a structure can be judged. Modal analysis techniques are a common method used to determine these structural properties. One of the popular modal analysis techniques for civil structures is the eigensystem realization algorithm (ERA). This study provides an experimental verification of the ERA method. The verification was carried out using the shake table from the University Consortium on Instructional Shake Tables (UCIST) project. The experimental verification was based on several experimental test structures. The identified vibration parameters from the ERA were compared with the values based on classical structural dynamic theory and with frequency response values of the experimental models. The findings of this study will be used to gauge the accuracy of the ERA when used with the UCIST instructional shake table for implementation into a structural health monitoring program that, in the future, can be used to determine vibration parameters using models appropriate for classroom instruction.

Background

Structural health monitoring can be defined as the analysis of the dynamic behavior of civil structures to observe and examine the integrity of those structures. This area of study has led to research involving parameter and damage identification. There are different levels of parameter and damage identification. Figure 1 illustrates the three stages of parameter identification of a civil structure. The research presented involves the first stage of parameter identification. A system of classification defining four levels can be applied to damage identification (Rytter 1993). They are determination that damage is present in the structure, determination of the geometric location of the damage, quantification of the severity of the damage, and prediction of the remaining service life of the structure.

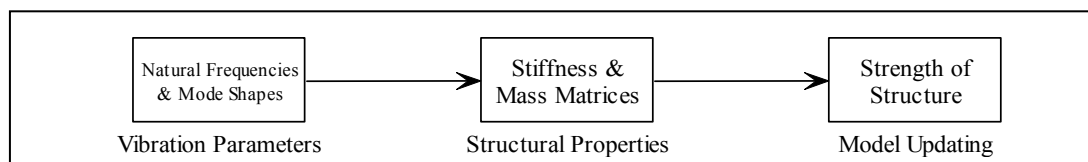


Figure 1. Stages of parameter identification

All civil structures require some form of routine maintenance. The purpose of this maintenance is to preserve structural integrity and prevent damage or failure. Visual inspection is still the predominant tool used to assess structural conditions. The main disadvantage of structural health monitoring (SHM) is its inability to classify invisible damage. Structural health monitoring has the potential to identify certain kinds of invisible damage.

The instructional shake table used to carry out the experimental procedure was provided by the University Consortium on Instructional Shake Tables (UCIST) (Dyke 1999). The UCIST Consortium consists of 23 member institutions associated with the earthquake research engineering centers; the Pacific Earthquake Engineering Research Center (PEER), the Mid America Earthquake Center (MAE), and the Multidisciplinary Center for Earthquake Engineering Research (MCEER). The instructional shake tables were provided by the consortium (NSF Grant No. DUE-9950340) for the purpose of exposing emerging technologies and modern methods to reinforce theoretical concepts of structural dynamics through experimentation. Some objectives of the UCIST project are:

- To develop an understanding and an intuition regarding the dynamic nature of civil structures in undergraduate students.
- To provide non-engineering students with exposure to the potential consequences of earthquakes and to the dynamic behavior of civil structures.
- To provide exposure to emerging technologies and modern methods in seismic resistant design.

This article presents an experimental verification analysis of a modal analysis technique to determine the modal parameters of experimental test models for SHM purposes. Thus, eventually allowing the development of a comprehensive program based on the modal analysis theory that can be used to identify the dynamic properties structural models for use on the UCIST shake table. This research will be used to develop teaching modules for civil engineering students using the ERA method.

Literature Review

The traditional maintenance philosophy of civil structures utilizes schedule-based maintenance inspections. The in-service conditions of a structure are generally unknown; therefore, service manuals dictate the maintenance schedule. By incorporating SHM into the maintenance philosophy allows the maintenance and inspection procedures to be updated. This is known as performance-based maintenance. Incorporating SHM allows the service conditions to dictate the maintenance schedule.

Modal analysis is an important technique for SHM. Its fundamental application is to use modal testing methods to identify the vibration parameters of civil structures. There are numerous modal analysis testing methods. Here are a few of the available methods that can be used to identify the vibration parameters of a structure. The first is the Complex Exponential method (Maia, 1997). Most time domain parameter identification methods were derived from this method. It analyzes the free decay of the vibration responses in the time domain, as well as the other two methods. It is a simple method that is sensitive to noise. Next is the Ibrahim Time Domain method (Ibrahim, 1977). It uses the free vibration response of a structure to identify its vibration parameters. It is a vibration parameter identification method that is unable to provide system realizations. The method

used for this research was the Eigensystem Realization Algorithm (ERA) (Juang, 1984). It is one of the most commonly used parameter identification methods. Not only is the ERA a vibration parameter identification method, it is also a system realization method.

Jer-Nan Juang and Richard Pappa developed the ERA in 1985. It is a modal parameter identification and model reduction algorithm of dynamic systems from test data. In addition, a minimum order realization technique, the ERA is an extension of the Ho-Kalman algorithm that incorporates singular value decomposition to counteract inherent noise.

Methodology

Sixteen experimental test structures were analyzed during these experiments. Aluminum and steel were the materials used to construct the test structures. Figures 2 and 3 shown below are of the test materials used to perform the experiments and the experimental test set-up, respectively. There were four 1-DOF experimental test structures used in this experiment. The test structures consisted of two aluminum and two steel models. The structures will be referred to using the following notation: *AL15*, *AL20*, *ST15*, & *ST20*. There were six 2-DOF test structures used in this experiment. Three aluminum, two steel, and one composite model with the following notations: *AL15AL15*, *AL20AL20*, & *AL20AL15* and *ST15ST15*, *ST20AL20*, & *ST20ST15*. There were also six 3-DOF experimental test structures analyzed. The *AL15AL15AL15*, *AL20AL20AL20*, & *AL20AL20AL15* and *ST15ST15ST15*, *ST20AL20AL20*, & *ST20ST15ST15* were the designations used for the three aluminum, two steel, and one composite test structures respectively.



Figure 2. Experimental test materials.



Figure 3. Experimental set-up.

This was the experimental procedure undertaken to identify the natural frequencies and mode shapes. The impulse force was exerted onto the test structure at random locations. The impulse response measurements were recorded and saved. There was a lag in the data. The lag was the time when the sensors started recording and the impulse was exerted. Figure 4 illustrates a typical impulse response from a test structure that includes the lag. To create the impulse response the lag was removed from the data sets. The experimental vibration parameters were obtained using the ERA method.

The theoretical and frequency response methods were used as verification tools to compare with the identified natural frequencies and mode shapes. For the theoretical method, the classical approach to structural dynamics was used to obtain the

theoretical vibration parameters. The theoretical values were based on the material properties of the test structures. The frequency response natural frequencies were obtained by determining the peaks off the frequency response plots (FRP). The FRP for a 2-DOF test structure is shown below in Figure 5. The peaks of the FRP's correspond to the natural frequencies of the test structure.

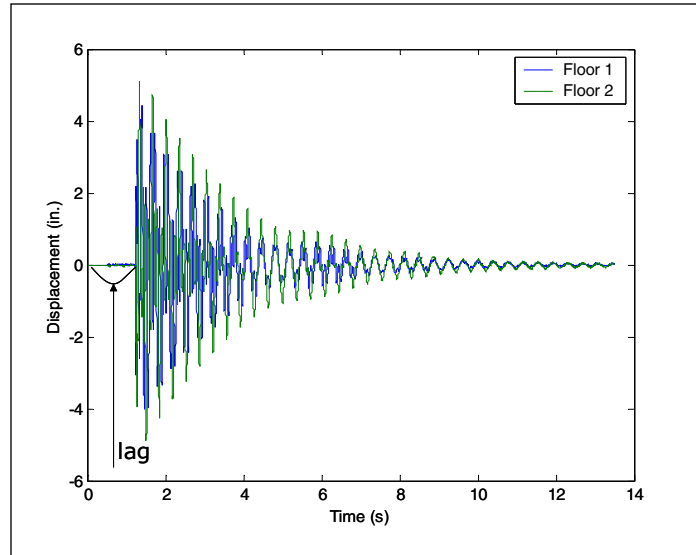


Figure 4. Impulse response with lag.

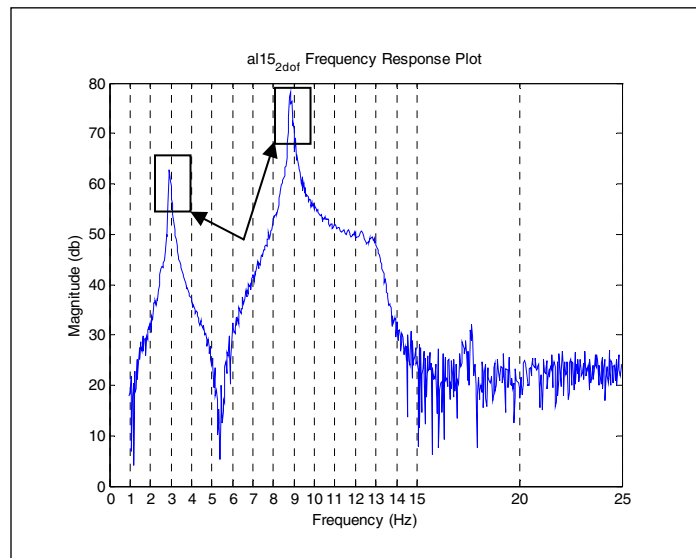


Figure 5. Frequency response plot of test structure.

Results

Tables 1 and 2, and Tables 3 and 4, contain the comparison data from the experiment. The ERA values were compared to the theoretical and frequency response values as a verification of the ERA

method using the instructional shake table. Figures 6 and 7 contain the theoretical and ERA identified mode shape plots of the first and second mode respectively of a 2-DOF experimental test structure.

Table 1. Summary of results for ERA & theoretical values.

1DOF Natural Frequency Comparison (rad/s)			
Model	ERA	Theoretical	% Difference
<i>AL</i> ₁₅	33.27	37.08	10.28
<i>AL</i> ₂₀	21.49	23.28	7.67
<i>ST</i> ₁₅	35.02	32.77	-6.86
<i>ST</i> ₂₀	19.23	19.95	3.63

Table 2. Summary of results for ERA & frequency response values.

1DOF Natural Frequency Comparison (rad/s)			
Model	ERA	Frequency Response	% Difference
<i>AL</i> ₁₅	33.27	33.55	0.84
<i>AL</i> ₂₀	21.49	21.87	1.71
<i>ST</i> ₁₅	35.02	36.95	5.22
<i>ST</i> ₂₀	19.23	20.67	6.99

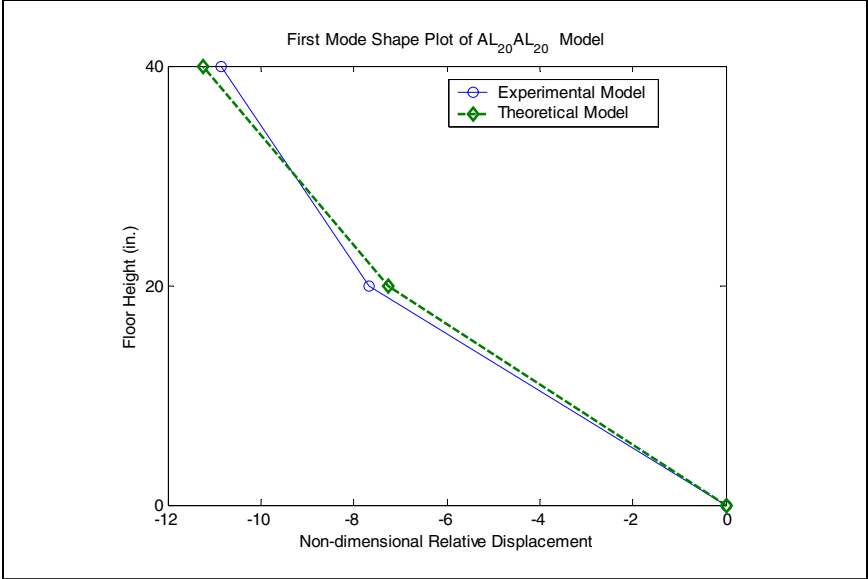


Figure 6. Mode shapes for 2-DOF theoretical and experimental models.

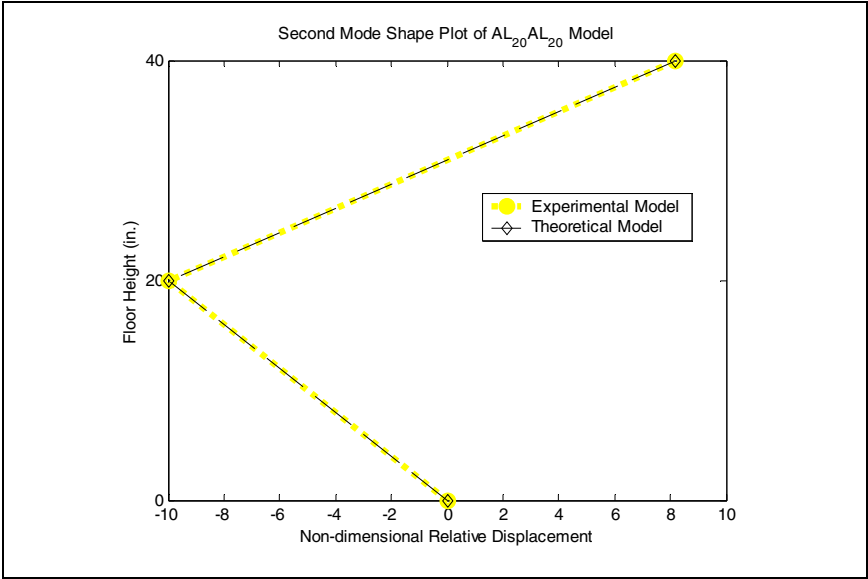


Figure 7. Mode shapes for 2-DOF theoretical and experimental models.

Table 3. Summary of results for ERA & theoretical values.

3DOF Natural Frequency Comparison (rad/s)			
Model	ERA	Theoretical	% Difference
<i>AL₁₅AL₁₅AL₁₅</i>	12.97	15.12	14.23
	40.58	41.73	2.76
	62.95	58.93	1.82
<i>AL₂₀AL₂₀AL₂₀</i>	8.05	9.39	14.22
	25.15	25.86	2.72
	38.77	36.35	-6.65
<i>AL₂₀AL₂₀AL₁₅</i>	8.39	9.85	14.86
	28.60	29.24	2.21
	52.69	50.08	-5.21
<i>ST₁₅ST₁₅ST₁₅</i>	12.92	12.95	0.30
	42.11	35.58	-18.37
	63.79	49.65	-28.50
<i>ST₂₀AL₂₀AL₂₀</i>	8.22	9.21	12.45
	24.29	23.93	6.04
	37.96	35.29	-4.42
<i>ST₂₀ST₁₅ST₁₅</i>	8.27	9.85	16.03
	33.94	32.25	-5.27
	62.00	50.28	-23.31

Table 4. Summary of results for ERA & frequency response values.

3DOF Natural Frequency Comparison (rad/s)			
Model	ERA	Frequency Response	% Difference
<i>AL₁₅AL₁₅AL₁₅</i>	12.97	12.88	-0.66
	40.58	39.84	-1.86
	62.95	61.83	-1.84
<i>AL₂₀AL₂₀AL₂₀</i>	8.05	8.23	2.18
	25.15	25.64	1.88
	38.77	38.77	0.00
<i>AL₂₀AL₂₀AL₁₅</i>	8.39	8.48	1.09
	28.60	29.15	1.90
	52.69	53.09	0.76
<i>ST₁₅ST₁₅ST₁₅</i>	12.92	12.75	-1.26
	42.11	41.09	-2.48
	63.79	63.02	-1.23
<i>ST₂₀AL₂₀AL₂₀</i>	8.22	7.85	-4.63
	24.29	23.37	-3.93
	37.96	37.39	-1.54
<i>ST₂₀ST₁₅ST₁₅</i>	8.27	8.67	4.62
	33.94	35.19	3.53
	62.00	67.48	8.12

Conclusions

The ERA was effective in identifying the vibration parameters of the experimental test structures. The ERA and theoretical natural frequencies, ERA and frequency response natural frequencies, and ERA and theoretical mode shapes were in good agreement.

This experimental procedure can be used as an educational experiment. There are several benefits of using this research as an educational experiment. It can be easily reproduced and it can also provide hands-on experiments to develop an understanding of the concepts of SHM. It can also be used as a lab experiment and shared with other UCIST institutions. These are a few benefits of using this research as an educational experiment.

Future Work

Consideration of the effects of magnitude and location of the impulse force on the experimental test structures should be considered in future studies. Further work can also be done to compare the ERA with other modal analysis techniques to further gauge their accuracy against theoretical approximations of vibration parameters. In practice, it is nearly impossible to obtain an impulse response of a structure outright. Therefore, to use the ERA as an analysis tool for real structures the impulse response will need to be generated. Future studies can couple the ERA with the Natural

Excitation Technique (NExT), which uses ambient vibrations of a system to generate an impulse response of that system.

Acknowledgements

This research was carried out under the supervision of Makola M. Abdullah, Ph.D. and supported by the GAANN Fellowship.

References

- Chopra, A.K. (2001): *Dynamics of Structures*. Prentice Hall, Inc.
- Dyke, S. (1999): University Consortium on Instructional Shake Tables. <http://www.ucist.cive.wustl.edu>.
- Ibrahim, S.R., and Mikulcik, E.C. (1977): A Method for the Direct Identification of Vibration Parameters from the Free Response. *The Shock and Vibration Bulletin*, 47(4), 183-198.
- Juang, J.N., and Pappa, R.S. (1977): An Eigensystem Realization Algorithm for Modal Parameter Identification and Model Reduction. *Journal of Guidance, Control and Dynamics*, 8(5), 620-627.
- Maia, N.M.M., and Silva, J.M. (1997): *Theoretical and Experimental Modal Analysis*. Research Studies Press Ltd.
- Tedesco, J.W., McDougal, W.G., and Ross, C.A. (1999): *Structural Dynamics*. Addison Wesley Longman, Inc.
- Rytter, A. (1993): Vibration Based Inspection of Civil Engineering. Ph.D. Dissertation, University of Aalborg, Denmark.

Evolutionary Methodologies for Decision Support

Yufeng Hu

Graduate Student, Department of Civil, Structural & Environmental Engineering, University at Buffalo

Research Supervisor: Gary Dargush, Professor

Summary

One of the primary objectives of the MCEER research program is to contribute toward the development of disaster resilient communities. As a result, there is a general need to model, understand and ultimately direct the behavior of a wide variety of complex multi-scale systems. Within the context of a critical care facility, these not only include the structural and non structural systems that shape the physical environment, but also the organizational systems that define the social and economic climate. Evolutionary methodologies (Holland, 1992) may be ideally suited to study and provide guidance for many of these tasks. Robust computational approaches are developed for decision support that incorporates both engineering and sociotechnical aspects. Furthermore, we attempt to create a theoretical and computational framework that may have applicability for complex decision-making in general.

Introduction

During the past two decades, there has been increasing interest in the concept of complex adaptive systems, originally formulated by Holland (1962, 1992). Physical and social systems often involve the complicated, nonlinear interaction amongst numerous components or agents. In many cases, the agents are free to aggregate at multiple scales in response to an uncertain or changing environment. As a result, such systems may demonstrate an ability to evolve over time and to self-organize. In the process, these complex adaptive systems may display collective attributes acquired through adaptation that could not be achieved either by individual agents acting independently, or by agents under strict top-down control. Standard examples include a rain forest, the human central nervous system and the local economy. However, from the definition above, a single critical care facility or critical care network also may function as a complex adaptive system. Key characteristics of these complex systems include: Environmental uncertainty; Multi-scale behavior; Large decision space; Temporal dimension.

Tsympkin (1971) presented perhaps the first major work on adaptation in automated systems. His approach was based primarily on the existing methods of optimal control theory. Holland (1992), on the other hand, developed a unified theory of adaptation for both natural and artificial systems. Ideas from biological evolution were central to his approach. Besides providing a general formalism for studying adaptive systems, this led to the development of evolutionary methods and, more specifically, to genetic algorithms.

In a genetic algorithm, the individual solutions are encoded as computational chromosomes, often using a binary string representation. The typical genetic operators include selection, crossover, mutation and replacement. At each generation, the best performing solutions are selected for reproduction. The genetic operators then work to increase the frequency of good qualities contained in the population, while continually exploring the space of possible solutions. Further details on genetic algorithms can be found in Holland (1992), Goldberg (1989) and Mitchell (1996).

Although in the original work by Holland the environment may be uncertain, most implementations and applications of genetic algorithms are limited to fixed environments. However, evolutionary methods are more appropriate for discovering robust solutions to problems involving uncertainty, ambiguity and risk. Of course, these are exactly the types of solutions required for the development of seismically resilient communities.

Framework of Evolutionary Methodologies

Figure 1 shows the overall decision support methodology. This methodological framework involves the geophysical (Frankel et al., 1996), earthquake (Papageorgiou, 2000), structural, damage and sociotechnical models.

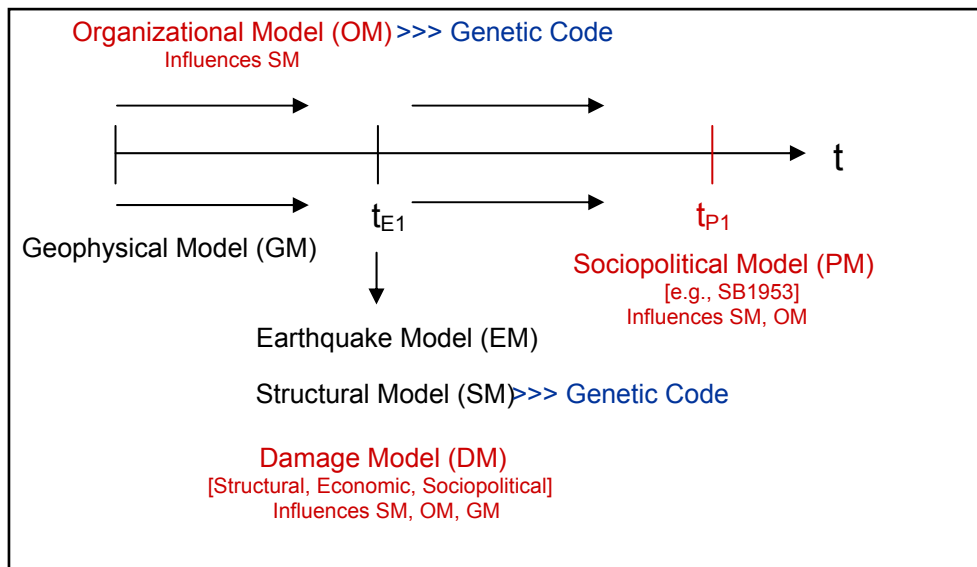


Figure 1. Evolutionary Decision Support

For the geophysical model and earthquake model, we employ the USGS Gutenberg-Richter seismicity database for eastern North America (Frankel, 1995; Frankel et al., 1996) and generate as many ground motions as necessary to evaluate proposed structural design and retrofit options. Following the USGS model, the entire geographical region of eastern North America is subdivided into bins, with each bin representing 0.1 degrees of longitude and latitude. The USGS database then provides Gutenberg-Richter parameters for each bin. We simulate the seismic environment by running Poisson processes in each bin to determine first arrival times of significant events that may occur during the intended life cycle of the structure. Once magnitude and epicentral distance are established for a significant event, the ground motion generation algorithm defined by Papageorgiou

(2000) is used to produce an appropriate synthetic accelerogram. This approach is used to simulate n_i environmental realizations independently for each individual structure at each generation.

Passive energy dissipation systems are now widely used for the seismic control of civil engineering structures and a wide variety of device types are available, including metallic yielding dampers, friction dampers, viscous fluid dampers and viscoelastic dampers (e.g., Soong and Dargush, 1997; Constantinou et al., 1998). The introduction of these passive energy dissipation concepts and systems presents the structural engineers with considerable freedom in aseismic design and retrofit, however further guidance may be needed to help direct the design process. In order to address this issue, several simplified design procedures have been in development over the past decade. These procedures are oriented mostly toward the design of simple uniform structures. Alternatively, one may attempt to develop new computational approaches that can provide insight into seismic performance, as well as design guidance both for simple structural systems and for complex irregular structures.

Here we adopt this latter approach and continue our development of an evolutionary approach for aseismic design and retrofit. Previous research on the application of genetic algorithms to passively damped structures includes the work by Singh and Moreschi (1999, 2000, 2002), Dargush and Sant (2000, 2002) and Dargush and Green (2002). In particular, the previous work is extended by introducing a parallel genetic algorithm for the design of robust passively damped structures within an uncertain seismic environment.

Organizational Decision Support

While the evolutionary approach for aseismic design and retrofit is useful in distinguishing the various design alternatives, decisions regarding whether or not to retrofit an existing structure are seldom based strictly on engineering grounds. The sociotechnical nature of organizational decision-making must be considered. For the general problems, March and Olsen (1973) proposed a garbage can model for organizational decisions. Recently, Petak and Alesh (2004) have tailored and augmented the March-Olsen model for earthquake hazard risk reduction in healthcare organizations. They also emphasize the importance of the temporal dimension of decision-making and the need within the organization to actively seek solutions.

This Petak-Alesh descriptive model is very helpful for identifying the prerequisites for organizational action. Additional qualitative and quantitative models of organizational behavior and performance are needed to support the decision-making process. Currently we are concentrating on the development of succinct differential models using ideas from system dynamics (Forrester, 1961, 1969, 1971) and interacting species formulations (May, 1973).

System dynamics originated in the 1960s with the work of Jay W. Forrester. System dynamics is a method of analyzing problems in which time is an important factor, and which involves the study of how a system can be defended against, or made to benefit from, the shocks which fall upon it from the outside world. A system dynamics model is a practical, operational decision-making model with interdisciplinary ties. The basic structures of a system dynamics model include stocks, flows, converters and connectors. For critical care facilities, the present system dynamic model utilizes patients, employees, building and equipment, and monetary assets as the four stocks, which are four key variables characterizing organizational behavior. Essentially, the system dynamics model can be represented by a set of Ordinary Differential Equations (ODEs). The four stocks in the system dynamics model are the four major dependent variables of the ODE set with time as the

independent variable. From the system dynamics model, we get a set of simplified dimensionless formulations. This permits analytical investigation using well-established qualitative methods for ODEs. The critical points, limit cycles and stability issues are analyzed.

As soon as the organizational dynamics model is established, decision space S should be identified. In our model, we focus on three sets of policies which need decision-making:

- Policies regarding seismic retrofit: including evaluation frequency (how often should we examine whether or not the facility needs to be retrofitted), retrofit criteria (under what financial conditions can we perform retrofitting), retrofit level (what performance level is expected after retrofitting).
- Policies regarding building and equipment investment: including investment rate, patients vs. building and equipment target ratio and major equipment investment criteria.
- Policies regarding human resource management: including employee hiring rate, patient vs. employee target ratio and employee hiring monetary criteria.
- Policies regarding close/open wings of the hospital: including close/open criteria (under what conditions can we close/open wings), close/open level (what percentage of the total buildings and equipments should be closed/opened).

Again a Genetic Algorithm is applied to find a robust solution, where each solution corresponds to a specific set of organizational policies. The overall flow of the genetic algorithm for organizational decision support is provided in Figure 2. Currently, the fitness can be defined as one or several of the following objectives: maximizing building and equipment; maximizing monetary assets; maximizing patients served; minimizing accumulated damage; minimizing patient-days lost.

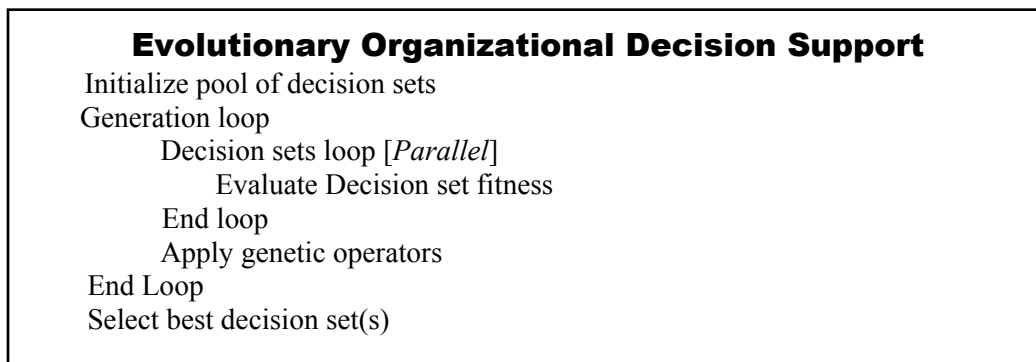


Figure 2. Evolutionary Organizational Decision Support Flow Diagram

A five story steel frame hospital is used as a preliminary example. We assume the lifetime $T_f=50$ years. For the genetic algorithm, we utilize a string length $N_f=26$ in a population of $n_p=16$ policy scenarios for a total of $n_g=32$ generations and assume maximizing building and equipment is the only measurement of fitness. The dimensionless initial condition is: Initial patients $P_0 = 1.5$, initial employees $E_0 = 1.0$, initial building and equipment $B_0 = 1.25$, initial monetary assets $M_0 = 1.0$. Whenever a decision is made to retrofit the hospital, the robust designs of the appropriate level

from evolutionary aseismic retrofit design are utilized. Results with six sets of organizational decisions which have highest fitness are shown in Figure 3. We can see decision sets A and D have the highest survival rate above 80%. Decision set A has gone through a large number of realizations and earthquakes, but, the averaged monetary assets are negative. From this simulation, decision set A seems to be a robust decision solution but it might not be suitable for a profitable hospital. However, we should emphasize that this is only a preliminary example intended to illustrate the methodology. Much more work is needed to provide a reliable decision support tool for critical care facilities.

	A	B	C	D	E	F
Realizations:	3392	4928	1088	1408	1472	1152
Fitness :	1.38	1.37	1.36	1.36	1.35	1.35
<u>Retrofit Policy</u>						
Frequency :	8 yr	-	8 yr	2 yr	8 yr	8 yr
Criteria :	R	-	M	R	R	Always
Level :	3	None	3	3	3	3
<u>Building & Equipment Investment Policy</u>						
Rate :	Slow	Slow	Slow	Slow	Slow	Slow
B/P Target :	Highest	Highest	Highest	Highest	Highest	Highest
Threshold :	Lowest	Lowest	Lowest	Lowest	Lowest	Lowest
<u>Human Resource Management Policy</u>						
Rate :	Slow	Slowest	Fast	Slowest	Slowest	Slowest
E/P Target :	Lowest	Lowest	Lowest	Lowest	Lowest	Lowest
Threshold :	Low	Low	Low	Low	Low	Low
<u>Retrofit Status</u>						
Fraction :	0.77	0.00	0.33	0.78	0.75	0.84
Time :	11.59	0.00	19.89	8.05	11.14	8.03
<u>Earthquake Response</u>						
Attempt :	236	317	85	79	97	81
Survive :	193	202	52	66	75	60
Survive Rate:	0.82	0.64	0.61	0.84	0.77	0.74
<u>Overall Performance</u>						
B :	1.38	1.37	1.36	1.36	1.35	1.35
M :	-0.17	0.73	-0.31	0.65	0.63	0.55
P Admit :	6.27	6.22	6.34	6.12	6.07	6.02
Damage :	0.03	0.07	0.09	0.02	0.04	0.06

Figure 3. Organizational decision support preliminary example

Conclusion

A general evolutionary framework has been developed to provide support for complex decision processes. Beyond the engineering aspects of the mitigation problem, there are many associated socioeconomic issues that must enter into the decision-making process. Consequently, we focus on developing evolutionary formulations for decision support toward seismic risk reduction in critical care organizations. Our present work is concentrated on the development of quantitative organizational models to approximate the overall behavior and to couple with the existing geophysical and structural models in the evolutionary decision support framework. Although many research challenges remain, we believe that this new approach has considerable potential to provide guidance at the level of a single critical care facility and also for regional planning of critical care networks.

Acknowledgements

This research was primarily supported by the Earthquake Engineering Research Centers Program of the National Science Foundation, under award number EEC-9701471. This financial support is gratefully acknowledged.

References

- Constantinou, M.C., Soong, T.T. and Dargush, G.F., (1998), *Passive Energy Dissipation Systems for Structural Design and Retrofit*, Monograph No. 1, Multidisciplinary Center for Earthquake Engineering Research, University at Buffalo.
- Dargush, G.F. and Sant, R.S., (2000), "Computational Aseismic Design and Retrofit: Application to Passively Damped Structures," *Mitigation of Earthquake Disaster by Advanced Technologies-2*, Las Vegas, NV, MCEER-01-0002, Multidisciplinary Center for Earthquake Engineering Research, University at Buffalo, pp. 175-185.
- Dargush, G.F. and Sant, R.S., (2002), "Computational Aseismic Design and Retrofit with Application to Passively Damped Structures," *Seventh U.S. National Conference Earthquake Engineering*, EERI, Boston, MA.
- Dargush, G.F. and Green, M.L., (2002), "Evolutionary Aseismic Design and Retrofit," *KEERC-MCEER Joint Seminar*, Buffalo, NY.
- Forrester, J.W., (1961), *Industrial Dynamics*, M.I.T. Press, Cambridge, MA and John Wiley & Sons, New York, NY.
- Forrester, J.W., (1969), *Urban Dynamics*, M.I.T. Press, Cambridge, MA.
- Forrester, J.W., (1971), *World Dynamics*, Wright-Allen Press, Cambridge, MA.
- Frankel, A., (1995), "Mapping Seismic Hazard in the Central and Eastern United States," *Seism. Res. Lett.*, Vol. 66, pp. 8-21.
- Frankel, A., Mueller, C., Barnhard, T., Perkins, D., Leyendecker, E.V., Dickman, N., Hanson, S. and Hopper, M., (1996), *National Seismic-Hazard Maps: Documentation*, U.S. Geological Survey, Open-File Report 96-532, 110 pp.

- Goldberg, D.E., (1989), *Genetic Algorithms in Search, Optimization and Machine Learning*, Addison-Wesley, Reading, MA.
- Holland, J.H., (1962), "Outline for a Logical Theory of Adaptive Systems", *J. Assoc. Comp. Mach.*, Vol. 9, 297-314.
- Holland, J.H., (1992), *Adaptation in Natural and Artificial Systems*, MIT Press, Cambridge, MA, 1st Edition 1975.
- March, J.G. and Olsen, J.P., (1973), *Ambiguity and Choice in Organizations*, Univeritetsforlaget, Bergen, Norway.
- May, R.M., (1973), *Stability and Complexity in Model Ecosystems*, Princeton University Press, Princeton, NJ.
- Mitchell, M., (1996), *An Introduction to Genetic Algorithms*, MIT Press, Cambridge, MA.
- Papageorgiou, A., (2000), "Ground Motion Prediction Methodologies for Eastern North America," *Research Progress and Accomplishments, 1999-2000*, Multidisciplinary Center for Earthquake Engineering Research, University at Buffalo.
- Petak, W.J and Alesch, D.J. (2004), "Organizational Decision Making with Respect to Extreme Events: Healthcare Organizations Respond to California's SB 1953," *Research Progress and Accomplishments, 2003-2004*, Multidisciplinary Center for Earthquake Engineering Research, University at Buffalo.
- Singh, M.P. and Moreschi, L.M., (1999), "Genetic Algorithm-based Control of Structures for Dynamic Loads," *Proc. IA-99*, Osaka University, Japan.
- Singh, M.P. and Moreschi, L.M., (2000), "Optimal Seismic Design of Building Structures with Friction Dampers," *Proc. US-China Millennium Symposium Earthquake Engrg.*, Beijing, China.
- Singh, M.P. and Moreschi, L.M., (2002), "Optimal Placement of Dampers for Passive Response Control," *Earthquake Engrg. Struct. Dyn.*, Vol. 31, pp. 955-976.
- Soong, T.T. and Dargush, G.F., (1997), *Passive Energy Dissipation Systems in Structural Engineering*, Wiley, London and New York.
- Tsympkin, Y.Z., (1971), *Adaptation and Learning in Automatic Systems*, Academic Press, New York.

Fragility Based Rehabilitation Decision Analysis

Cagdas Kafali

Graduate Student, School of Civil and Environmental Engineering, Cornell University

Research Supervisor: Mircea Grigoriu, Professor

Summary

A method is presented for assessing the seismic performance of structural/nonstructural systems and developing rational strategies for increasing the seismic resilience of these systems. The seismic performance is measured by fragility surfaces, that is, the probability of system failure as a function of moment magnitude and site-to-source distance, consequences of system damage and failure, and system recovery time following seismic events. The input to the analysis consists of (i) seismic hazard, (ii) structural/nonstructural systems properties, (iii) performance criteria, (iv) rehabilitation strategies, and (v) a reference time. Estimates of losses and recovery times can be derived using fragility information, financial models, and available resources. A structural/nonstructural system located in New York City is used to demonstrate the methodology. Fragilities are obtained for structural/nonstructural components and systems for several limit states. Also, statistics are obtained for life time losses and recovery times corresponding to different rehabilitation alternatives.

Introduction

Capital allocation decisions for a health care facility include, for example, opening a new unit, extending or closing some existing units, buying new equipment, and relocating the hospital building. These decisions are based on life cycle capacity, viewed as the level of performance defined for a service, and cost estimates. Existing geotechnical, structural/nonstructural systems can be left as they are or can be retrofitted using one of the available rehabilitation alternatives. Leaving a system as it is seems to be reasonable for short-term decisions but retrofitting the system, despite its initial costs, might be beneficial in the long run. A probabilistic methodology is required to make a rehabilitation decision since seismic hazard and system performance are uncertain. Most of the existing earthquake loss estimation methodologies usually calculate losses including direct and indirect economic and social losses for a given region, based on the maximum credible earthquake. The ATC-13 (ATC, 1985) methodology provides damage and loss estimates, based on expert-opinion, for industrial, commercial, residential, utility and transportation facilities. HAZUS (FEMA, 1999) estimates potential losses on a regional basis and these estimates are essential to decision-making at all levels of government, providing a basis for developing mitigation policy, and response and recovery planning. Both methods were developed to estimate losses for a large number of facilities in a specified region using the maximum credible earthquake and should not be applied to an individual facility. Losses estimated by using the maximum credible earthquake may not be accurate (Kafali and Grigoriu, 2004a).

The main objective of this paper is the development of a methodology for evaluating the seismic performance and development of optimal rehabilitation strategies of individual health care facilities

during a specified time interval. The seismic performance is measured by fragility surfaces, that is, the probability of system failure as a function of moment magnitude and site-to-source distance, consequences of system damage and failure, and system recovery time following seismic events. Estimates of losses and recovery times, referred to as life cycle losses and recovery times, can be derived using fragility information, financial models, and available resources. A health care facility located in New York City is used to demonstrate the methodology. Fragilities and statistics for lifetime losses are obtained for this structural system and some of its nonstructural components.

Proposed Loss Estimation Method

The proposed loss estimation method is based on (i) seismic hazard analysis, (ii) fragility analysis and (iii) capacity/cost estimation. Figure 1 shows a chart summarizing the loss estimation methodology.

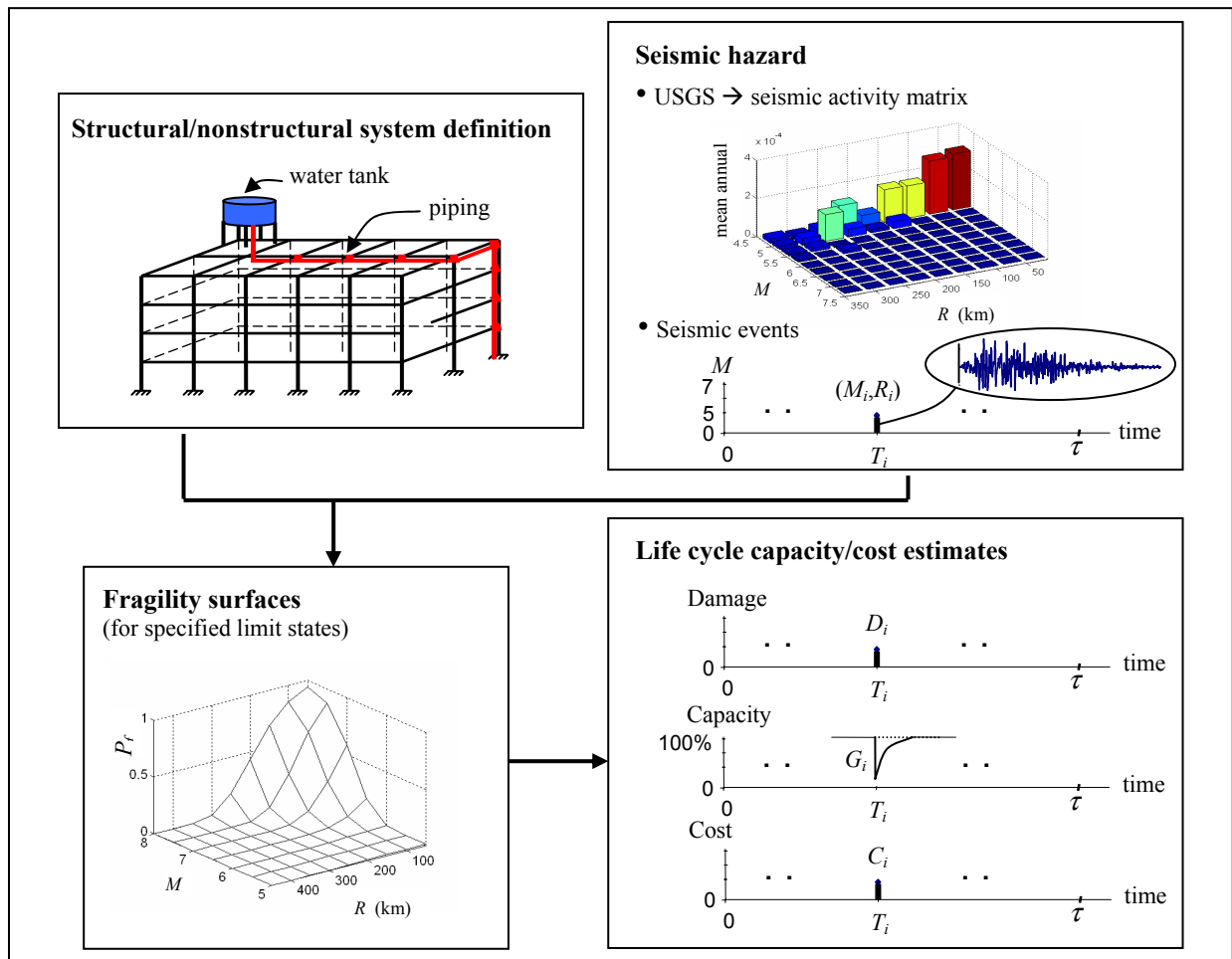


Figure 1. Loss estimation

Seismic Hazard Analysis

The input to the seismic hazard model consists of (1) seismic activity matrix at the site, (2) the projected life τ of a system, and (3) soil properties at the site. The seismic activity matrix is calculated using the deaggregated matrices available at USGS website (<http://eqhazmaps.usgs.gov/index.html>). Deaggregation matrices at a site give the percent contribution of earthquakes with different moment

magnitude ranges M_i and rings R_j to the seismic hazard at the site. USGS provides several deaggregated seismic hazard matrices for any location in the United States at hazard levels of 1%, 2%, 5% and 10% probability of exceedance in 50 years, where a hazard level is defined as the probability that a ground motion parameter (*e.g.* peak ground acceleration) exceeds a reference value during a given period of time. The mean annual rate ν_{ij} of earthquakes from bin (M_i, R_j) can be calculated from deaggregation matrix (Kafali and Grigoriu, 2004a). A Monte Carlo algorithm can be developed for generating (i) random samples of the seismic hazard at the site during a given period of time τ using the seismic activity matrix, and (ii) seismic ground acceleration samples for these seismic hazard samples. Each seismic hazard sample is defined by the number of earthquakes during the time τ , temporal distribution, and magnitude and source-to-site distance of each of them.

Total number of earthquakes $N(\tau)$ is assumed to follow a Poisson distribution with mean annual rate $\nu = \sum_{i,j} \nu_{ij}$, and the probability that an earthquake having a magnitude in the range M_i and coming from a source in the ring R_j can be obtained from $P[M \in M_i, R \in R_j] = \nu_{ij} / \nu$. The ground acceleration $A(t)$ is modeled by a non-stationary stochastic process $A(t) = w(t)A_s(t)$, where t is the time, $w(t)$ is a deterministic envelope function and $A_s(t)$ is a stationary Gaussian process whose spectral density function is given by the specific barrier model. Input parameters of this model are the moment magnitude, source-to-site distance of the earthquake and the soil condition at the site. The description of specific barrier model and how to generate samples of ground acceleration time histories can be found elsewhere (Papageorgiou and Aki, 1983 a and b; Kafali and Grigoriu, 2003a). Figure 2 shows (i) the deaggregation matrix for 1% probability of exceedance in 50 years, (ii) the seismic activity matrix, and (iii) a sample of seismic hazard scenario over a life time of 50 years, for New York City (NYC) area.

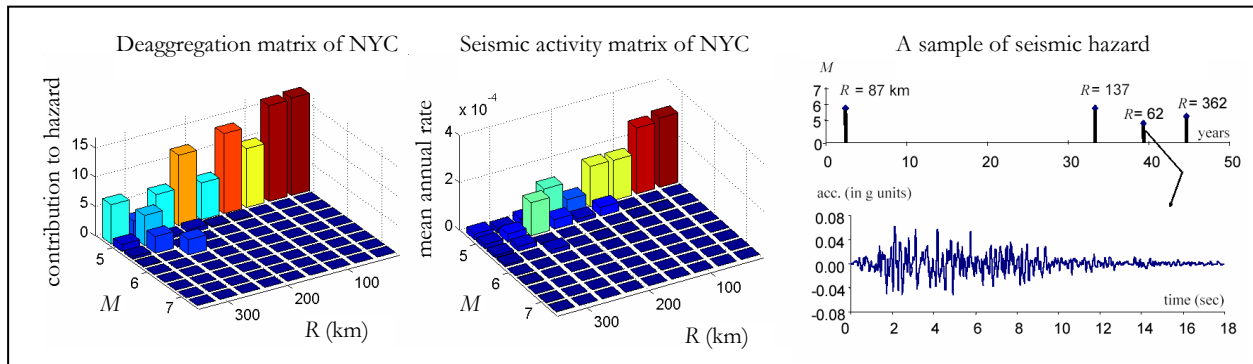


Figure 2. Seismic hazard

Fragility Analysis

The probability that a system response exceeds a limit state viewed as a function of M and R is called system fragility surface. Monte Carlo simulation and crossing theory of stochastic processes can be used to calculate fragility surfaces of linear/nonlinear systems and their components for different limit states (Kafali and Grigoriu, 2003b, 2004b). Fragility is used to characterize the damage in the structural/nonstructural systems. Let D_i be a discrete random variable characterizing the damage state of a nonstructural system after seismic event i characterized by (M_i, R_i) , $i=1, \dots, N(t)$, where $N(t)$ is the number of seismic events in $[0, t]$. Assume that the nonstructural system is in damage state d_k with probability $p_{k,i}$ for $k=1, \dots, n$, where n is the number of damage states. The probabilities $p_{k,i}$ are obtained from the fragility information of the nonstructural system and are functions of the limit

state defining the damage state d_k and (M_p, R_i) . Similarly, we can define random variables characterizing the damage in structural system and components of the selected nonstructural system.

Capacity and Cost Estimation

Capacity, for example patient per day capacity in a service, and total cost are estimated for the case of no rehabilitation and for different retrofitting techniques. Using these estimates efficient solutions can be determined. We assume that loss of capacity is caused solely by damage of nonstructural systems. The capacity at time t is

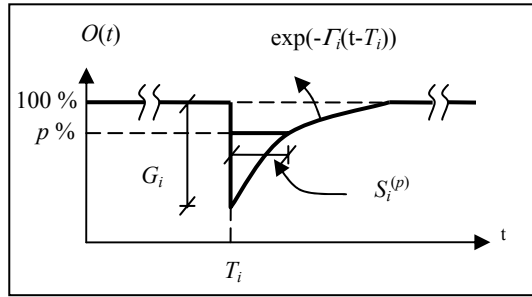


Figure 3. Capacity model

$$O(t) = 1 - \sum_{i=1}^{N(t)} G_i \exp(-\Gamma_i(t - T_i)),$$

where T_i is the arrival time of event i , G_i and Γ_i are the loss in the capacity and the rate of recovery, after event i , respectively (Fig.3). Note that

$$S_p(t) = \sum_{i=1}^{N(t)} S_i^{(p)},$$

represents the total time the system spends at or below $p\%$ -level capacity in $[0, t]$.

The cost relates to (i) structural failure, (ii) retrofitting, (iii) repair, (iv) loss of capacity in services, and (v) loss of life. Rehabilitation is only considered for the nonstructural system. Costs due to (i), (iii), (iv) and (v) are random. The total cost in dollars at time t in net present value is

$$TC(t) = ic + \sum_{i=1}^{N(t)} C_i / (1 + dr)^{T_i},$$

where ic is initial cost related to the rehabilitation, dr is the discount rate, T_i is the time of arrival of event i , and C_i is the cost related to event i . Assume that $C_i = CS_p$, if structure fails and $C_i = CR_i + CC_i + CL_p$, otherwise. CS_i is the cost related to structural failure, CR_i is the repair cost of the nonstructural system, CC_i is the cost due to the loss in capacity, and CL_i is the cost of life losses. It is expected that with an increasing initial cost ic , the cost C_i due to event i will decrease and for some rehabilitation alternative we will have the optimum solution.

Numerical Example

An MCEER Demonstration Hospital Project located in NYC is used to demonstrate the proposed methodology. Three different levels of rehabilitation, namely, (i) no rehabilitation (rehab.1), (ii) life safety (rehab.2) and (iii) limited downtime (rehab.3) are considered. It is assumed that the structure is linear elastic and cascade analysis applies, that is, the nonstructural system does not affect the dynamics of the supporting structure. The nonstructural system considered consists of a water tank (comp.1) and a power generator (comp.2) located at the roof and at the first floor, respectively. It is assumed that (i) the components are not interacting, (ii) water tank is drift sensitive, (iii) power generator is acceleration sensitive, and (iv) both components are linear single degree of freedom oscillators. An illustration of the hospital model with two components attached to it, the required

modal properties of the structure (damping ratio is 3% for all modes), and natural frequencies and damping ratios of the components for the different rehabilitation alternatives are show in Figure 4.

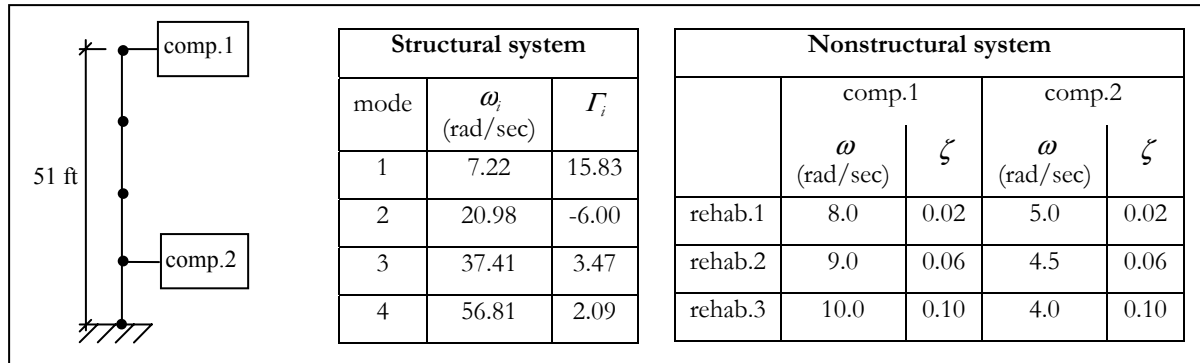


Figure 4. System properties

Fragility surfaces are obtained for the structural/nonstructural systems, comp.1 and comp.2 for different limit states assuming stationary ground accelerations. Structural system is assumed to fail when the roof displacement exceeds 5". Limit states are {0.12",0.25",0.50"} and {1.0g,1.5g} for comp.1 and 2, respectively. The nonstructural system has three damage states (i) no damage, when both components have no damage; (ii) extensive damage, when either of its components fails; and (iii) moderate damage, otherwise. Figure 5 shows fragility surfaces of structural/nonstructural systems and comp.1 and comp.2 for different rehabilitation alternatives and limit states.

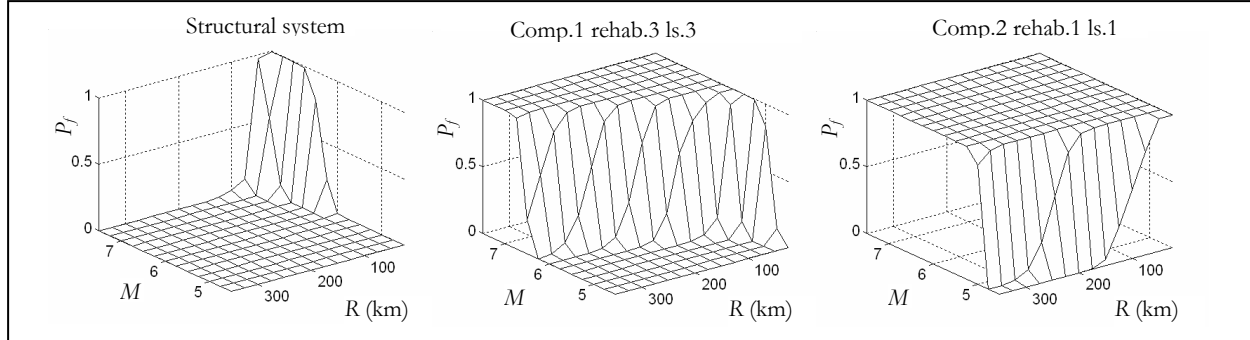


Figure 5. Fragility surfaces

Estimates of the total time the system spends at or below 80%-level capacity and the total cost TC , during a projected life of $\tau=100$ years, for the three rehabilitation alternatives are obtained by Monte Carlo simulation. Following information is used to obtain these estimates. G_i and Γ_i are discrete random variables taking values {0,0.5,0.9} and {0,0.5,0.3}, respectively, with probabilities obtained from the nonstructural system fragility. The discount rate is 7% and the rehabilitation cost ic takes values {0,1000000,5000000}, for no rehabilitation, life safety and limited downtime rehabilitation, respectively. $CR_i=C_{1,i}+C_{2,i}$ where $C_{1,i}$ and $C_{2,i}$ are discrete random variables taking values {0,600000,1400000,2000000} and {0,500000,1000000}, respectively, with probabilities obtained from the corresponding component fragility surfaces, and they represent the repair costs for comp.1 and 2, respectively. $CS_i=c_s.q_i$, where $c_s=47000000$ is the cost related to the downtime and the construction of a new facility and q_i is the probability of system failure obtained from the structural

system fragility. $CL_i = cl \cdot X_i$, where $cl = 2200000$ is the cost of one person's life loss and X_i is a binomial random variable with parameters $n_x = 100$ and $p_x = 0.1$, representing the number of people losing their lives, respectively. $CC_i = \alpha \cdot RT_i$, where $\alpha = 2300$ is the cost due to the loss in capacity per day and RT_i is the time to reach 100% capacity given by $RT_i = 0$ for $G_i = F_i = 0$, and $RT_i = -\ln(0.001/G_i)/F_i$ otherwise. Figure 6 shows $P(S_p(t)/\tau > s/\bar{t})$ and $P(TC(t) > c)$.

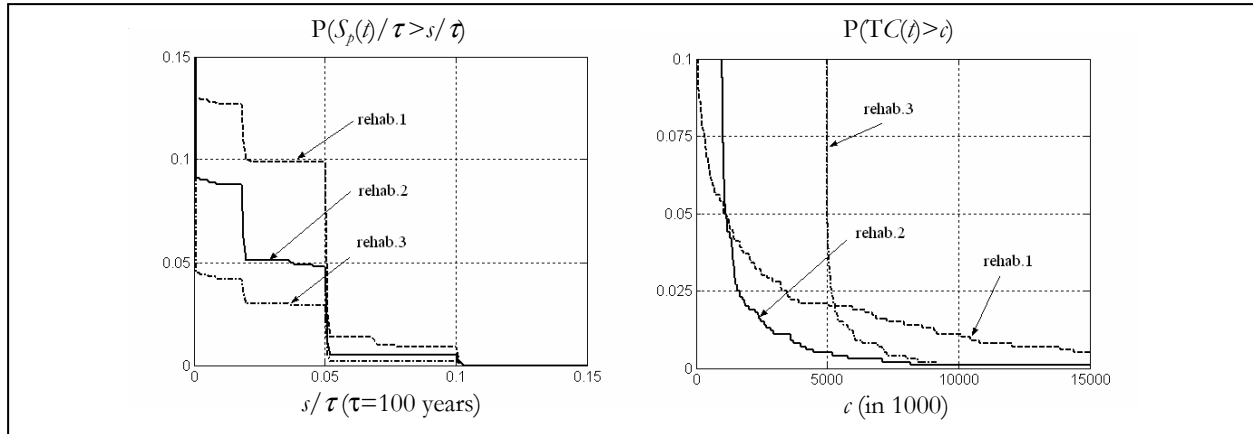


Figure 6. Estimates of the capacity and total cost

A possible measure for comparing the effectiveness of different rehabilitation alternatives is the probability that the total cost exceeds a level c . Accordingly, the optimal solution is the one with the lowest $P(TC(t) > c)$, and depends on the selected value of c (see Fig.6). For example, the optimal solutions are rehabilitation alternatives 1 and 2, for $c = 500000$ and $c = 4000000$, respectively.

Concluding Remarks

A method was developed to identify an optimal retrofitting technique for structural/nonstructural systems. The method (i) considers a realistic seismic hazard model rather than using the maximum credible earthquake, (ii) includes all components of costs, that is, the costs related to the structural failure and downtime, retrofitting, repair, loss of capacity in services, and loss of life, and (iii) is designed for individual facilities rather than a large population of them. The method is based on Monte Carlo simulation, probabilistic seismic hazard, fragility surfaces and capacity/cost analyses.

Acknowledgements

This research was carried out under the supervision of Dr. M. Grigoriu, and supported by the Multidisciplinary Center for Earthquake Engineering Research under NSF award EEC-9701471.

References

ATC-13 (1985): *Earthquake damage evaluation data for California*. Applied Technology Council, Redwood City, CA.

FEMA (1999): *HAZUS 99: Estimated annualized earthquake losses for the United States*, FEMA, Washington, D.C.

Kafali, C. and Grigoriu, M. (2003a): *Non-Gaussian model for spatially coherent seismic ground motions*. In proceedings of the ICASP9, San Francisco, CA., pp. 321–327.

Kafali, C. and Grigoriu, M. (2003b): *Fragility analysis for nonstructural systems in critical facilities*, In proceedings of ATC-29-2 seminar, Newport Beach, CA, pp. 375–385.

Kafali, C. and Grigoriu M. (2004a): *Rehabilitation decision analysis*. In preparation.

Kafali, C. and Grigoriu, M. (2004b): *Seismic fragility analysis*. In proceedings PMC2004, Albuquerque, N.M.

Papageorgiou, A. S. and Aki, A. K. (1983a): *A specific barrier model for the quantitative description of the inhomogeneous faulting and the prediction of strong ground motion. Part I*, Bulletin of the Seismological Society of America 73, 693–722.

Papageorgiou, A. S. and Aki, A. K. (1983b): *A specific barrier model for the quantitative description of the inhomogeneous faulting and the prediction of strong ground motion. Part II.* Bulletin of the Seismological Society of America 73, 953–978.

A Wavelet Based Approach for Estimating the Steady State Response of Nonlinear Systems

Jale Tezcan

Graduate Student, Department of Civil & Environmental Engineering, Rice University

Research Supervisor: Pol D. Spanos, L. B. Ryon Chair of Engineering

Summary

A wavelet based equivalent linearization method is presented for estimating the steady state response of systems with cubic nonlinearity, excited by non-stationary processes. Harmonic wavelets are used to decompose the excitation into components with non-overlapping frequency components. The original nonlinear system is then decomposed into linear time varying subsystems, each responding only to a particular frequency band of the excitation process. Response for each subsystem is calculated using the equivalent stiffness values obtained from the proposed algorithm. The total response of the original system is then found by adding up the responses from individual subsystems. Finally, records of the Kocaeli, Turkey earthquake (8/17/1999) are used to demonstrate the applicability of the proposed method to a lightly damped oscillator with cubic nonlinearity in stiffness. It has been concluded that the numerical approach developed in this paper gives a reliable estimate of the steady state response of nonlinear systems, excited by non-stationary processes.

Introduction

An inherent difficulty in dealing with nonlinear vibration problems is that the superposition principle is not applicable. The fact that most linear analysis techniques are based on the idea of finding a general solution by superimposing particular solutions, has led many researchers to find alternative formulations for nonlinear analysis (Nigam 1983, Roberts and Spanos 1986, Lin, Y.K. and G.Q. Cai, 1995).

While Fourier transform has been an indispensable tool in signal processing, it is now recognized that by breaking a signal into a series of trigonometric basis functions, time varying features cannot be captured. The fact that non-stationary features characterize many processes of interest has led to the development of alternative transforms that rely on bases with compact support. As Fourier basis functions are localized in frequency but not in time, one alternative was introduced by Gabor to localize the Fourier Transform through the short time Fourier transform. However, the constraints of the Heisenberg uncertainty principle prompt an alternative approach to time-frequency analysis, featuring basis functions that have compact support in both frequency and time to yield a multi resolution analysis called the wavelet transform (Carmona et. al. 1998, Mallat 1989a, Mallat 1989b).

This paper is organized as follows. To illustrate the basic ideas involved, next section is devoted to the discussion of wavelet theory, where Newland's harmonic wavelets are introduced. Later, a wavelet based numerical approach for determining nonlinear system response was developed and the proposed procedure is applied to the response estimation problem. Finally, concluding remarks are made, and other possible applications are discussed.

Wavelet Transform

The wavelet transform is a linear transform, which decomposes a signal $x(t)$ via basis functions that are simply dilations and translations of the mother wavelet $\psi(t)$ through the convolution,

$$W_{\psi}x(s, b) = \frac{1}{\sqrt{s}} \int_{-\infty}^{\infty} x(t) \psi^* \left(\frac{t-b}{s} \right) dt \quad (1)$$

where $\psi^*(t)$ is the complex conjugate of the wavelet function $\psi(t)$, s is the dilation parameter and b is the location parameter of the wavelet. The wavelet coefficients $W_{\psi}x(s, b)$ represent the measure of similarity between the scaled and translated wavelet at and the signal at scale s around time $t=b$.

The harmonic wavelets were introduced by Newland, in an attempt to create a wavelet basis, equivalent to dilation wavelets with infinite number of coefficients that would occupy a narrow band region in frequency domain (Newland, 1993). Specifically, the mother wavelet of the harmonic transform is defined in the frequency domain as,

$$W_{m,n,r}(\omega) = \frac{1}{(n-m)2\pi} e^{\frac{-i\omega r}{n-m}}, \quad m2\pi \leq \omega \leq n2\pi \quad (2)$$

$$W_{m,n,r}(\omega) = 0, \quad \text{else,}$$

where m and n are any positive real numbers. This is the expression for a harmonic wavelet centered at time $t=r/(n-m)$ and frequency $(m+n)\pi$ with bandwidth $(n-m)/(2\pi)$.

Wavelets-based Equivalent Linearization Procedure

The most commonly used approach for finding approximate answers to nonlinear dynamic problems is to replace the nonlinear system with a linear system. For a system with nonlinearity in stiffness, one replaces,

$$\ddot{x} + \beta \dot{x} + k x + h(x) = g(t) \quad (3)$$

with

$$\ddot{x} + \beta \dot{x} + k x + k_{nl}x = g(t) \quad (4)$$

where k_{nl} is the additional stiffness introduced by the nonlinearity. On minimizing the mean square of the error over one cycle of the response, k_{nl} is obtained as,

$$k_{nl} = \frac{\oint h(x) x dt}{\oint x^2 dt}. \quad (5)$$

From the linear vibration theory, for an excitation described as a sum of sinusoids,

$$g(t) = F_1 \text{Sin}(\omega_1 t) + F_2 \text{Sin}(\omega_2 t) + \dots + F_N \text{Sin}(\omega_N t) \quad (6)$$

the steady state response can be written as,

$$x(t) = X_1 \text{Sin}(\omega_1 t + \phi_1) + X_2 \text{Sin}(\omega_2 t + \phi_2) + \dots + X_N \text{Sin}(\omega_N t + \phi_N) \quad (7)$$

where,

$$X_i^2 = \frac{F_i^2}{(k - \omega_i^2)^2 + (\beta \omega_i)^2} \quad \text{and} \quad \phi_i = \tan^{-1} \frac{\beta \omega_i}{k - \omega_i^2} \quad (8)$$

Substituting $x(t)$ from Eq(7) in Eq(5), and assuming that the stiffness nonlinearity is given by,

$$h(x) = k_{nl} x = \lambda k x^3, \quad (9)$$

the additional stiffness due to the nonlinearity can be found for each frequency of excitation as;

$$\begin{aligned} k_{nl.1} &= \frac{3}{4} \lambda k X_1^2 \left[1 + 2 \left(\frac{X_2}{X_1} \right)^2 + 2 \left(\frac{X_3}{X_1} \right)^2 + \dots + 2 \left(\frac{X_N}{X_1} \right)^2 \right] \\ k_{nl.2} &= \frac{3}{4} \lambda k X_2^2 \left[2 \left(\frac{X_1}{X_2} \right)^2 + 1 + 2 \left(\frac{X_3}{X_2} \right)^2 + \dots + 2 \left(\frac{X_N}{X_2} \right)^2 \right] \\ &\quad \vdots \\ &\quad \vdots \\ k_{nl.N} &= \frac{3}{4} \lambda k X_N^2 \left[2 \left(\frac{X_1}{X_N} \right)^2 + 2 \left(\frac{X_2}{X_N} \right)^2 + 2 \left(\frac{X_3}{X_N} \right)^2 + \dots + 1 \right]. \end{aligned} \quad (10)$$

The solution of this system of equations requires an iterative scheme. Starting with

$$k_{nl.i} = 0 \quad \text{and} \quad X_i = \frac{F_i}{\sqrt{(-\omega_i^2 + k + k_{nl.i})^2 + (\beta \omega_i)^2}} \quad \text{for } i = 1:N \quad (11)$$

the updated k_{nl} values are calculated using Eq(10). It was observed that the solution converges quickly, usually in a few steps. Total response can then be calculated by summing up all the response components as,

$$x(t) = \sum_{i=1}^N x_i(t). \quad (12)$$

As an example, this procedure is applied to the system defined as,

$$\ddot{x} + \beta \dot{x} + kx + \lambda kx^3 = g(t) \quad (13)$$

with $\beta=0.5$, $k=16\pi^2$, $\lambda=1$ and $g(t)=15 \sin(4t)+10 \sin(8t)+ 5 \sin(12t)+ 5 \sin(16t)$ and the excitation and response processes are shown in (Figure 1). It is seen that the procedure yields a very good approximation of the true response for this problem.

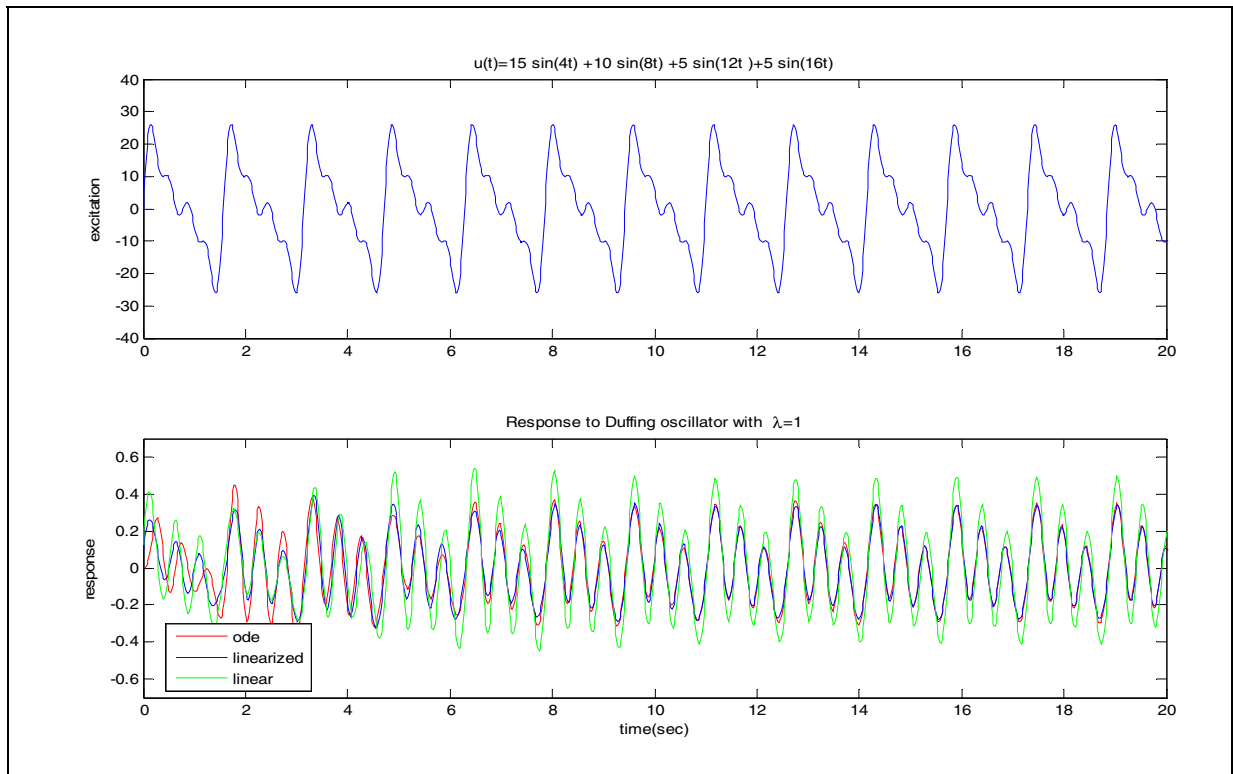


Figure 1. Equivalent Linearization for Stationary Input

The method described above works well for systems subjected to stationary processes. Since real signals are nonstationary, a modified version of the linearization procedure to account for the time dependence of the system response is proposed. For each frequency band, wavelet coefficients of the response are calculated by the method described by Newland, using the generalized wavelet scheme (Newland, 1997). Exploiting the direct relationship between the absolute values of the Fourier coefficients of the response and its wavelet coefficients, scale dependent equivalent stiffness values are calculated as,

$$\begin{aligned}
k_{nl,m} &= 3\pi^2 (n-m)^2 \lambda k A_m^2 \left[1 + 2 \left(\frac{A_{m+1}}{A_m} \right)^2 + 2 \left(\frac{A_{m+2}}{A_m} \right)^2 + \dots + 2 \left(\frac{A_{n-1}}{A_m} \right)^2 \right] \\
k_{nl,m+1} &= 3\pi^2 (n-m)^2 \lambda k A_{m+1}^2 \left[2 \left(\frac{A_m}{A_{m+1}} \right)^2 + 1 + 2 \left(\frac{A_{m+2}}{A_{m+1}} \right)^2 + \dots + 2 \left(\frac{A_{n-1}}{A_{m+1}} \right)^2 \right] \\
&\vdots \\
&\vdots \\
k_{nl,n-1} &= 3\pi^2 (n-m)^2 \lambda k A_{n-1}^2 \left[2 \left(\frac{A_m}{A_{n-1}} \right)^2 + 2 \left(\frac{A_{m+1}}{A_{n-1}} \right)^2 + 2 \left(\frac{A_{m+2}}{A_{n-1}} \right)^2 \dots + 1 \right]
\end{aligned} \tag{14}$$

and the transfer function is updated accordingly. In Equation(14), A_i represents the i^{th} component of the Fourier transform of the wavelet coefficients of the response, As one can see from Eq.(14), for scale (m,n), there are (n-m) equivalent stiffness values, each $1/(n-m)$ units apart on the time axis. The process is iterated until the solution converges. It was seen that convergence is usually achieved in a few steps.

To demonstrate its validity, the procedure described above has been applied to the system defined in Eq.(13) and the steady state system response from the linearization is compared to that from the numerical analysis (4th order Runge Kutta algorithm) in Figure(2). Here, the excitation is a recorded accelerogram from the Kocaeli, Turkey earthquake (8/17/1999).

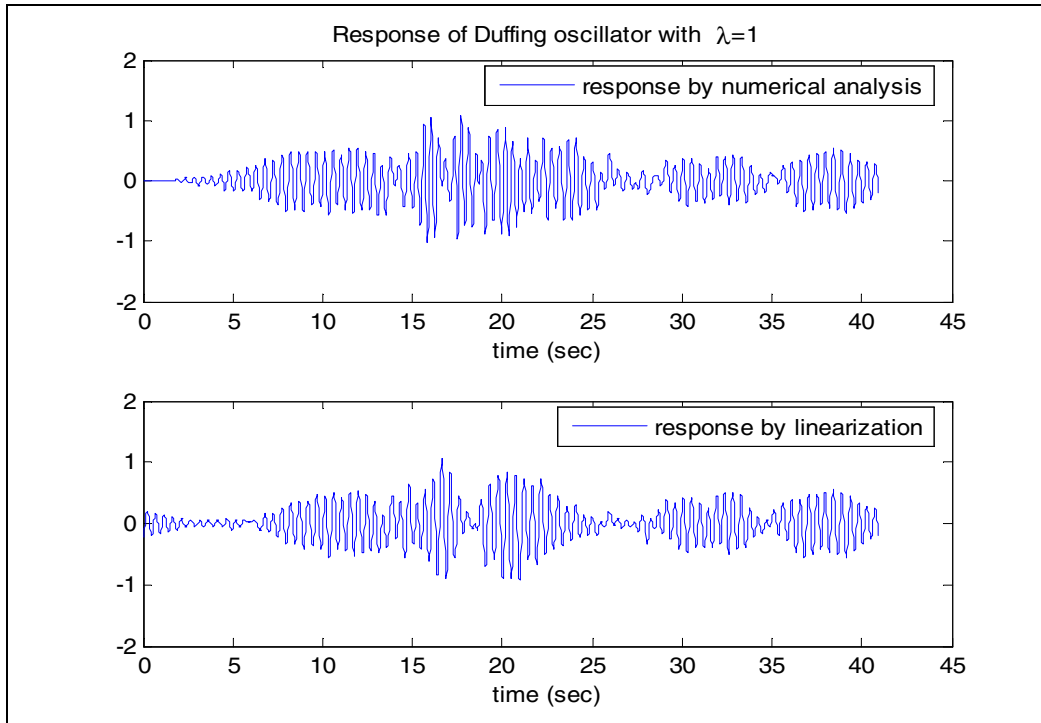


Figure 2. a) Numerical solution b)Wavelet based solution for $\lambda = 1$

Conclusions

A numerical approach for determining steady state response for a system with cubic nonlinearity in stiffness is proposed. Generalized harmonic wavelets are used to define scale dependent equivalent stiffness values. Starting from the frequency response function of the linear system, an iterative method is applied to update the equivalent stiffness values such that the mean square error between the nonlinear system and its linear equivalent is minimized. No assumptions have been made regarding the probability distribution of the excitation or the response. Numerical results pertaining to the response of an oscillator with cubic nonlinearity in stiffness with nonlinearity parameter $\lambda=1$ have been presented. It is concluded that the numerical approach developed in this paper gives a reliable estimate of the steady state response of systems with cubic nonlinearity in stiffness, when subjected to nonstationary excitations. Future research will focus on the applicability of this procedure on systems with hysteretic nonlinearity.

Acknowledgements

This research was supported by the Earthquake Engineering Research Centers Program of the National Science Foundation, under award number EEC-9701471. This financial support is gratefully acknowledged.

References

- Carmona, R., W.J. Hwang, and B. Torresani, *Practical Time-Frequency Analysis*. 1998: Academic Press.
- Lin, Y.K. and G.Q. Cai, *Probabilistic Structural Dynamics: Advanced Theory and Applications*. 1995, New York: McGraw-Hill.
- Mallat, S., *A Theory for Multiresolution Signal Decomposition: The wavelet Representation*. IEEE Pattern Analysis and Machine Intelligence, 1989a. 11(7): p. 674-693.
- Mallat, S., *Multi-resolution Approximations and Wavelets*. Transactions of the American Mathematical Society, 1989b. 315: p. 69-88.
- Newland, D.E., *An introduction to Random Vibrations, Spectral and Wavelet Analysis*. 1993, New York: Longman Scientific & Technical.
- Newland, D.E. *Practical Signal Analysis: Do Wavelets Make Any Difference?* in *Proceedings of 16th ASME Biennial Conference on Vibration and Noise*. 1997. Sacramento.
- Nigam, N.C., *Introduction to Random Vibrations*. 1983, Cambridge, MA: M.I.T Press.
- Roberts, J. and P.D. Spanos, *Random Vibration and Statistical Linearization*. 1986, New York: Wiley.
- Spanos, P.D., J. Tezcan, and P. Tratskas, *Stochastic Processes Evolutionary Spectrum Estimation via Harmonic Wavelets*. Computer Methods in Applied Mechanics and Engineering, 2004

Floor Response of Single Degree of Freedom Systems with Metallic Structural Fuses

Ramiro E. Vargas

Graduate Student, Department of Civil, Structural & Environmental Engineering, University at Buffalo

Research Supervisor: Michel Bruneau, Professor

Summary

The floor demands of Single-Degree-of-Freedom (SDOF) systems designed or retrofitted with metallic structural fuses are studied in this article. Floor velocity and acceleration are obtained and comparisons are made between the floor response of bare frames and the floor response of systems with metallic fuses. Furthermore, velocity and acceleration spectra are developed from the floor time history responses to assess how the behavior of nonstructural components may be influenced by the use of metallic fuses.

Introduction

In the 1964 Alaska and 1971 San Fernando earthquakes, extensive damage of nonstructural components was observed, which resulted in substantial economic losses with serious casualties and impediments to the buildings operation, although structural damage was found to be less significant (Lagorio, 1990). Consequently, since the 1970's, many research projects have focused on providing guidance to design, retrofit, and improve the seismic performance of nonstructural elements. An inventory and summary of past research, as well as comparisons of existing regulations to seismically design nonstructural components can be found in Filiatrault et al. (2002), where, as part of the study, recommendations are made for the development of rational research plans to investigate the seismic performance of nonstructural building components.

In Vargas and Bruneau (2004), the structural fuse concept was investigated as a way to protect primary moment frame structures from experiencing inelastic behavior of beams and columns, by concentrating all damage on easily replaceable elements. Furthermore, limiting story drift indirectly allows mitigation of damage to nonstructural components that are sensitive to lateral deformations (i.e., elements that are generally attached to consecutive floors). However, many nonstructural elements are only attached to one floor, which makes them vulnerable to shifting or overturning. Damage to the internal components of sensitive equipment may also occur due to severe floor vibrations. In order to protect these components, floor acceleration and, in some cases, floor velocity (e.g., in the case of toppling of furniture) should be kept under certain limits.

This article studies the floor velocity and acceleration response of SDOF systems designed with metallic dampers acting as structural fuses. Comparisons are made between the floor response of bare frames and the floor response of systems with metallic fuses. Furthermore, velocity and acceleration spectra are developed from floor time history responses to assess how the behavior of

nonstructural components may be affected by the use of metallic fuses. Finally, an equivalent sine-wave floor acceleration response is proposed to generate acceleration and velocity spectra, that may be used to seismically design nonstructural components.

Floor Response

A parametric study was conducted to obtain floor accelerations and velocities for SDOF systems with metallic fuses, using the set of parameters previously considered in Vargas and Bruneau (2004). Figures 1a and 1b show an example of the results obtained from the parametric study for floor acceleration, S_a , and floor velocity, S_v , respectively. The solid line in both figures corresponds to the NEHRP elastic design spectrum, and every curve corresponds to a different value of the strength ratio, η . Note that as structures become more flexible (i.e., $T \geq 2.0$ s), floor spectral accelerations progressively approach those obtained for elastic SDOF systems. Figure 1b shows, as expected, that the relative velocity is close to zero for short period systems. Like in the case of acceleration, floor velocity increases with η values, and for long period systems all the curves approach the NEHRP elastic design spectrum for $T \geq 2$ s.

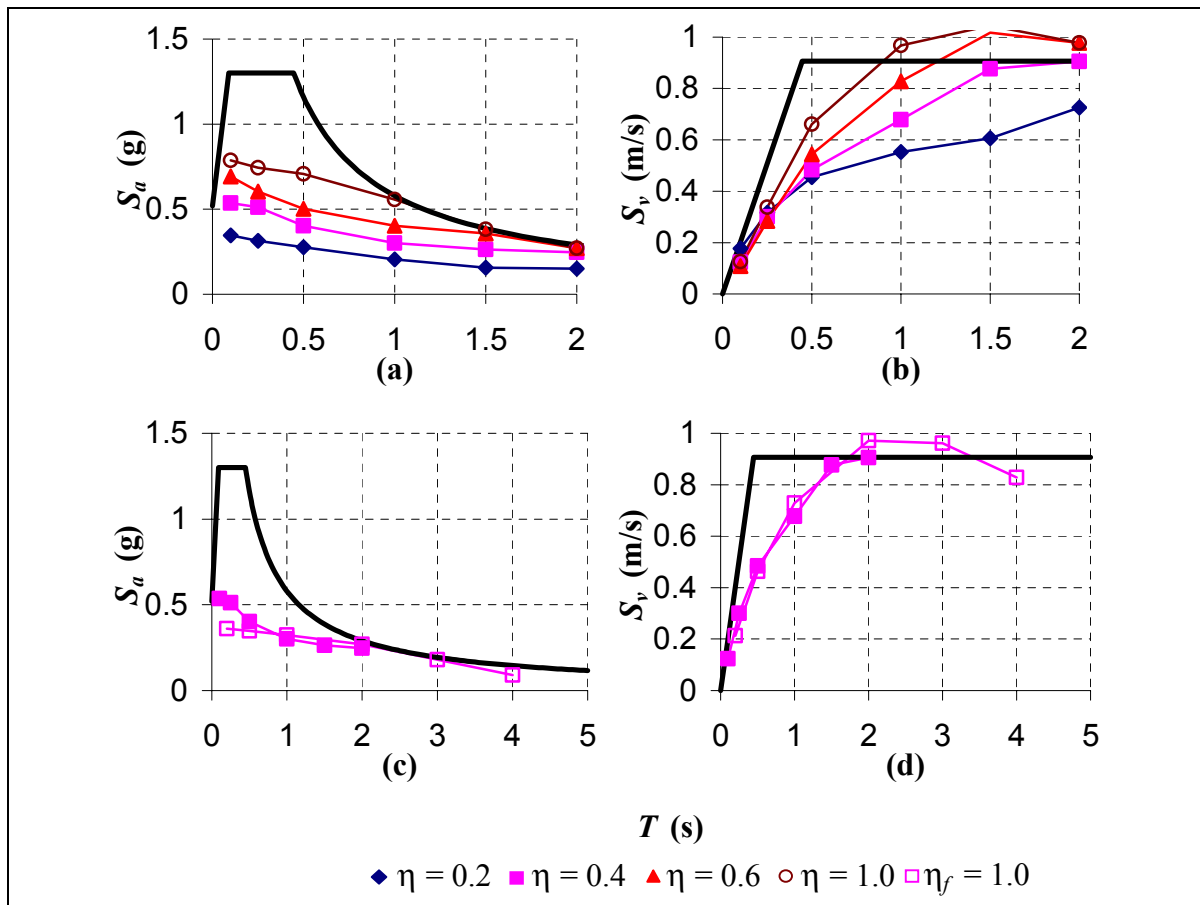


Figure 1. Floor Response; (a) Floor Acceleration, (b) Floor Velocity, (c) Floor Acceleration of Structural Fuse System and Bare Frame, (d) Floor Velocity of Structural Fuse System and Bare Frame

To analyze how metallic fuses modify the floor response, comparisons between the response of bare frames and the response of structural fuse systems were made, in terms of acceleration and velocity. Figure 1c shows an example of the floor acceleration of structural fuse systems, along with the floor acceleration of the corresponding bare frame (i.e., without metallic dampers). Note that when metallic fuses are added to the system, the period of the system shortens. When comparing bare frame and retrofitted system response in Figure 1c, one cannot directly read up from the horizontal axis, but should rather compare the results point-by-point for the six cases considered (alternatively, the figures could have been plotted as a function of the bare frame period on the horizontal axis, but it was felt worthwhile to also visually see the shift in period corresponding to each case). Figure 1c also shows that, in most of the cases, floor acceleration is increased by adding metallic fuses to the system. Furthermore, Figure 1d shows the floor response, in terms of velocity, for bare frames and structural fuse systems. In this case, the periods are also “shifted” to lower values. Unlike acceleration, velocity either decreases or remains equal in most of the cases, which implies that adding metallic fuses do not seem to change the velocity response of the systems.

As a case study to illustrate in more details the above results, a SDOF system designed with unbonded braces to satisfy the structural fuse concept was selected. The frame is a single-story one-bay structure composed of W14 x 211 columns and a W12 x 190 beam, with unbonded braces made of rectangular plates (57 x 25 mm) in a chevron configuration. General properties for this example are: $L = 4877$ mm, $H = 3810$ mm, $m = 0.35$ kN·s²/mm, $F_{yf} = 345$ Mpa, and $T = 0.53$ s. In this case study, results obtained from time history analysis (or directly read from Figures 1c and 1d) indicate that floor spectral acceleration, S_a , and floor spectral velocity, S_v , are 0.40 g and 484 mm/s, respectively. Prior to adding the unbonded braces, properties of the system were $\eta_f = 0.52$ and $T_f = 1.04$ s. Figures 1c and 1d also show that S_a and S_v on the bare frame are respectively 0.32 g and 728 mm/s. In this particular example, it may be noted that adding unbonded braces to the system result in an increase of 25% in the floor acceleration, and a reduction of 33% in the floor velocity.

Floor Spectra

Floor acceleration response histories of SDOF systems have been taken as the input signal to generate elastic floor acceleration and velocity spectra, to analyze the response of nonstructural components attached to the floor of bare frame systems, and structures designed with metallic fuses. A damping ratio of 5% was selected for this study.

Figures 2a and 2b show an example of the floor acceleration spectra, $S_{a,nc}$, and the floor velocity spectra, $S_{v,nc}$, respectively, for the selected structural fuse systems, and their corresponding bare frame systems, where the subscript “nc” denotes “nonstructural component.” In these plots, the horizontal axis corresponds to the elastic period of the nonstructural components, T_{nc} , since floor spectra were built to analyze the response of secondary elements attached to the floor of the primary structure. Note that, even though peak floor acceleration was found to increase in most of the cases, in floor acceleration spectra, two regions are defined by the critical period of the nonstructural component, T_c , where both spectra intersect. Nonstructural elements with a period shorter than this critical period are subjected to acceleration demands greater in structural fuse systems, than in the corresponding bare frame; whereas for components with a period longer than critical, the acceleration demand decreases for structural fuse systems. Approximately, the critical period, T_c , may be determined as the average between the period of the bare frame, T_f , and the period of the structural fuse system, T .

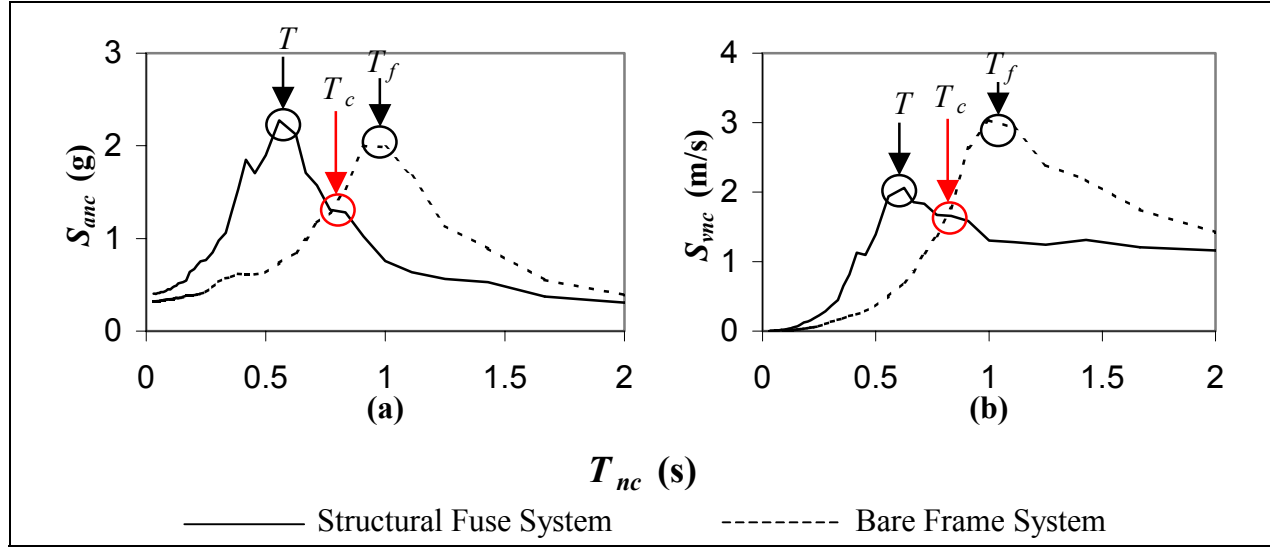


Figure 2. Floor Spectra; (a) Floor Acceleration Spectra, (b) Floor Velocity Spectra

Figures 2a and 2b demonstrate that, in a retrofit situation, the seismic behavior of the nonstructural components may (or may not) be improved with the addition of metallic dampers to the structural system. Positive or negative results may be obtained, depending on the dynamic characteristics of the nonstructural elements, relative to the properties of the retrofitted system. For example, for the case study described in the former section, the critical period is approximately equal to 0.83 s (see Figures 2a and 2b). In this case, nonstructural components with an elastic period less than 0.83 s would experience an increase in acceleration and velocity by the addition of metallic dampers. On the other hand, components having a period greater than 0.83 s are more likely to be subjected to lower levels of acceleration and velocity when metallic dampers are added.

Equivalent Sine-wave Floor Spectra

This section investigates whether an equivalent sine-wave floor acceleration response history could be used as a simplified way to generate acceleration and velocity spectra for that purpose. The dynamic response of a nonstructural component attached to the floor of a structural fuse system can be obtained through the following expression:

$$m_{nc} \ddot{u}_{nc} + c_{nc} \dot{u}_{nc} + k_{nc} u_{nc} = -m_{nc} \ddot{u}_F \quad (1)$$

where, again, the subscript “nc” denotes “nonstructural component”, and \ddot{u}_F is the floor acceleration (i.e., the input signal exciting the nonstructural component). Substituting an equivalent harmonic sine-wave motion for \ddot{u}_F gives, after arranging terms:

$$\ddot{u}_{nc} + \left(\frac{4\pi\xi_{nc}}{T_{nc}} \right) \dot{u}_{nc} + \left(\frac{4\pi^2}{T_{nc}^2} \right) u_{nc} = PFA_{eff} \sin\left(\frac{2\pi t}{T} \right) \quad (2)$$

where ξ_{nc} , T_{nc} are the damping ratio and the period of the nonstructural component, respectively, and PFA_{eff} is the effective peak floor acceleration, defined here as the average of the absolute values of the peaks of the floor acceleration response history, between the first and last exceedances of a threshold acceleration (arbitrarily set at 25% of the maximum floor acceleration in this study). Results for effective peak floor acceleration using this procedure, indicate that PFA_{eff} may be conservatively determined as 50% of the peak floor acceleration (i.e., $PFA_{eff} \approx 0.50 S_a$). Figure 3 shows the first 15 seconds of an actual floor acceleration response history, and its equivalent sine-wave floor acceleration response history generated per the above procedure.

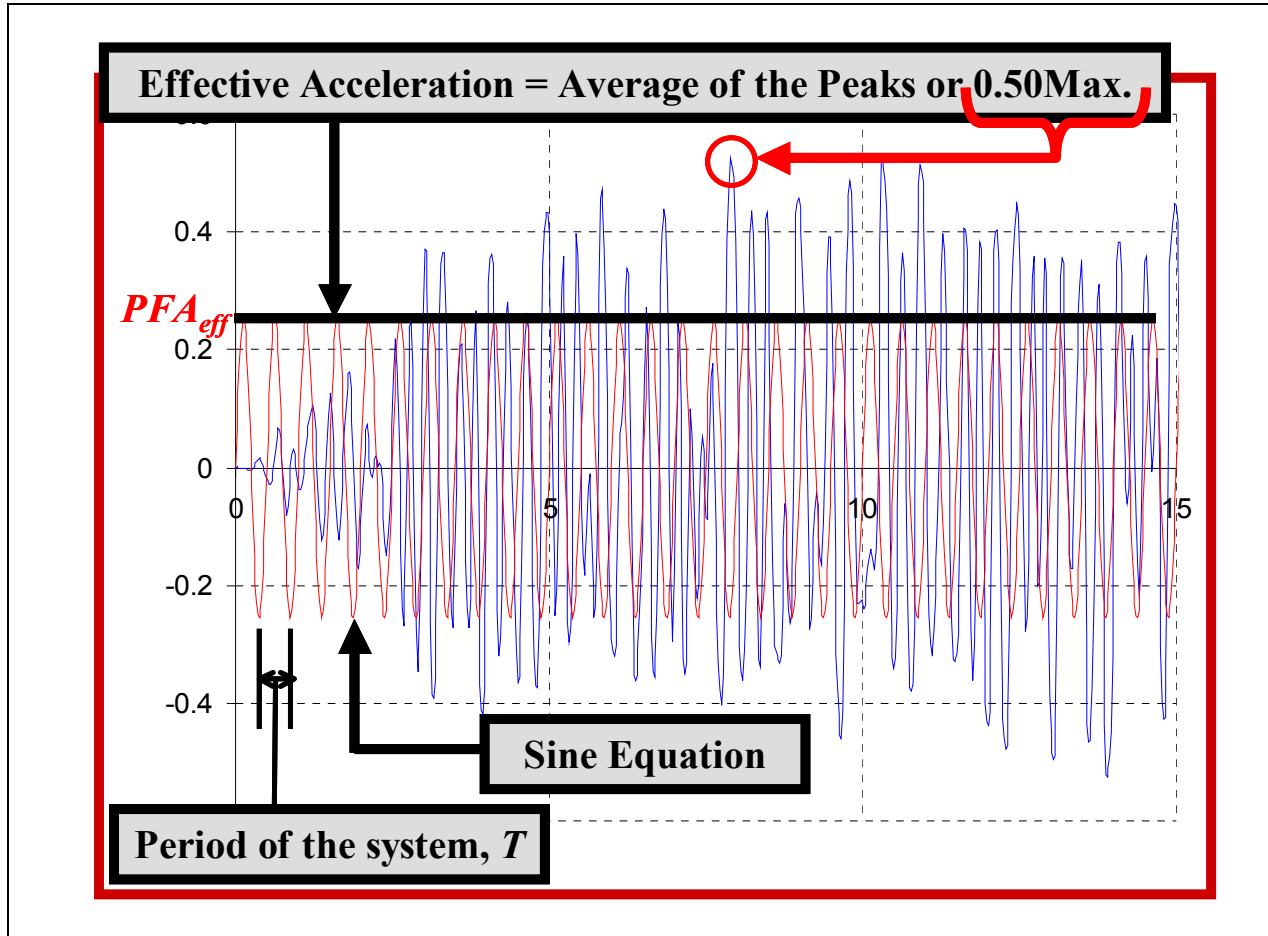


Figure 3. Equivalent Sine-Wave Floor Acceleration Response History of a SDOF System with Metallic Fuses

Closed form solutions for the spectral acceleration, S_{anc} and velocity, S_{vnc} , of nonstructural components for the equivalent sine-wave floor acceleration may be obtained from Equation (2). Figures 4a and 4b show an example of actual acceleration and velocity spectra, respectively, along with the sine-wave response obtained from Equation (2), assuming a damping ratio of 5% for the nonstructural components (i.e., $\xi_{nc} = 5\%$).

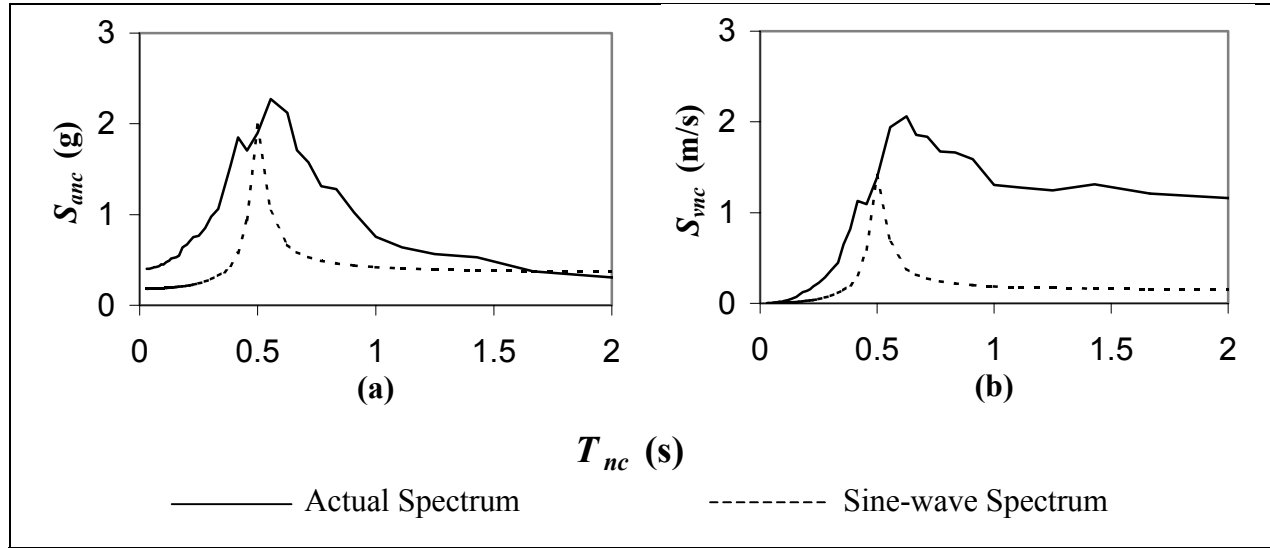


Figure 4. Actual and Sine-wave Response Spectra; (a) Acceleration Spectra, (b) Velocity Spectra

As an example, the case study from former sections will be subjected to a peak floor acceleration of 0.40 g at the roof level (Figure 1a). Conservatively, taking an effective peak floor acceleration of 0.50 S_p and assuming a damping ratio of 5% (i.e., $PFA_{eff} = 0.20$ g, and $\xi_{nc} = 5\%$), a nonstructural component located at the roof level of the building, may be conservatively designed to resist an acceleration, $S_{anc} = 2.2$ g, and a velocity, $S_{vnc} = 1.56$ m/s. These results are corroborated by Figures 4a and 4b.

Conclusions

Floor accelerations and velocities for SDOF systems with metallic fuses have been studied in this chapter through a parametric analysis. It was found that, in most of the cases, floor acceleration increases when using metallic fuses.

It was also found that the critical period, T_c , is an useful indicator to identify when using metallic fuses can increase or decrease the dynamic acceleration and velocity response of nonstructural components. It was observed that nonstructural elements having a period shorter than T_c may be susceptible to greater acceleration (which would increase their likelihood of sliding on their support if unrestrained, for example), and greater velocity (which would for example increase their probability of overturning) when metallic fuses are added. On the other hand, it was found that retrofit works may improve the seismic behavior of flexible nonstructural components that have a period longer than T_c ; however, adequate judgement must be exercised in retrofitting these elements.

Furthermore, using the equivalent sine-wave criterion, it is also possible to determine spectral acceleration and velocity to conservatively design nonstructural components and/or their anchorages. This criterion may be applied to multi-degree of freedom systems assuming a linear variation of floor acceleration over the building height.

Acknowledgements

This research was carried out under the supervision of Dr. Michel Bruneau, and supported by the National Science Foundation, under a grant awarded to the Multidisciplinary Center for Earthquake Engineering Research. This financial support is gratefully acknowledged.

References

Filiatrault, A., Christopoulos, C., and Stearns, C. (2002): Guidelines, Specifications, and Seismic Performance Characterization of Nonstructural Building Components and Equipment. *Report No. PEER-2002/05*, Pacific Earthquake Engineering Research Center, University of California, Berkeley.

Lagorio, H.J. (1990): Earthquakes, and Architect's Guide to Nonstructural Seismic Hazards. John Wiley & Sons Inc., New York.

Vargas, R., Bruneau, M. (2004): Seismic Response of Single Degree (SDOF) Structural Fuse Systems. *13th World Conference on Earthquake Engineering*, Paper No. 3277. Vancouver, Canada.

Response of Seismically Isolated Bridges Considering Variation in the Mechanical Properties of Individual Isolators

Gordon Warn

Graduate Research Assistant, Department of Civil Structural and Environmental Engineering, University at Buffalo

Research Supervisor: Andrew Whittaker, Professor

Summary

This paper summarizes an analytical study investigating how changes in the mechanical properties of individual seismic isolators affect the response of isolated bridge structures subjected to earthquake excitation. Nonlinear response-history analyses are conducted utilizing a simple seismically isolated bridge model, twenty sets of bilinear isolator properties and bins of recorded earthquake ground motion pairs. Variations in the mechanical properties are considered using factors to modify the appropriate bilinear isolator parameter. The results of analyses considering nominal and modified isolation systems are used to systematically identify changes in system response as a function of the property modification factor. These results are used to determine threshold values of the property modification factor corresponding to specific increases in maximum shear force. Threshold values determined in this study are intended to aid engineers in the preliminary design and assessment of an isolation system prior to performing bounding analysis as now required by bridge and building design codes.

Introduction

Property modification factors were included in the 1999 American Association of State Highway and Transportation Officials' Guide Specifications for Seismic Isolation Design (AASHTO, 1999) to account for plausible changes in the mechanical properties of individual seismic isolators over the design life of a seismically isolated bridge. The Guide Specification for Seismic Isolation Design recommends that minimum and maximum property modification factors, denoted λ_{\min} and λ_{\max} , respectively, be determined either through system characterization tests, as prescribed by the specifications, or using the default values provided in Appendix A of the Guide Specification. The process and default values are based on the work of Constantinou et al. (1999). Engineers typically opt for the latter approach where λ_{\min} and λ_{\max} are determined based on the type of seismic isolation bearing (i.e., elastomeric or friction) and various factors affecting the mechanical properties of the isolator, including aging, contamination, scragging, travel and temperature. Typically the minimum property modification factor, λ_{\min} , is assumed to be unity, corresponding to the nominal mechanical properties. Once property modification factors are determined, bounding analysis with limiting values of isolator properties is performed to estimate critical design parameters for the isolators, substructure and superstructure. Although inclusion of property modification factors into the Guide Specification provides an important and necessary design consideration for seismically

isolated bridges (and buildings) the result is an increased number of response analyses required to determine key design parameters.

This paper summarizes an analytical study investigating how changes in the mechanical properties of individual seismic isolators affect system response in seismically isolated bridges subjected to earthquake excitation. Parametric nonlinear response-history analysis is performed using a simple isolated bridge model and three bins of recorded earthquake ground motion pairs to determine key response parameters. Variations in the mechanical properties are considered by modifying the appropriate bilinear parameter using a modification factor. The results of response-history analysis considering nominal and modified isolation system are used to quantify the change in system response as a function of the modification factor. The change in system response, more specifically the change in maximum shear force, is used to identify values of the modification factor corresponding to specific levels of increase in maximum shear force. For a chosen increase in maximum shear force, for example 50-percent, corresponding threshold λ values were determined for each bilinear system and presented as a function of the bilinear parameters: Q_d/W , the zero-displacement force-intercept normalized by the weight acting on the isolator and T_b , the second-slope period. Threshold λ values determined in this study are intended to provide engineers with a design aid for the preliminary assessment of seismic isolation systems prior to performing bounding analysis and not to circumvent bounding analysis as required by bridge and building design codes.

Property Modification Factors

Appendix A of the Guide Specification provides component property modification factors (λ values) for both sliding and elastomeric seismic isolators (AASHTO, 1999). Values of λ are provided for each factor affecting the mechanical properties of isolators including factors for, aging, contamination, cumulative travel, scragging (elastomeric systems), temperature and velocity. Property modification factors for sliding isolators are based largely on research conducted by Constantinou et al. (1999). Recent work by Thompson et al. (2000) provided improved values for high-damping elastomeric seismic isolators with respect to velocity and scragging. The maximum property modification factor is calculated using an equation provided in the Guide Specification and presented here

$$\lambda_{\max} = \lambda_{\max,t} \times \lambda_{\max,a} \times \lambda_{\max,v} \times \lambda_{\max,tr} \times \lambda_{\max,c} \times \lambda_{\max,scrag} \quad (1)$$

where $\lambda_{\max,t}$ accounts for temperature; $\lambda_{\max,a}$ accounts for aging; $\lambda_{\max,v}$ accounts for velocity effects assumed to be equal to 1.0 for all scenarios considered in this study; $\lambda_{\max,tr}$ accounts for cumulative travel (wear); $\lambda_{\max,c}$ accounts for contamination (in sliding isolation systems) and $\lambda_{\max,scrag}$ accounts for scragging (in high-damping elastomeric systems). A range of modification factors was selected for the purpose of response-history analysis based on consideration of all plausible combinations (scenarios) of maximum property modification factors (λ_{\max}) for elastomeric and sliding isolation systems as prescribed in the Guide Specification. Noting, sliding isolation systems including bimetallic interfaces were not specifically addressed due to the large penalty assigned by the Guide Specification to such systems. Table 1 presents the range of λ values and appropriately bilinear parameter(s) to be modified for the three types of isolator considered in this study, namely, Friction Pendulum™ (FP), Elastomeric (E) and Lead-rubber (LR).

Table 1. Modification factors considered for response-history analysis.

Type	Bilinear Parameter	λ							
		0.5	0.85	1.0	1.15	1.5	2.0	3.0	4.0
Friction Pendulum	Q_d	0.5	0.85	1.0	1.15	1.5	2.0	3.0	4.0
Elastomeric	Q_d and K_d	0.5	0.85	1.0	1.15	1.5	2.0	3.0	
Lead-rubber	K_d	0.5	0.85	1.0	1.15	1.5	2.0	3.0	

Shown in Fig. 1 are the three different modified bilinear force-displacement relationships used to account for the change in mechanical properties of FP, E and LR isolators. In Fig. 1, nominal and appropriately modified bilinear plots are shown using nominal properties: $Q_d/W=0.06$, $T_d=2.5$ seconds, and a property modification factor, $\lambda=2.0$. Also illustrated in Fig. 1 are the assumed yield displacements for FP, E and LR isolators chosen to be 0.5 mm, 12.7 mm and 12.7 mm, respectively. For FP isolators, Q_d is modified, as shown in Fig. 1, to account for changes in the frictional properties of the sliding interface while K_d , the second-slope stiffness, remains constant as it is a function of the radius of curvature of the concave plate and the supported weight (assumed to be constant). For E isolators, both Q_d and K_d are modified to account for changes in the elastomer affecting the shear modulus. Similarly, for LR isolators, K_d is modified, again accounting for changes in the elastomer. For this study, variations in the properties of the lead-core which govern Q_d were ignored.

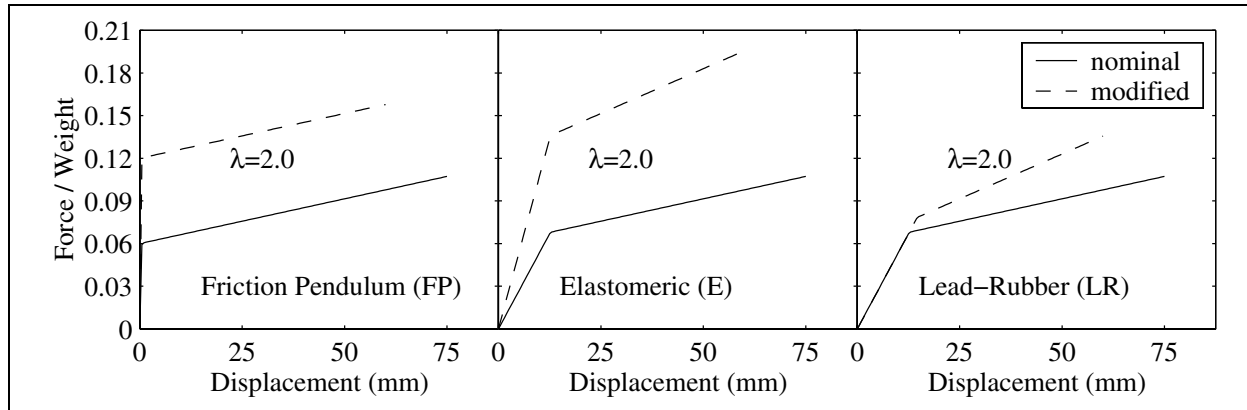


Figure 1. Nominal and modified bilinear force-displacement relationships.

Numerical Simulation

A simple seismically isolated bridge model is utilized to facilitate nonlinear response-history analysis. A schematic of this model is shown in Fig. 2 and assumes a rigid block superstructure supported by four seismic isolators, with three degrees-of-freedom, namely, translation in the longitudinal (x-direction) and transverse directions (y-direction) and rotation about the vertical axis (z-direction). The spatial distribution of isolators and physical properties of the bridge deck (excluding flexibility) are based on the middle span of a multi-span prototype bridge presented in an Applied Technology Council report (ATC, 1986). A more detailed description of this simple bridge model is provided in Warn and Whittaker (2004). The seismic isolators are modeled using a coupled plasticity formulation (Mosqueda, 2004) and characterized by a bilinear force-displacement relationship with defining parameters; Q_d the zero-displacement force-intercept; K_d the second-slope stiffness; and u_y an

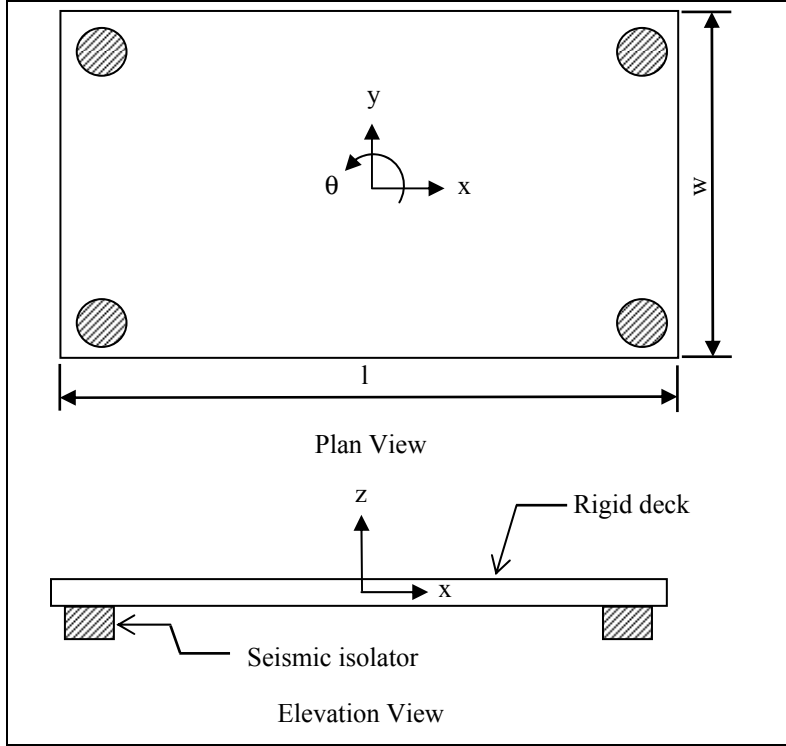


Figure 2. Schematic of simple isolated bridge model.

assumed yield displacement: the characterization assumed in the AASHTO Guide Specifications for Seismic Isolation Design.

Twenty nominal isolation systems were considered with Q_d/W ranging from 0.03 to 0.012 and T_b (a period calculated from the second-slope stiffness) ranging from 1.5 seconds to 4.0 seconds. To facilitate nonlinear response-history analysis three bins of ground motions pairs organized for a previous study (Warn et al. 2004) were utilized. The ground motion bins are denoted: Near-Field (NF), Large-Magnitude, Small-Distance (LMSD), and Large-Magnitude, Soft-Soil (LMSS). Details regarding the characteristics of the ground motion pairs and bin organization is provided in Warn and Whittaker

(2004). The response of the assumed isolated bridge model is determined using Newmark's Step-by-Step integration procedure implemented in Opensees (PEER, 2004). For each analysis, response data is mined to determine the maximum horizontal displacement across the isolation interface and maximum horizontal shear force transmitted by a seismic isolator to the support. Maximum values are determined from the square-root-sum-of-squares (SRSS) response calculated at each time step in the analysis.

Results

The results of response-history analysis considering nominal and modified isolation systems were utilized to quantify the change in system response as a function of the change in the mechanical properties of individual seismic isolators during earthquake excitation. This information is used to determine threshold values of λ as a function of the nominal isolator properties, i.e., Q_d/W and T_b , for specific changes in system response as measured as a percentage of the nominal value. For brevity only the results obtained using ground motion pairs contained in the LMSD bin are presented. Shown in Fig. 3 are sample results for the average change in maximum shear force (DF_{max}) plotted as a function of the modification factor (λ) for various isolation systems composed of FP, E and LR isolators. Also plotted in these figures are three reference lines: one horizontal, one vertical (both solid) and a line (dashed) with slope equal to 1.0. The average change in maximum shear force is calculated using Eq. (2)

$$DF_{max} = \sum_{i=1}^n \frac{F_{max}^{\lambda}}{F_{max}} \quad (2)$$

where F_{\max}^{λ} is the maximum horizontal shear force determined from response-history analysis using the i th pair of ground motions and isolator properties modified by λ ; F_{\max} is the maximum horizontal shear force determined using the i th pair of ground motions and nominal isolator properties; and n is the number of ground motion pairs contained in a particular ground motion bin.

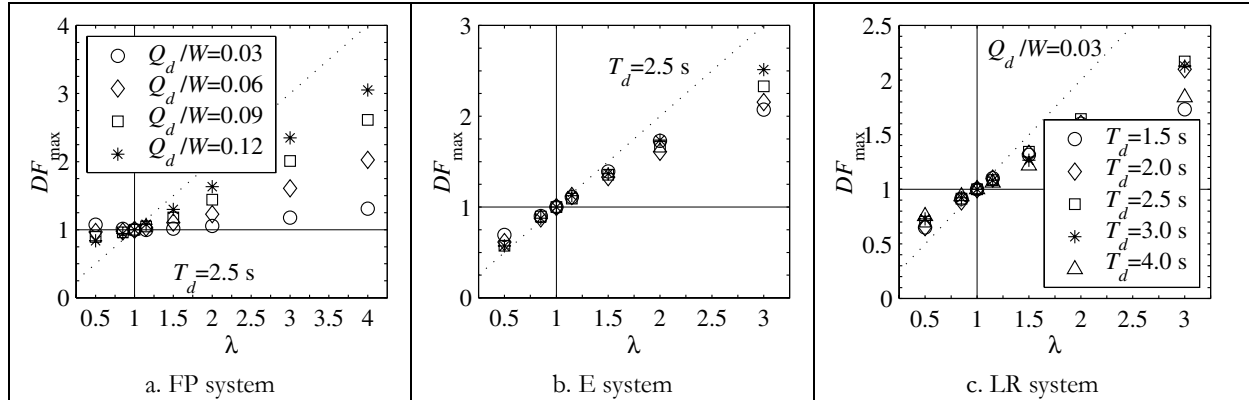


Figure 3. Sample results for change in maximum shear force isolation system composed of FP, E and LR isolators.

The change in maximum shear force data is used to calculate threshold values of λ corresponding to a specific increase in shear force for each type of isolator (FP, E and LR) and each set of nominal isolator properties. For a given increase in shear force (e.g. $DF_{\max} = 1.25$), the corresponding λ value was determined using linear interpolation. These threshold values are presented in graphical format using contour lines plotted as functions of the nominal bilinear parameters, Q_d/W and T_d , for a specific percent increase in shear force. Presented in Fig. 4 are threshold λ values corresponding to a 15-percent increase in maximum shear force for isolation systems composed of FP, E and LR isolators. Considering the results presented in Fig. 4a, for a FP isolation system with $Q_d/W = 0.08$ and $T_d = 2.5$ seconds (shown by the solid dot) a 15-percent increase in shear force is observed for a system with Q_d increased by a factor of 1.5.

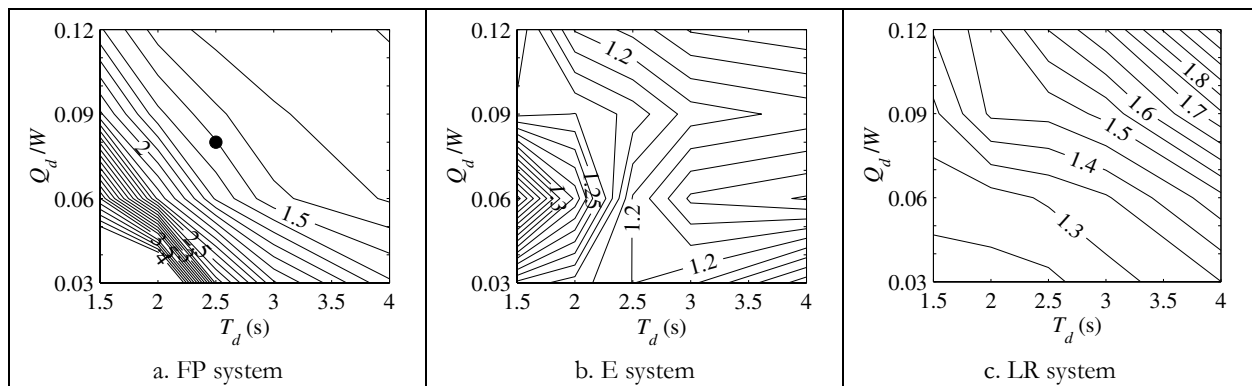


Figure 4. Threshold λ values corresponding to a 15-percent increase in maximum shear force.

Concluding Remarks

This paper served to summarize an analytical study investigating how changes in the mechanical properties of individual seismic isolators in isolated bridge structures effect system response and to present sample results. The results of response-history analysis considering a simple seismically isolated bridge model, twenty nominal isolation systems and a range of modification factors were used to quantify the change in system response: maximum displacement (not presented in this paper) and maximum shear force. The range of λ values selected and used for response-history analysis is based an investigation of those values presented in the current AASHTO Guide Specifications for Seismic Isolation Design for typical bridge isolation systems. System response data, more specifically the change in maximum shear force data, was translated into threshold values of λ , the property modification factor, for several levels of increases in maximum shear force. This paper presented threshold values corresponding to a 15-percent increase in maximum shear force. These threshold values are intended to provide design engineers a method of estimating a λ value corresponding to a specific increase in maximum shear force given a type of seismic isolator and assumed bilinear properties. In this manner, threshold values may be used, in a preliminary sense, to evaluate design alternatives prior to performing bounding analysis. It is important to note, the authors do not intend threshold values from this study to circumvent bounding analysis but rather to aid design engineers in the preliminary selection of design alternatives based on the likely impact that choice will have on the design of surrounding components, for example, substructure elements.

Acknowledgements

This research was carried out under the supervision of Professor Andrew Whittaker, and primarily supported by the Federal Highway Administration through Task D1.4 under award number DTFH 61-98-C-0094 to the Multidisciplinary Center for Earthquake Engineering Research.

References

- American Association of State Highway Officials (1999). Guide Specifications for Seismic Isolation Design, Washington, D.C.
- Applied Technology Council (1986). Seismic design guidelines for highway bridges. Report 6. Redwood City, CA.
- Constantinou M., Tsopelas P., Kasalanati A., and Wolff E. (1999). Property Modification Factors for Seismic Isolation Bearings. MCEER-99-0012, Multidisciplinary Center for Earthquake Engineering Research., Buffalo, NY.
- Mosquesda G, Whittaker A.S., and Fenves G.L. (2004). "Characterization and Modeling of Friction Pendulum Bearings Subjected to Multiple Components of Excitation." J. Structural Engineering. ASCE: 130(3): 433-442.
- Pacific Earthquake Engineering Research (2004). Open System for Earthquake Engineering Simulation. <http://opensees.berkeley.edu/>
- Warn G. and Whittaker A. (2004). "Performance estimates in seismically isolated bridge structures". Engineering Structures, 26, 1261-1278.
- Warn G. and Whittaker A. (2004). "Property modification factors for seismically isolated bridge structures", ASCE, J. Bridge Engineering. Submitted for review and possible publication.

A Novel Nonlinear Control System with Emphasis on Nonstructural Performance

Xin Xu

Graduate Student, Department of Civil, Structural & Environmental Engineering, University at Buffalo

Research Supervisor: Gary Dargush, Professor

Summary

Most control techniques in the structural engineering literature are aimed at improving performance of the primary structural part, but they may have limited or reverse effect on the nonstructural component during strong seismic events. In this paper, we emphasize the nonstructural performance using a cubic nonlinear active control system optimized in the frequency response functions of an SDOF nonlinear isolator. An eight-story base isolated benchmark building recently proposed by the ASCE community is studied as a demonstration. Both the structural and nonstructural performance indices are proposed in this research. We compare our cubic control effect with that of an LQG-based semiactive damping control system. It is shown from the simulation results that, in most design cases, the cubic control system has much better nonstructural performance while still maintaining good performance of the primary structural part. Further research of this cubic control system is also addressed.

Introduction

It is apparent, as demonstrated in the extensive literature on the subject, that the engineering profession has now recognized the importance of the seismic design of electrical and mechanical equipment, pipelines, parapets, elevators, tanks, and other nonstructural elements that are usually attached to the walls and floors of large multistory buildings, nuclear power plants, industrial facilities, and offshore platforms. More importantly, it also has been recognized that after the occurrence of a strong earthquake the survival of these so called secondary systems may be vital to provide emergency services, as it is the case for equipment in power stations, hospitals, or communication facilities. Up to now, the most accepted performance indices with respect to the nonstructural components attached to buildings are the peak and root-mean-square (RMS) absolute floor accelerations.

Base isolation, the most mature passive control technique, has been used widely to protect these critical facilities. But certain severe seismic events, such as some near fault earthquakes dominated by high frequency ground acceleration, will increase the isolation deformation, and also increase the superstructure absolute accelerations which are vital to the nonstructural seismic performance. Passive control devices, such as viscous dampers, may be used to augment damping (Soong and Dargush 1997) at the isolation level to reduce the isolation deformation, but heavy damping may increase superstructure accelerations and drifts (Gavin and Aldemir, 2001). Other optimal control systems, developed mainly in automatic control engineering, have been recently introduced to the structural engineering

profession, such as the Linear Quadratic Gaussian (LQG), Clipped-optimal and Skyhook semiactive control using Magneto-Rheological (MR) fluid dampers. The control effects of a base-isolated benchmark building employing these very mature and practical active/semiactive control systems are studied and compared in a recent paper (Nagarajaiah and Narasimhan 2004). The results show that, while all of these control systems can suppress the structural vibration, none of them can significantly reduce the floor acceleration demands and some of them may even have a reverse effect on the nonstructural performance. It should be also noticed that, LQG is a linear, full-state feedback control law and the Clipped-optimal and Skyhook are just heuristic nonlinear output feedback.

In this paper, we emphasize the nonstructural performance using a novel and more rigorous nonlinear output feedback control system. In the next section, we will describe the Krylov-Bogoliubov “averaging method” for obtaining analytical frequency response functions (FRFs) that approximate the periodic solution of second-order nonlinear differential equations containing cubic terms that we add in the controller intentionally. In nonlinear dynamics, this method has a wide range of applicability by enabling one to study the so-called “slowly varying” oscillation that is an extension to the linear oscillation theory commonly used by structural engineers today. The set of parameters where the single-degree-of-freedom (SDOF) oscillator behaves regularly are found, and the nonlinear oscillator is optimized for obtaining minimum relative deformation and absolute acceleration based on its FRFs. Thus we basically take a frequency domain approach to design the optimal nonlinear controller.

Furthermore, a base isolated building has some unique characteristics for which the SDOF nonlinear oscillation theory can apply. The natural vibration frequency of the “isolation mode” can be shown to be much lower than those of the “structural modes”, thus the dynamics of the MDOF base-isolated building can be estimated by a simpler analysis treating the superstructure as rigid (Chopra, 1995). Although the demonstrated building is a 3D model, we can still approximately treat it as an SDOF oscillator in each X and Y direction when designing the controller. Simulation results of the realistic structure verify the proposed nonlinear control system.

Method of Control Systems Design

The frequency response functions of both the relative deformation and absolute acceleration normalized by the corresponding sinusoidal base excitation counterpart for an SDOF linear oscillator have been well established and are replotted as the thin curves in Fig. 1 below. It should be noticed that, while heavy linear damping can significantly reduce the dynamic response near its resonant frequency, it increases the absolute acceleration throughout the high frequency range of the input (normalized frequency $w/w_1 > 1.41$). Thus, when a base isolated building that always has a low first natural frequency undergoes a strong ground motion containing high frequency contents (> 1 Hz), it will provide poor acceleration performance if it is heavily damped. To overcome this dilemma, we introduce algebraic cubic damping and stiffness terms in the equation of motion and use the averaging method (Vidyasagar, 1993) to obtain the analytical FRFs as the dotted curves shown below. Distortion of the FRFs for nonlinear systems is well known. We optimize their shapes to obtain the minimum response and meanwhile obtain the optimal set of parameters, p and ksi_3 , that control the cubic stiffness and cubic damping terms, respectively.

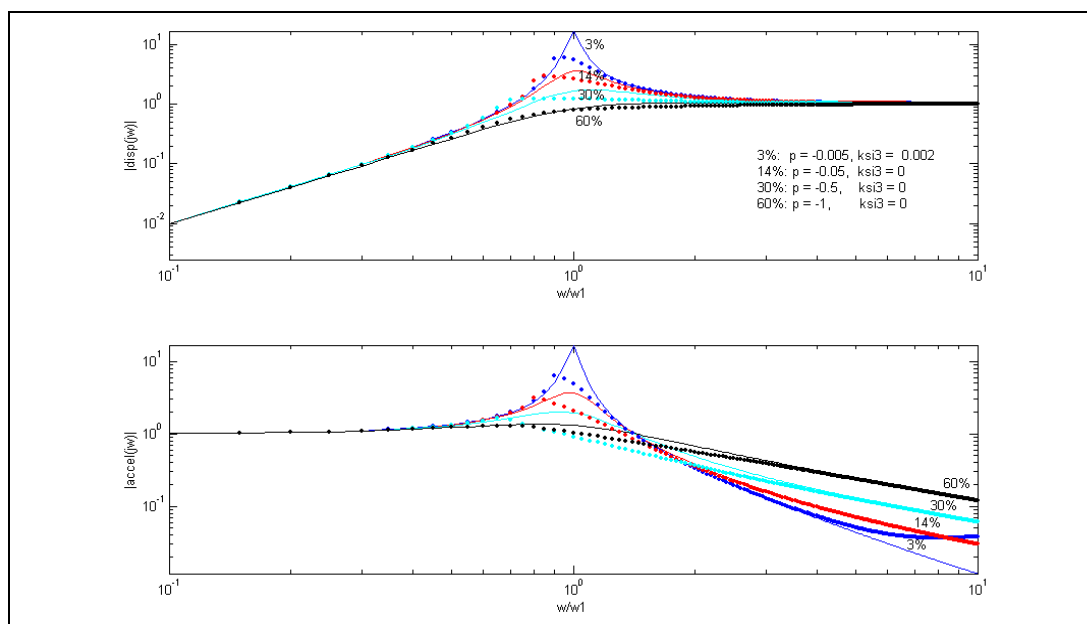


Figure 1. FRFs for linear and nonlinear oscillators with different linear damping ratio

These FRFs are all obtained to avoid the jump phenomenon when the FRFs become over-distorted and all of them are verified by the numerical integration in the time domain. It is clear from these FRFs that, the optimal control parameters are $p = -0.5$, $ksi3 = 0$ at this stage, corresponding to an intermediate damping ratio of 30% or so. This oscillator can attain the same steady state response near the resonant frequency as that of a heavy linear damping (60%) oscillator and also can keep the response in the high frequency range as small as that of a lightly damped oscillator. In addition, the distorted resonant frequency of this nonlinear oscillator shifts to 0.22 Hz without changing its linear stiffness and is farther away from the dominant frequency of most near fault earthquakes than the uncontrolled building (0.33 Hz). It should be emphasized that, in this paper the nonlinear controller is also Lyapunov stable by saturating the controls to keep the oscillator restoring force effective all the times. It should be further emphasized that all the nonlinear FRFs we obtained are dependent on the magnitude of the sinusoidal base excitation. Thus, when detailing the controller, we treat the whole input as a single sinusoidal excitation at its dominant frequency (1 Hz) so as to choose an appropriate input magnitude from the acceleration signals.

To compare our nonlinear control effect, the author also designed a set of semiactive viscous fluid dampers using the Hrovat algorithm (Hrovat et al., 1983) to trace the active LQG controller developed by Nagarajaiah et al. (Nagarajaiah and Narasimhan 2004b). The controller output voltage (0-10V) for each semiactive damper can be designed to be linearly dependent on the required damping coefficient between the upper and lower parameter bounds of the damper at each time instant to trace LQG. The simulation results show that our semiactive control system has almost the equivalent control performance as the active LQG control system. (Xu et al. 2004).

Benchmark Building Demonstration and Simulation Results

The configuration of the eight-story base isolated benchmark building is shown in Fig. 2.

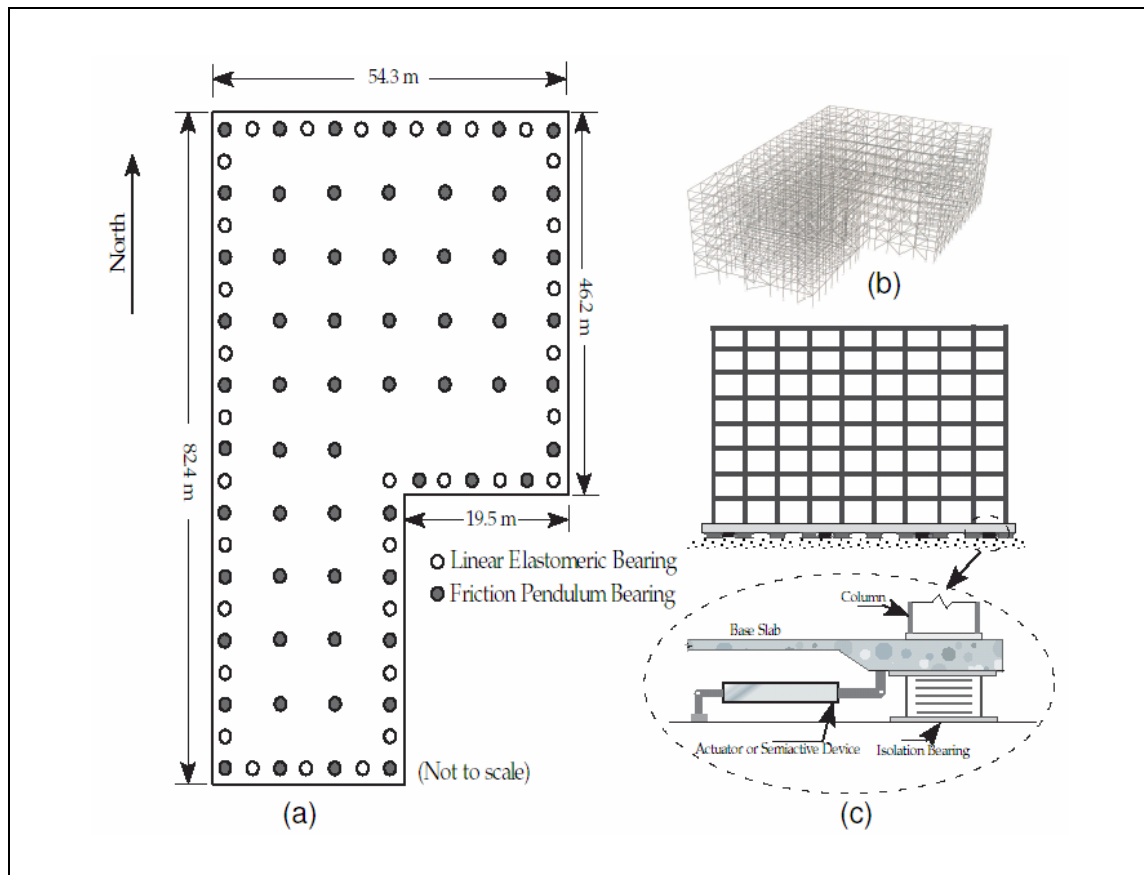


Figure 2. (a) Isolation Plan, (b) FEM Model of Superstructure, (c) Elevation View with Devices (adapted from Nagarajaiah and Narasimhan 2004)

There are seven bi-directional historical near fault earthquakes designated for this benchmark study. The results of the effectiveness for our nonlinear control (Nonlinear) and semiactive control (SAVD) systems are presented in Table 1. Time history response in the EW direction for the Newhall earthquake acting on the building is shown in Fig 3. The force-displacement loops for the two control systems are also shown in Fig 4.

Table 1. Results for Nonlinear Control and SAVFD Control Systems

	Case	J1	J2	J3	J4	J5	J6	J7	J8	J9
Newhall	Nonlinear	0.88	0.88	0.85	0.92	0.93	0.13	0.66	0.82	0.51
	SAVD	0.89	0.88	0.79	0.94	0.98	0.10	0.67	0.83	0.45
Sylmar	Nonlinear	0.77	0.80	0.81	0.84	0.88	0.12	0.65	0.71	0.50
	SAVD	0.89	0.91	0.89	0.94	0.95	0.10	0.70	0.82	0.47
ElCentro	Nonlinear	0.87	0.86	0.58	0.75	0.78	0.13	0.56	0.57	0.47
	SAVD	0.95	0.93	0.79	0.80	0.82	0.09	0.74	0.72	0.41
Rinaldi	Nonlinear	0.92	0.92	0.80	0.92	0.96	0.14	0.65	0.64	0.49
	SAVD	0.97	0.96	0.90	0.94	0.96	0.08	0.72	0.75	0.47
Kobe	Nonlinear	0.71	0.70	0.71	0.71	0.94	0.13	0.63	0.62	0.50
	SAVD	0.84	0.84	0.77	0.85	0.89	0.10	0.71	0.73	0.45
Jiji	Nonlinear	0.89	0.88	0.89	0.88	0.89	0.11	0.65	0.74	0.40
	SAVD	0.87	0.87	0.83	0.88	0.89	0.07	0.74	0.82	0.38
Erzinkan	Nonlinear	0.80	0.82	0.72	0.77	0.80	0.12	0.67	0.65	0.48
	SAVD	0.94	0.96	0.74	0.80	0.93	0.09	0.74	0.78	0.48

J1-J9 are nine performance indices defined for the benchmark problem and are briefly explained as follows. J1: Peak base shear (isolation-level) in the controlled structure normalized by the uncontrolled structure. J2: Peak structure shear (at first story level) in the controlled structure normalized by the uncontrolled structure. J3: Peak base displacement in the controlled structure normalized by the uncontrolled structure. J4: Peak inter-story drift in the controlled structure normalized by the uncontrolled structure. J5: Peak absolute floor acceleration in the controlled structure normalized by the uncontrolled structure. J6: Peak force generated by all control devices normalized by the peak base shear in the controlled structure. J7: RMS base displacement in the controlled structure normalized by the uncontrolled structure. J8: RMS absolute floor acceleration in the controlled structure normalized by the uncontrolled structure. J9: Total energy absorbed by all control devices normalized by energy input into the controlled structure.

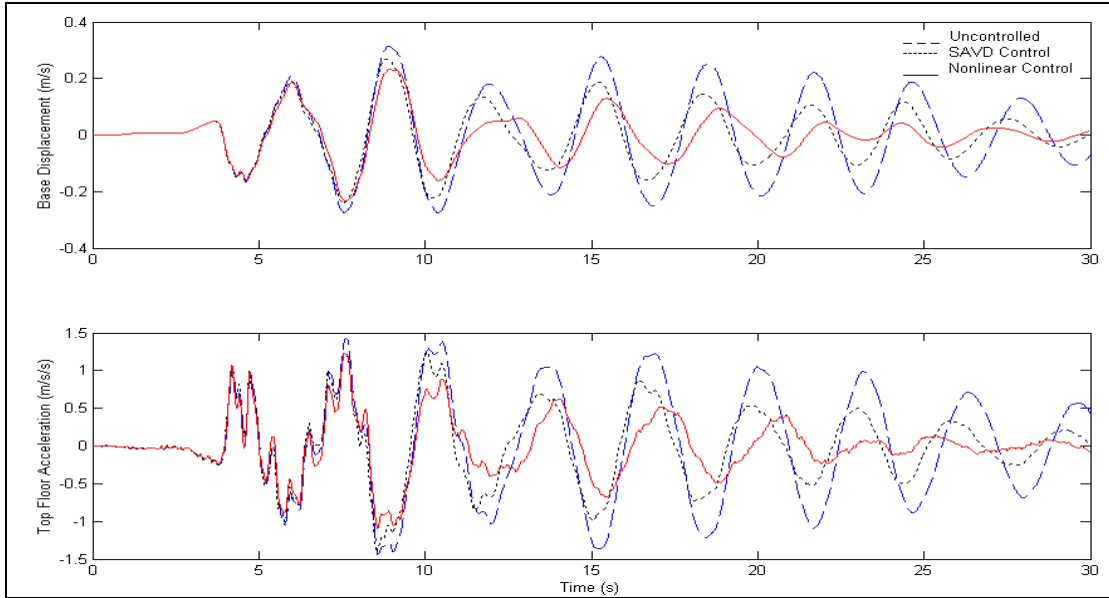


Figure 3. Time history responses of base displacement and top floor acceleration at the center of mass of the base and the top floor respectively in the EW direction for Newhall earthquake

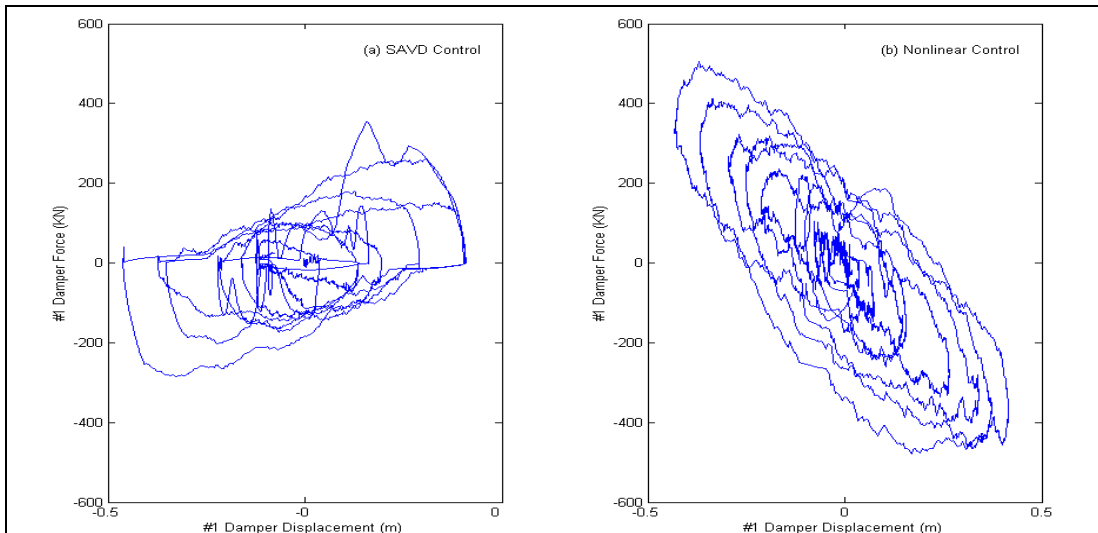


Figure 4. Force-Displacement Loops of #1 Control Device: (a) SAVD Control System, (b) Nonlinear Control System

Conclusions and Future Work

Our semiactive viscous damping control system shows that, the LQG control is mainly in the form of time varying damping force. Other control laws, such as Clipped-optimal and Skyhook, also provide time varying damping force. However, the nonlinear control system providing restoring forces has better performance of absolute floor acceleration, especially if the RMS evaluation criterion is considered, while still maintains good performance of isolation deformation. This result is in good agreement with the analytical nonlinear

frequency response functions and therefore this control system is very suitable to protect nonstructural contents in a critical base isolated structure. Also, from the force-displacement loops, we can see that the SAVD system has almost I, III quadrant forces in the control device while the nonlinear control system has II, IV quadrant forces in the control device. Thus, this nonlinear control law cannot be traced well by the smart viscous fluid dampers. Finally, the optimization of the cubic control system containing other nonlinearities, such as the phase II base isolated benchmark building with friction pendulum bearings or lead rubber bearings, merits further study.

Acknowledgements

This research was primarily supported by the Earthquake Engineering Research Centers Program of the National Science Foundation, under award number EEC-9701471. This financial support is gratefully acknowledged.

References

Chopra A. K. (1995): *Dynamics of structures*, Prentice-Hall, Englewood Cliffs, New Jersey.

Gavin, H., and Aldemir, U. (2001): Behavior and response of auto-adaptive seismic isolation. *Proc. 3rd U.S.-Japan Workshop in Urban Earthquake Disaster Mitigation.*, 15-16 August 2001, Seattle WA, 120-128.

Hrovat, D., Barak, P., and Rabins, M. (1983): Semiactive versus passive or active tuned mass dampers for structural control. *J. Eng. Mech.*, 109(3), 691-705.

Nagarajaiah, S. and Narasimhan, S. (2004): Phase I smart base isolated benchmark building - sample controllers for linear isolation system: Part II. *J. of Structural Control and Health Monitoring (in review)*.

Soong, T. T. and Dargush, G. F. (1997): *Passive energy dissipation systems in structural engineering*, Wiley, New York.

Vidyasagar, M. (1993): *Nonlinear systems analysis*, Prentice-Hall, Englewood Cliffs, New Jersey.

Xu, X., Dargush, G., and Singh, T. (2004): Active/semiactive control for phase I smart base isolated benchmark building with emphasis on nonstructural performance. *J. of Structural Control and Health Monitoring (in review)*.

Production Staff

- Jane E. Stoye, Managing Editor
- Michelle A. Zuppa, Layout and Design

Cover Images

Cover Images (from top left, then clockwise): Group photo taken at the 2004 MCEER Student Leadership Council Retreat in Reno, Nevada; Amanda Bonneau, Cornell University, Ramiro Vargas, University at Buffalo, and Marlon Hill, Florida A&M University are shown presenting posters at MCEER's 2004 NSF site review; This graph displaying construction investment appears in Michael Astrella's (University at Buffalo) discussion on changing the paradigm for performance-based design; Participants on the 2004 Student Field Mission to Japan are pictured at the Miki City E-Defense shake table--from left, Yufeng Hu, University at Buffalo, Elliot Goodwin, University of Nevada, Reno and Hwasung Roh, University at Buffalo--and at the geotechnical centrifuge facility of Soil Stabilization Division of Port and Airport Research Institute; Marlon Hill, Florida A&M University shows an experimental setup in this photo from his paper describing experimental verification of the Eigensystem Realization Algorithm for vibration parameter identification; Cagdas Kafali, Cornell University, shows structural/nonstructural system definition in this illustration from his study on fragility based rehabilitation decision analysis; Jeffrey Berman, University at Buffalo discusses testing of a laterally stable eccentrically braced frame for steel bridge piers--the photo shows a deformed link after testing. Anita Jacobson presents a methodology to assess seismic performance of water supply systems in her paper--the graph is a matrix comparing seismic activity in New York City and Los Angeles.

Acknowledgements

This work was supported primarily by the Earthquake Engineering Research Centers Program of the National Science Foundation under NSF Award Number EEC-9701471.

Any opinions, findings and conclusions or recommendations expressed in this material are those of the author(s) and do not necessarily reflect those of the National Science Foundation.



MULTIDISCIPLINARY CENTER FOR EARTHQUAKE ENGINEERING RESEARCH

A National Center of Excellence in Advanced Technology Applications

University at Buffalo, State University of New York

Red Jacket Quadrangle ■ Buffalo, New York 14261

Phone: (716) 645-3391 ■ Fax: (716) 645-3399

E-mail: mceer@mceermail.buffalo.edu ■ WWW Site <http://mceer.buffalo.edu>



University at Buffalo *The State University of New York*